energies

MDPI

Review

A Systematic Review on Heat Transfer and Pressure Drop Correlations for Natural Refrigerants

Alberta Carella and Annunziata D'Orazio *

Department of Astronautical, Electrical and Energy Engineering, Sapienza University of Rome, Via Eudossiana 18, 00184 Rome, Italy; alberta.carella@uniroma1.it
* Correspondence: annunziata.dorazio@uniroma1.it

Abstract: Due to environmental concerns, natural refrigerants and their use in refrigeration and air conditioning systems are receiving more attention from manufacturers, end users and the scientific community. The study of heat transfer and pressure drop is essential for accurate design and more energy efficient cycles using natural refrigerants. The aim of this work is to provide an overview of the latest outcomes related to heat transfer and pressure drop correlations for ammonia, propane, isobutane and propylene and to investigate the current state of the art in terms of operating conditions. Available data on the existing correlations between heat transfer coefficients and pressure drops for natural refrigerants have been collected through a systematic search. Whenever possible, validity intervals are given for each correlation, and the error is quantified. It is the intention of the authors that this paper be a valuable support for researchers and an aid to design, with particular reference to heat pumps. A procedure based on the Preferred Reporting Items for Systematic Reviews and Meta-Analyses (PRISMA) statement was adopted, and the Scopus database was used to query the relevant literature. A total of 135 publications qualified for inclusion in the survey; 34 articles report experimental investigations for unusual geometric conditions. Of the 101 selected papers related to usual geometric conditions, N = 50 deal only with HTC, N = 16 deal only with pressure drop and the remainder (N = 35) analyse both HTC and pressure drop. Among the 85 HTC papers, N = 53 deal with the evaporating condition, N = 30 with condensation and only N = 2 with the heat transfer correlations under both conditions. Most of the 101 articles concern propane and isobutane. The high temperatures are less widely investigated.

Keywords: natural refrigerants; two-phase flow; heat transfer; pressure drop; correlations; systematic review

Citation: Carella, A.; D'Orazio, A. A Systematic Review on Heat Transfer and Pressure Drop Correlations for Natural Refrigerants. *Energies* **2024**, *17*, 1478. https://doi.org/10.3390/en17061478

Academic Editor: Christopher Micallef

Received: 5 February 2024
Revised: 11 March 2024
Accepted: 14 March 2024
Published: 19 March 2024

1. Introduction

Refrigeration and air conditioning play an important role in modern society, providing thermal comfort and food safety. However, the widespread use of synthetic refrigerants, particularly fluorinated gases (F-gases), has led to serious environmental concerns, as they contribute significantly to the greenhouse effect and climate change. In response to these problems, international regulations have imposed restrictions on the use of F-gases, pushing industry towards the adoption of more sustainable solutions. In this context, natural refrigerants have gained increasing attention as environmentally friendly and low-impact alternatives [1].

These refrigerants, such as ammonia (R717), hydrocarbons and carbon dioxide (R744), have been studied to replace CFCs, HCFCs and HFCs in refrigeration, air conditioning and heat pump systems. They have zero ozone depletion potential (ODP), and most have near-zero global warming potential (GWP) compared to CFCs and HCFCs.

However, the use of natural refrigerants will be complex, mainly due to the need to adapt refrigeration and air conditioning systems to their characteristics.

In this context, the experimental study of heat transfer and pressure drop and their correlations becomes very important in optimising the energy efficiency of the system and to ensure reliable performance. In addition, the flow pattern studies will help to determine how natural refrigerants behave under different operating conditions, contributing to a more accurate design.

Sunden et al. [2], in their systematic review, presented a meta-analysis and regression analysis of the available pressure drop and heat transfer data for both single-phase and two-phase flows for several refrigerants with attention to enhanced configurations of heat exchangers.

Cavallini et al. [3] provide a comprehensive review of recent research on the heat transfer and pressure drop of natural refrigerants (CO_2, NH_3, C_3H_8, R600a, nitrogen) in mini channels, with the aim of properly designing heat transfer equipment.

The review by Thome et al. [4] focuses on flow boiling heat transfer, two-phase pressure drop and the flow patterns of ammonia and hydrocarbons. A comparison of experimental data in smooth tubes with four flow boiling correlations is presented. It is suggested that more experimental data be obtained from properly conducted experiments and that new correlations or modified correlations be made on the basis of the existing ones.

This article presents a systematic review to evaluate the available correlations regarding the heat transfer (HT) and pressure drop (PD) of natural refrigerants such as ammonia (R717) and hydrocarbons (R290, R600a, R1270). The most common geometries and operating conditions are analysed for each refrigerant.

Whenever possible, validity intervals are given for each correlation and the error is quantified. It is the intention of the authors that this could be a valuable support for researchers and an aid to design, with particular reference to heat pumps.

2. Materials and Methods

A systematic review of heat transfer and pressure drop correlations for natural refrigerants was conducted following the PRISMA guidelines [5]. This approach to literature review aims to collect all evidence that meets pre-defined eligibility criteria to answer a specific research question. It uses explicit, systematic methods to minimise bias and, thus, provide reliable findings from which conclusions can be drawn and decisions made.

The workflow consists of four phases: identification, screening, eligibility and inclusion. In the first phase, a number of research questions were formulated to accurately identify the objectives of the systematic review and, consequently, to examine the available literature:

- Are there heat transfer and pressure drop correlations that can predict the experimental data of natural refrigerants?
- How accurate are the current correlations?
- Which natural refrigerants receive more attention?

Specifically, for this research, the Scopus database was queried, using a combination of keywords and Boolean operators to find relevant studies. Specifically, the keywords in the following items were searched in the "Article title, Abstract and Keywords" fields:

1. "Heat transfer" OR "heat transmission";
2. "Pressure drop" OR "frictional pressure gradient";
3. "Natural refrigerant" OR hydrocarbons OR propane OR R290 OR C_3H_8 OR isobutane OR R600a OR C_4H_{10} OR propylene OR R1270 OR C_3H_6 OR ammonia OR R717 OR NH_3;
4. Correlation OR "prediction method" OR "predictive method" OR "relationship" OR "as a function of";
5. Combustion OR kerosene OR coal (only for "Article Title and Keywords" fields).

The queries from #1 to #5 were combined as follows: #1 OR #2 AND #3 AND #4 AND NOT #5.

Inclusion and exclusion criteria were then defined and applied through the identification, screening and inclusion steps to select the relevant studies for the review, which were then analysed in detail.

Inclusion criteria:

- The research must include heat transfer and/or pressure drop correlations.
- Natural refrigerants must be evaluated, in particular R717, R290, R600a and R1270.
- The papers can be reviews but also reporting data and correlations.

Exclusion criteria:

- The articles focus on combustion, toxicity, flammability and risk.
- The studies concern particular natural refrigerants (e.g., CO_2) that are not considered in this review.
- The papers partly deal with heat transfer and pressure drop, but no correlations are reported.
- The studies refer to synthetic refrigerants and/or refrigerant blends.
- The papers are conference papers.
- The papers are purely reviews, not reporting data and correlations.
- The language is not English.

In the screening phase, the titles and the abstracts of all the articles identified in the first stage were rigorously assessed against the defined inclusion and exclusion criteria. The papers that met the criteria were analysed in more detail through a full reading of the text (eligibility stage).

A period of 15 years was chosen to give priority to more recent studies, and only those written in English were selected.

The division of labour consisted of a first phase in which the first author independently selected the relevant material, followed by a second stage in which both authors reviewed all papers. In cases of doubt, the senior author made the final decision.

3. Results

A total of 1366 articles were analysed in the first identification step. Duplicates of 24 articles were removed before the screening phase. As shown in Figure 1, of the 1342 original articles, N = 728 were excluded because their titles did not meet the inclusion criteria and N = 213 were excluded because of their abstracts. From the 401 articles obtained, those for which the full text was not available were subtracted. This resulted in N = 353 papers that were assessed for eligibility. A thorough reading of the full text of the articles and the application of the exclusion criteria resulted in a final sample of 135 articles that were assessed in the review.

The 135 articles included are summarised in Tables 1–4.

It should be noted that the tables are constructed with some assumptions and conventions, which are specified below.

Table 1 shows the source of the data used for the correlation and the geometry studied, highlighting the main focus of the article. As in Table 3, the reader is referred to the citing article in this review (first column) when the number of external databases is greater than 3.

Table 2 shows the operating conditions and correlations for only the natural refrigerants of interest in this review (R717, R290, R600a, R1270). Different refrigerants appear in the table in the case of universal correlations and have, therefore, been developed with different refrigerants.

The most frequent dimensionless parameters used in the correlations reported in Tables 2 and 4 are summarised in the Nomenclature Section.

The "R" column refers only to the refrigerants used to develop the correlation. If the experimental data available in the literature and related to the refrigerant of interest for the present work are used to test the correlation, the corresponding error is reported in the "*AAD*" column.

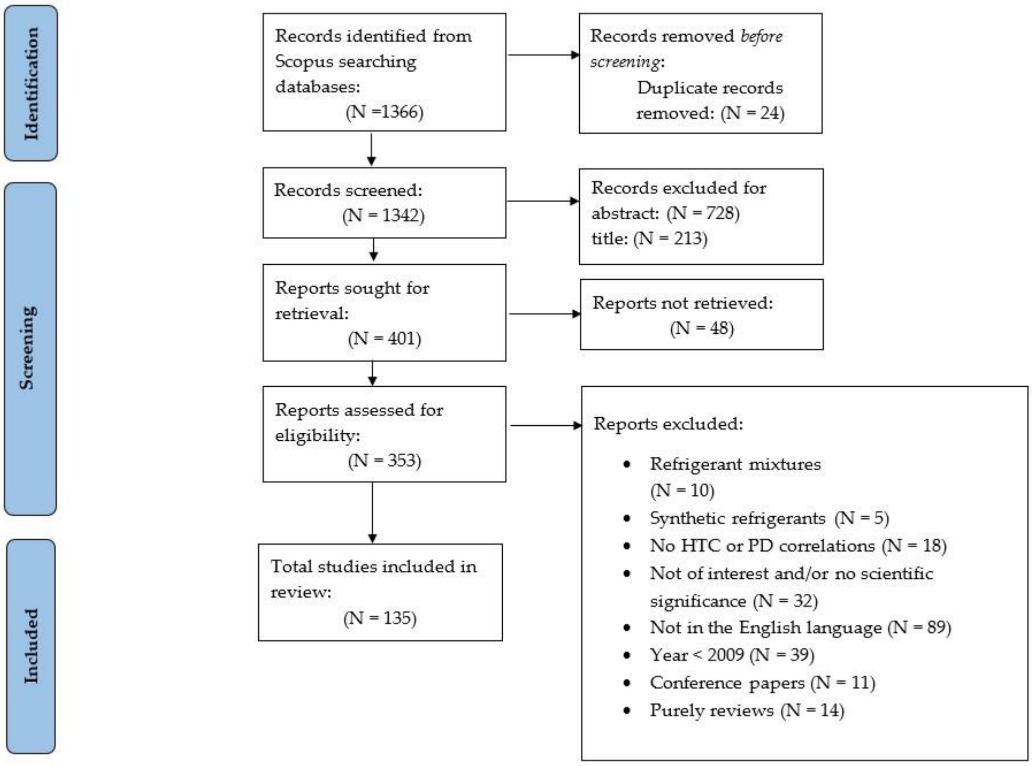

Figure 1. PRISMA flowchart for studies included in this review.

When the experimental results related to the refrigerant of interest for the present work are coupled with an existing correlation, the corresponding error is reported in the table (column "*AAD*") together with the corresponding reference.

The error between the model prediction and the experimental data is reported as average absolute deviation (*AAD*), calculated according to Equation (1):

$$AAD = \frac{1}{N}\sum_{i=1}^{N}\left|\frac{y(i)_{pred} - y(i)_{exp}}{y(i)_{exp}}\right| \quad (1)$$

It should be noted that some authors expressed the error in a different way. Some expressed error as the percentage of data falling within a certain range, others as the coefficient of determination (R^2). This is indicated with an asterisk in Tables 2 and 4. The error values related to the mean deviation without the absolute value are indicated by *AD*.

Table 3 shows the source of the data used for the correlation and the geometry studied, highlighting the main focus of the article in cases of unusual configurations.

Table 4 shows the operating conditions and correlations for only the natural refrigerants of interest in this review, in cases of unusual configurations.

Table 1. Summary of the type of data, geometries and research highlights of the articles included in this review.

First Author/Year	R	Data	Geometry/Material/Orientation	Research Highlights
Ağra (2012) [6]	R600a	Analytical model and experimental study	Horizontal smooth copper tube, d_i = 4 mm	TP annular flow condensation HT
Ahmadpour (2019) [7]	R600a	Experimental study	Horizontal straight copper tube, d_i = 8.7 mm	Condensation HT, effect of lubricating oil on condensation HT
			Horizontal U-shaped copper tube, d_i = 8.7 mm	
Akbar (2021) [8]	R290	Experimental study	Horizontal smooth stainless steel tube, d_i = 3 mm	TP flow boiling HT

Ali (2021) [9]	R1234yf R152a R600a, R134a	Experimental study	Vertical stainless steel tube, d_i = 1.60 mm, L_h = 245 mm	Flow boiling frictional PD
Allymehr (2020) [10]	R290	Experimental study	A smooth tube, MF1, MF2, d_o = 5 mm	Flow boiling HT and PD
Allymehr (2021) [11]	R600a R1270	Experimental study	A smooth tube, MF1, MF2, d_o = 5 mm	Evaporation HT and PD
Allymehr (2021) [12]	R290 R600a R1270	Experimental study	A smooth tube, MF1, MF2, d_o = 5 mm	Condensation HT and PD
Amalfi (2016) [13]	R134a, R245fa, R236fa, R717, R290 R600a, R1270, R1234yf R mixtures	External experimental database [14]	Brazed/gasketed/welded/shell and plate heat exchanger (PHE), β = 27–70°, d_h = 1.7–8 mm	Flow boiling HT and TP frictional PD
Anwar (2015) [15]	R600a	Experimental study	Vertical stainless steel tube, d_i = 1.60 mm, L_h = 245 mm	Flow boiling HT and dryout characteristics
Arima (2010) [16]	R717	Experimental study	Vertical plate evaporator	Flow patterns and forced convective boiling HT
Asim (2022) [17]	R600a	Experimental study	Vertical stainless steel tube, d_i = 1.60 mm, L_h = 245 mm	Flow boiling HT
Ayub (2019) [18]	R717, R134a R410A	External experimental database (see [18])	PHE, β = 0–65°	Evaporation HT
Basaran (2021) [19]	R600a	Steady-state numerical simulations (CFD code ANSYS Fluent 19.2)	Horizontal smooth circular microchannel, d_i = 0.2–0.6 mm	Condensation HT and TP PD
Basaran (2021) [20]	R600a	Experimental study and thermal simulation model	Microchannel, d_h = 0.2–0.6 mm	Condensation HT and PD
Butrymowicz (2022) [21]	R134a, R507A, R600a	Experimental study	Horizontal copper tubular channel, d_i = 12 mm	Flow boiling HT under near critical pressure
Butrymowicz (2022) [22]	R290	Experimental study	Aluminium mini channel condenser and evaporator	Condensation and evaporation frictional PD
Cao (2021) [23]	R600a	Experimental study	Aluminium mini channel, d_i = 8 mm, vertical/horizontal inclined angles 0°–180°	Condensation HT and frictional PD
Choi (2009) [24]	R290	Experimental study	Horizontal smooth stainless steel mini channels, d_i = 1.5, 3.0 mm	TP flow boiling HT and PD
Choi (2014) [25]	R744, R717 R290, R1234y	Experimental study	Horizontal circular stainless steel smooth tube, d_i = 1.5, 3 mm	Evaporation HT
Cioncolini (2011) [26]	R22, R32, R134a R290, R600a R718, R12 R236fa, R245fa	External experimental database (see [26])	Vertical/horizontal tubes, d_i = 1.03–14.4 mm	Liquid film thickness, void fraction and convective boiling HT
Da Silva (2023) [27]	R600a	Experimental study	Horizontal aluminium multiport extruded tube, d_i = 1.47 mm	Flow patterns, void fraction distribution and flow boiling PD
Da Silva Lima (2009) [28]	R717	Experimental study	Horizontal smooth stainless steel tube, d_i = 14 mm	Flow patterns, diabatic and adiabatic frictional PD
Dalkilic (2010) [29]	R600a	Experimental study	Horizontal smooth copper tube, d_i = 4 mm	Annular flow condensation frictional PD
Darzi (2015) [30]	R600a	Experimental study	Horizontal copper smooth round tube, d_h = 8.7 mm Horizontal copper flattened tubes, d_h = 5.1–8.2 mm	Condensation HT and PD

De Oliveira (2016) [31]	R600a	Experimental study	Horizontal smooth stainless steel tube, d_i = 1.0 mm, L_h = 265 mm	TP flow patterns and flow boiling HT
De Oliveira (2017) [32]	R290 R600a	Experimental study	Horizontal stainless steel tube, d_i = 1.0 mm, L_h = 265 mm	Flow patterns and TP flow boiling frictional PD
De Oliveira (2018) [33]	R290	Experimental study	Horizontal smooth stainless steel tube, d_i = 1.0 mm, L_h = 265 mm	Flow patterns and flow boiling HT
De Oliveira (2020) [34]	R1270	Experimental study	Horizontal stainless-steel circular tube, d_i = 1 mm	Flow patterns and flow boiling HT
De Oliveira (2023) [35]	R1270	Experimental study	Horizontal stainless-steel circular tube, d_i = 1 mm	Flow patterns and flow boiling frictional PD
Del Col (2014) [36]	R290	Experimental study	Horizontal copper mini channel, d_i = 0.96 mm, Ra = 1.3 μm	TP condensation and flow boiling HT, frictional PD
Del Col (2017) [37]	R1270	Experimental study	Horizontal copper mini channel, d_i = 0.96 mm, Ra = 1.3 μm	Condensation and flow boiling HT, adiabatic TP PD
ElFaham (2023) [38]	R290 R600 R600a	External experimental database (see [38])	Horizontal/vertical stainless steel/copper tubes, d_i = 0.168–7.7 mm	TP flow boiling HT
Fang, Xiande (2019) [39]	R717 R290 R600a	External experimental database (see [39])	Horizontal/vertical upward copper/ stainless steel single circular tubes, d_h = 0.96–14 mm	Saturated flow boiling HT
Fang, Xianshi (2023) [40]	R600a	External experimental database [41]	Horizontal copper circular smooth and spiral coil inserted tubes, d_i = 8.1 mm	Condensation frictional PD
Fries (2019) [42]	R290	Experimental study	Horizontal mild steel plain tubes, d_i = 14.65, 20.8 mm	Condensation HT and PD
Fries (2020) [43]	R290 R1270	Experimental study	Copper tube, d_i = 15 mm Mild steel tube, di = 14.65 mm	PD in TP flow
Fronk (2016) [44]	R717	External experimental database [45]	Horizontal smooth stainless steel tube, d_i = 0.98–2.16 mm	Pure ammonia condensation HT, high-temperature-glide zeotropic ammonia–water mixtures
Gao (2018) [46]	R717	Experimental study	Horizontal smooth stainless steel tube, d_i = 4 mm	Flow boiling HT, adiabatic TP frictional PD
Gao (2019) [47]	R717	Experimental study	Horizontal smooth stainless steel tube, d_i = 4, 8 mm	TP PD
Ghazali (2022) [48]	R290	External experimental database (see [48])	Horizontal smooth stainless steel tubes, d_i = 1–6 mm	Pre-dry out TP evaporation HT, genetic algorithm optimization
Ghorbani (2017) [49]	R600a	Experimental study	Horizontal flattened copper tube, d_h = 7.29 mm	Condensation HT, R600a–oil–nanoparticle mixtures
Guo (2018) [50]	R1234ze(E) R290 R161 R41	Experimental study	Horizontal smooth copper tube, d_i = 2 mm	Condensation HT
Huang (2012) [51]	R134a R507a R12, R717	Experimental study and external experimental database [52]	Brazed PHE, β = 28–60°, d_h = 3.51 mm	TP flow boiling HT and PD
Ilie (2022) [53]	R717	Experimental study	PHE, β = 60°, d_h = 10 mm	Boiling HT
Inoue (2018) [54]	R32, R410a R1234ze(E) R152a	Experimental study	Horizontal smooth copper tube, d_i = 3.48 mm	Condensation HT
Kanizawa (2016) [55]	R134a R245fa R600a	External experimental database (see [55])	Horizontal smooth stainless steel tube, d_i = 0.38–2.60 mm	Flow boiling HT
Khan, T.S. (2012) [56]	R717	Experimental study	PHE, β = 60°	TP evaporation HT and PD

Khan, M.S. (2012) [57]	R717	Experimental study	PHE, β = 30°	TP evaporation HT and PD
Koyama (2014) [58]	R717	Experimental study	Titanium plate evaporator, channel height = 1, 2, 5 mm	Flow boiling HT
Lee (2010) [59]	R290 R600a	Experimental study	Horizontal smooth copper tube, d_i = 5.80–10.07 mm	Condensation HT
Lillo (2018) [60]	R290	Experimental study	Horizontal circular smooth stainless steel tube, d_i = 6 mm, L_h = 193.7 mm	TP flow boiling HT and PD, dry-out incipience vapor quality
Liu (2016) [61]	R290	Experimental study	Horizontal square stainless steel mini channel, d_h = 0.952 mm, Ra = 3.2 µm	Condensation HT and PD
Liu (2018) [62]	R600a R227ea, R245fa	Experimental study	Vertical rectangular copper mini channel, d_h = 2.76	Flow patterns and flow boiling HT
Longo (2012) [63]	R600a R290 R1270	Experimental study	Brazed PHE, β = 60°, d_h = 10 mm	Vaporization HT and frictional PD
Longo (2017) [64]	R290 R1270	Experimental study	Horizontal smooth tube, d_i = 4 mm	Forced convection condensation HT, condensation frictional PD
Longo (2020) [65]	R600a	Experimental study	Horizontal smooth copper tube, d_i = 4 mm	Flow boiling HT and frictional PD
Longo (2023) [66]	R290 R1270	Experimental study	Brazed PHE, β = 65°	Nucleate boiling HT
López-Belchí (2016) [67]	R290	Experimental study	Horizontal square aluminium multiport mini channel tube, d_i = 1.16 mm	TP condensation HT and frictional PD
Macdonald (2016) [68]	R290	Experimental study	Horizontal smooth copper tubes, d_i = 7.75, 14.45 mm	Condensation HT and frictional PD
Macdonald (2016) [69]	R290	Experimental study	Horizontal smooth copper tubes, d_i = 7.75, 14.45 mm	Flow visualization, condensation HT and frictional PD
Macdonald (2017) [70]	R290	Experimental study	Horizontal circular smooth tube, d_i = 7.75 mm	Flow visualization and condensation HT
Maher (2020) [71]	R134a, R245fa R125, R744 R236ea, R22, R152a R32, R410a R1234ze(E), R290 R600a, R1234yf R1234yf	External experimental database (see [71])	Horizontal circular tubes, d_i = 0.509–8.0 mm	Two-phase flow frictional PD
Maqbool (2012) [72]	R717	Experimental study	Vertical circular stainless steel mini channel, d_i = 1.70, 1.224 mm	Flow boiling TP PD
Maqbool (2012) [73]	R717	Experimental study	Vertical circular stainless steel mini channel, d_i = 1.70, 1.224 mm	Flow boiling HT
Maqbool (2013) [74]	R290	Experimental study	Vertical circular stainless steel mini channel, d_i = 1.70 mm, Ra = 0.21 µm, L_h = 245 mm	TP flow boiling HT and frictional PD
Mohd-Yunos (2020) [75]	R290	External experimental database (see [75])	Vertical/horizontal tubes, d_i = 1–6 mm	TP evaporation HT and genetic algorithm optimization
Moreira (2021) [76]	R134a, R600a R290, R1270	Experimental study	Horizontal smooth stainless steel tube, d_i = 9.43 mm	Flow patterns and convective condensation HT
Morrow (2021) [77]	R717 R290 R600a	External experimental database (see [77])	Horizontal/vertical, round/square/rectangular/flat, smooth tubes, d_i = 0.952–10.07 mm	Flow condensation HT
Murphy (2019) [78]	R290	Experimental study	Vertical aluminium mini channel, d_i = 1.93	Condensation HT and PD

Nasr (2015) [79]	R600a	Experimental study	Horizontal smooth copper tube, d_i = 8.7 mm	Flow patterns and flow boiling HT
Oh (2011) [80]	R22, R134a, R410A, R290, R744	Experimental study	Horizontal circular smooth stainless steel tubes, d_i = 0.5, 1.5, 3.0 mm	Flow patterns and TP flow boiling HT
Pamitran (2009) [81]	R290	Experimental study	Horizontal smooth stainless steel mini channels, d_i = 1.5, 3.0 mm	TP flow boiling HT
Pamitran (2011) [82]	R290 R717	Experimental study	Horizontal circular stainless steel smooth tube, d_i = 1.5, 3 mm	Evaporation HT
Patel (2018) [83]	R290, R22 R1234yf, R1234ze, R410a, R32	External experimental database (see [83])	Horizontal mini channel, d_h = 0.952–1.150 mm	Condensation TP frictional PD
Pham (2019) [84]	R22, R32, R410a R290	Experimental study	Horizontal aluminium multiport rectangular mini channel, d_h = 0.83 mm	Condensation HT and TP frictional PD
Qiu (2015) [85]	R600a	Experimental study	Horizontal smooth copper tube, d_i = 8 mm	Saturation flow boiling HT and adiabatic frictional PD
Sempértegui-Tapia (2017) [86]	R134a R1234ze(E), R1234yf R600a	Experimental study	Horizontal stainless steel tube, d_i = 1.1 mm	Flow boiling HT
Sempértegui-Tapia (2017) [87]	R134a, R1234ze(E) R1234yf, R600a	Experimental study	Horizontal circular/square/triangular stainless steel tube, d_h = 0.634–1.1 mm	TP frictional PD
Shafaee (2016) [88]	R600a	Experimental study	Horizontal copper smooth tube, d_i = 8.1 mm	Flow boiling HT, effect of coiled wire inserted tubes on HT
Shah (2009) [89]	R718 halocarbon Rs HC Rs organics	External experimental database (see [89])	Horizontal/vertical/downward inclined tubes, d_h = 2–49 mm	Condensation HT
Shah (2016) [90]	R718, R744, halocarbon Rs, HC Rs	External experimental database (see [90])	Horizontal round/square/rectangle/semi-circle/triangle/barrel-shaped single- and multi-channels, d_h = 0.1–2.8 mm	Condensation HT
Shah (2017) [91]	R718, R744 R717 halocarbon Rs cryogens HC Rs	External experimental database (see [91])	Horizontal/vertical, round/rectangular/triangular single- and multi-port channels, d_h = 0.38–27.1 mm	Saturated boiling HT prior to critical heat flux
Shah (2017) [92]	R718, R744 cryogens, R12, R113 R22, R134a HC R (R50, R290)	External experimental database (see [92])	Horizontal/vertical tubes, d_h = 0.98–25 mm	Dispersed flow film boiling HT
Shah (2021) [93]	R718, HC Rs, R717, halocarbon Rs	External experimental database (see [93])	PHE, β = 30–75°	Condensation HT
Shah (2022) [94]	R718, R744 halocarbon R, HC, R717 cryogens, chemicals	External experimental database (see [94])	Horizontal/vertical, round/rectangular/triangular single- and multi-port channels, d_h = 0.38–41 mm	Saturated boiling HT
Tao (2019) [95]	HFCs, HC Rs HFOs, R744	External experimental database (see [95])	Brazed/gasketed PHE, β = 25.7–70°, d_h = 3.23–8.08 mm	Condensation HT and frictional PD
Tao (2020) [96]	R717	External experimental database [97]	PHE, β = 63°, d_h = 2.99 mm	Flow patterns, condensation HT and TP frictional PD
Turgut (2016) [98]	R717	External experimental database [28]	Horizontal circular smooth stainless steel tube, d_i = 14 mm	Flow pattern map, flow boiling TP PD

Turgut (2021) [99]	R290	External experimental database (see [99])	Vertical/horizontal smooth stainless steel/copper tubes, d_h = 0.3–7.7 mm	Saturated TP flow boiling HT
Turgut (2022) [100]	R717	External experimental database (see [100])	Horizontal smooth stainless steel tube, d_h = 3–14 mm	Flow boiling HT
	R600a		Horizontal smooth stainless steel tube, d_h = 1.1–8.0 mm	
Umar (2022) [101]	R290	Experimental study	Horizontal stainless steel smooth tube, d_i = 3 mm	TP flow boiling PD
Wang, S. (2014) [102]	R290	Experimental study	Horizontal smooth copper tube, d_i = 6 mm	TP saturated flow boiling HT and frictional PD
Wang, H. (2016) [103]	R717	External experimental database (see [103])	Horizontal/vertical stainless steel/aluminium/carbon steel tube, d_i = 1.224–32 mm	Flow boiling HT
Wen (2018) [104]	R290	Numerical simulation CFD software ANSYS Fluent 16.1	Horizontal circular smooth mini channel, d_h = 1 mm	Condensation HT and frictional PD
Yang (2017) [105]	R600a	Experimental study	Horizontal smooth copper tube, d_i = 6 mm	Flow patterns, flow boiling HT and TP frictional PD
Yuan (2017) [106]	R134a, R22, R717, R744, R236fa, R245fa, R1234ze	External experimental database (see [106])	Horizontal smooth circular stainless steel/aluminium/copper tube, d_i = 0.5–14.0 mm	Annular flow boiling HT
Zhang, Y. (2019) [107]	R290 R600a	External experimental database (see [107])	Horizontal smooth stainless steel/copper tube, d_i = 1–6 mm	Boundary layer theory and flow boiling HT
Zhang, J. (2021) [108]	R134a R236fa, R245fa R1233zd (E) R1234ze(E) R290, R600a	Experimental study	Brazed PHE, β = 65°, d_h = 3.4 mm	Condensation HT and frictional PD
Zhang, J. (2021) [109]	R134a R236fa, R245fa R1233zd (E) R1234ze(E) R290, R600a	Experimental study	Brazed PHE, β = 65°, d_h = 3.4 mm	Flow boiling HT and frictional PD
Zhang, R. (2021) [110]	R717	Experimental study	Horizontal smooth stainless steel tube, d_i = 3 mm	Flow patterns, TP flow boiling HT and frictional PD, dry out phenomenon
Zhang, R. (2022) [111]	R717	Experimental study	Horizontal smooth steel tube, d_i = 3 mm	Flow boiling TP, HT and TP frictional PD, dry out phenomenon

R = refrigerant, TP = two phase, HT = heat transfer, PD = pressure drop, PHE = plate heat exchanger, β = chevron angle, MF = microfin, d_i, d_h, d_o = inner, hydraulic, outer diameter, L_h = heated length, *Ra* = roughness, HC Rs = hydrocarbon refrigerants.

Table 2. Summary of the operating conditions, HTC and PD correlations of the papers included in this review.

First Author/Year	R	ST/SP/VQ	Heat Flux (kW/m²)	Mass Flux (kg/m²s)	Best Reported HTC Correlation/New HTC Correlation	*AAD* (%)	Best Reported PD Correlation/New PD Correlation	*AAD* (%)
Ağra (2012) [6]	R600a	T_{sat} = 30–43 °C – –	–	G = 47–116	$h = \frac{-k\frac{dT}{dy_{y=0}}}{(T_{sat}-T_w)}$ $T_w = tube\ wall\ temperature$	* ±20%	–	–
Ahmadpour (2019) [7]	R600a	– p_{sat} = 510–630 kPa x = 0.04–0.80	–	G = 140–280	Straight tube: Cavallini and Zecchin [112], Shah [113] U-shaped tube: Traviss et al. [114] Shah [89]	* ±20	–	–
Akbar (2021) [8]	R290	T_{sat} = 0–11 °C – x = 0–1	q = 5–20	G = 50–180	Aizuddin et al. [115]	11.6	–	–
Ali (2021) [9]	R1234yf R152a R600a, R134a	T_{sat} = 27, 32 °C – –	–	G = 50–500	–	–	Based on Cavallini et al. [116] $F = \frac{x^{0.9525}(1-x)^{0.414}}{3.25}$	* 71.78% ± 30%
Allymehr (2020) [10]	R290	T_{sat} = 0, 5, 10 °C – x = 0.14–1	q = 15–33	G = 250–500	ST: Liu and Winterton [117] MF1: Rollmann and Spindler [118] MF2: Rollmann and Spindler [118]	6.2 14.8 26.3	ST: Xu and Fang [119] MF1: Diani et al. [120] MF2: Diani et al. [120]	11.7 3 12.7
Allymehr (2021) [11]	R600a	T_{sat} = 5, 10, 20 °C – x = 0.11–1	q = 15–34	G = 200–515	ST: Shah [121] MF: Rollmann and Spindler [118]	6.4 –	ST: Xu and Fang [119] MF: Diani et al. [120]	6.6 –
	R1270				ST: Liu and Winterton [117] MF: no reliable correlation	8.5 –	ST: Xu and Fang [119] MF: Diani et al. [120]	4.4 –
Allymehr (2021) [12]	R290	T_{sat} = 35 °C – x = 0.12–0.89	–	G = 200–500	ST: Dorao and Fernandino [122] MF1: Cavallini et al. [123]	4.9 7.9	ST: Macdonald and Garimella [69] MF: Diani et al. [120]	7.9 –
	R600a				ST: Dorao and Fernandino [122] MF1: Cavallini et al. [123]	5.8 7.8	ST: Xu and Fang [124] MF: Diani et al. [120]	11.0 –
	R1270				ST: Dorao and Fernandino [122] MF1: Cavallini et al. [123]	11.0 13.6	ST: Macdonald and Garimella [69] MF: Diani et al. [120]	6.4 –
Amalfi (2016) [13]	R134a, R245fa, R236fa R717, R290 R600a, R1270, R1234yf mixtures	T_{sat} = −25–39 °C – x = 0–0.95	q = 0.1–50.0	G = 5.5–610	For Bd < 4, $\mathrm{Nu_{tp}} = 982\beta^{*1.101}\mathrm{We}_m^{0.315}\mathrm{Bo}^{0.320}\rho^{*-0.224}$; For Bd >= 4, $\mathrm{Nu_{tp}} = 18.495\beta^{*0.248}\mathrm{Re}_v^{0.135}\mathrm{Re}_{lo}^{0.351}\mathrm{Bd}^{0.235}\mathrm{Bo}^{0.198}\rho^{*-0.223}$	22.1 (all data)	$f_{tp} = 15.698\mathrm{C}\mathrm{We}_m^{-0.475}\mathrm{Bd}^{0.255}\rho^{*-0.571}$ $\mathrm{C} = 2.125\beta^{*9.993} + 0.955$	21.5 (all data)
Anwar (2015) [15]	R600a	T_{sat} = 27, 32 °C – x = 0–0.8	q = 20–130	G = 50–350	Li and Wu [125]	−0.48 (AD)	–	–
Arima (2010) [16]	R717	T_{sat} = 13.9, 17.9, 21.6 °C p_{sat} = 0.7, 0.8, 0.9 x = 0.1–0.4	q = 15, 20, 25	G = 7.5, 10, 15	$\frac{h_{loc}}{h_{lo}} = 16.4\left(\frac{1}{X_{vv}}\right)^{1.08}$ $h_{lo} = 0.023\frac{\lambda_l}{d_h}\left[\frac{G(1-x)d_h}{\mu_l}\right]^{0.8}\mathrm{Pr}_l^{0.4}$	* ±25%	–	–

Asim (2022) [17]	R600a	T_{sat} = 27, 32 °C – –	q = 5–245	G = 50–500	Mahmoud and Karayiannis [126]	14.17	–	–
Ayub (2019) [18]	R717, R134a R410A	– p_{sat} = 0.136–1.445 MPa –	–	–	$\mathrm{Nu} = \left(1.8 + 0.7\ {}^{\beta}/_{\beta_{max}}\right)\mathrm{Re}_{eq}^{\left(0.49-0.3\frac{\sigma_{Ref}}{\sigma_{ammonia}}\right)}\mathrm{Bo}_{eq}^{-0.2}$ $\beta_{max} = 65°$	* ±30% (all data)	–	–
Basaran (2021) [19]	R600a	T_{sat} = 40 °C – x = 0.3–0.9	q = 40	G = 200–600	$\mathrm{Nu} = \frac{HTCd_h}{\lambda_l}$ $\mathrm{Nu} = \begin{cases} 0.2516\mathrm{Re}_{eq}^{0.6860}, for\ \mathrm{Re_{eq}} < 2300 \\ 0.3215\mathrm{Re}_{eq}^{0.6548}, for\ \mathrm{Re_{eq}} > 2300 \end{cases}$	10.22	$f = \Delta p \frac{d_h}{L}\frac{2\rho_{tp}}{G^2}$ $f = \begin{cases} 0.8393\mathrm{Re}_{eq}^{-0.2200}, for\ \mathrm{Re}_{eq} \le 2300 \\ 0.7344\mathrm{Re}_{eq}^{-0.2260}, for\ \mathrm{Re}_{eq} > 2300 \end{cases}$	17.42
Basaran (2021) [20]	R600a	T_{sat} = 0.82056 °C – –	–	G = 200–600	$\mathrm{Nu} = 0.2963\mathrm{Re}_{eq}^{0.6642}$	** 6.8 (p_o)	Sakamatapan and Wongmisses [127]	–
Butrymowicz (2022) [21]	R134a, R507A, R600a	– p_r = 0.501–0.985 x = 0.1–1	q = 0.4–10	G = 60–200	Based on Gungor–Winterton [128], $h = h_{GW}exp[-45.8(1 - \mathrm{Bo_m^{-0.016}})]$ $h_{GW} = h_{conv}\mathrm{E} + h_{pb}\mathrm{S}$ $h_{conv} = 0.023\frac{\lambda}{D_i}\mathrm{Re}_l^{0.80}\mathrm{Pr}^{0.40}$ $h_{pb} = 55\mathrm{p}_r^{0.12}(-log\mathrm{p}_r)^{-0.55}M^{-0.50}q^{0.67}$ $\mathrm{E} = 1 + 24000\mathrm{Bo}^{1.16} + 1.37\mathrm{X}^{-0.86}$ $\mathrm{S} = [1 + 1.15 \times 10^{-6}\mathrm{E}^2\mathrm{Re}_{ri}^{1.17}]^{-1}$	* R^2 = 0.51 (all data)	–	–
Butrymowicz (2022) [22]	R290	$T_{sat,e}$ = 8 °C $T_{sat,c}$ = 34 °C – –	–	G = 50–160	–	–	Based on Müller-Steinhagen [129], $\Delta p = \Delta p_{vo}\beta$ $\beta = \mathrm{C}_f(1 + \zeta)$ Condensation: $\zeta = \frac{64}{0.3164}\frac{\mu_l}{\mu_v^{0.25}}\frac{\rho_v}{\rho_l}(Gd_h)^{-0.75}$ $\mathrm{C}_f = 1.858 + 6.154 \times 10^{-5}\mathrm{Re}_{vo}$	* R^2 = 0.832
							Evaporation: $\mathrm{C}_f = 3.925 + 4.120 \times 10^{-5}\mathrm{Re}_{vo}$	* R^2 = 0.555
Cao (2021) [23]	R600a	– p_{sat} = 530–620 kPa –	–	G = 25–41.25	$h_{tp} = 0.012\mathrm{Re}_l^{0.81}\mathrm{Pr}_l^{1.42}\Phi_l\frac{\lambda_l}{d_h}$ $\phi_l^2 = 1 + \frac{\mathrm{C}}{\mathrm{X}_{tt}} + \frac{1}{\mathrm{X}_{tt}^2}$ $\mathrm{C} = 21(1 - e^{-0.319d_h})$	9.8	$\mathrm{f}_l = 0.35\mathrm{Re}_l^{-0.36}$ $where\ \mathrm{Re}_l < 2000$	7.3
Choi (2009) [24]	R290	T_{sat} = 0, 5, 10 °C – x = 0–1	q = 5–20	G = 50–400	$h = 55\mathrm{p}_r^{0.12}(-0.4343ln\mathrm{p}_r)^{-0.55}M^{-0.5}q^{0.67}$ $\mathrm{F} = MAX(0.5\phi_f, 1)$ $\mathrm{S} = 181.485(\phi_f^2)^{0.002}\mathrm{Bo}^{0.816}$ $\phi_f^2 = 1 + \frac{\mathrm{C}}{\mathrm{X}} + \frac{1}{\mathrm{X}^2}$ $\mathrm{C} = 1732.953\mathrm{Re}_{tp}^{-0.323}\mathrm{We}_{tp}^{-0.24}$	9.93	$\mathrm{C} = \left(\phi_f^2 - 1 - \frac{1}{\mathrm{X}^2}\right)\mathrm{X}$ $= 1732.953\mathrm{Re}_{tp}^{-0.323}\mathrm{We}_{tp}^{-0.24}$	10.84

Choi (2014) [25]	R744 R717 R290 R1234yf	T_{sat} = 0–10 °C – x = 0–1	q = 5–60	G = 50–600	$h_{tp} = Fh_{lo} + Sh_{pb}$ $h_{lo} = 0.023\frac{k_l}{D}\left[\frac{G(1-x)d}{\mu_l}\right]^{0.8}\left(\frac{c_{pl}\mu_l}{k_l}\right)^{0.4}$ $F = Max[(0.007(\varphi_l^2)^{1.15} + 0.95), 1]$ $h_{pb} = 55p_r^{0.12}(-0.4343 ln p_r)^{-0.55}M^{-0.5}q^{0.67}$ $S = C_{ref}(\Phi_f^2)^{0.3421}Bo^{0.0469}$ $C_{ref,R717} = 0.5018$ $C_{ref,R290} = 0.12$	12.28 (all data) 11.09 (R717) 10.02 (R290)	–	–
Cioncolini (2011) [26]	R22, R32, R134a, R290 R600a R718, R12 R236fa R245fa	– p = 0.1–7.2 MPa x = 0.19–0.94	q = 3–736	G = 123–3925	$1 + \alpha_t^+ = \frac{ht}{k_l}Nu = 77.6 \times 10^{-3}t^{+0.90}Pr_l^{0.52}$ $10 \leq t^+ \leq 800; \quad 0.86 \leq Pr_l \leq 6.1$ $t = (1-e)(1-x)\frac{Gd}{4\mu_l}$	13.0 (all data)	–	–
Da Silva (2023) [27]	R600a	T_{sat} = 24 °C p_{sat} = 340.3 kPa x = 0.09–0.98	q = 4.5–18.5	G = 35–170	–	–	Hwang and Kim [130]	7.96 (AD)
Da Silva Lima (2009) [28]	R717	T_{sat} = −14–14 °C – x = 0.05–0.6	q =12–25	G = 50–160	–	–	Moreno Quibén and Thome [131]	9.5
Dalkilic (2010) [29]	R600a	T_{sat} = 30–43 p_{sat} = 4–5.73 bar x = 0.45–0.9	–	G = 75–115	–	–	Chen et al. [132] Mishima and Hibiki [133]	* ±30%
Darzi (2015) [30]	R600a	– – x = 0.1–0.8	q = 17	G = 154.8–265.4	Based on Shah [89], $h_{flat} = 1.3\left(\frac{d}{d_h}\right)^{0.8}\left(\frac{x}{1-x}\right)^{-0.0008(G-205)}h_{shah}$	* 90%±17	Jung and Radermacher [134]	* 80%±25
De Oliveira (2016) [31]	R600a	T_{sat} = 25 °C – x = 0–0.92	q = 5–60	G = 240–480	Kim and Mudawar (2013) [135]	4.4 (AD)	–	–
De Oliveira (2017) [32]	R290	T_{sat} = 25 °C – –	q = 5–60	G = 240–480	–	–	Zhang et al. [136]	21.66 (AD)
	R600a						Mishima and Hibiki [133]	−5.54 (AD)
De Oliveira (2018) [33]	R290	T_{sat} = 25 °C p_{sat} = 952.2 kPa –	q = 5–60	G = 240–480	Li and Wu [125]	−8.5 (AD)	–	–
De Oliveira (2020) [34]	R1270	T_{sat} = 25 °C p_{sat} = 1154.4 kPa x = 0.01–0.99	q = 5–60	G = 240–480	Bertsch et al. [137]	22.8 (AD)	–	–
De Oliveira (2023) [35]	R1270	T_{sat} = 25 °C p_{sat} = 1154.4 kPa –	q = 5–60	G = 240–480	–	–	Hwang and Kim [130]	2.65 (AD)
Del Col (2014) [36]	R290	$T_{sat,aPD,cHT}$ = 40 °C $T_{sat,bHT}$ = 31 °C	$q_{,bHT}$ = 10–315	$G_{,aPD}$ = 200–800 $G_{,cHT}$ = 100–1000	cHT: Moser et al. [138] bHT: Thome et al. [139]	7.22 3.9 (AD)	Del Col et al. [140]	9.1

		– x = 0.05–0.6		$G_{,\mathrm{bHT}}$ = 100–600				
Del Col (2017) [37]	R1270	$T_{sat,\mathrm{aPD,cHT}}$ = 40 °C $T_{sat,\mathrm{bHT}}$ = 30 °C – –	$q_{,\mathrm{bHT}}$ = 10–244	$G_{,\mathrm{aPD}}$ = 400, 600 $G_{,\mathrm{cHT}}$ = 80–1000 $G_{,\mathrm{bHT}}$ = 100–600	cHT: Moser et al. [138] bHT: Sun and Mishima [141]	16.4 8.6	Friedel [142]	7.3
ElFaham (2023) [38]	R290 R600 R600a	T_{sat} = −35–43 °C – x = 0–1	q = 5–315	G = 50–1100	Kew and Cornwell [143]	24.6 (all data)	–	–
Fang, Xiande (2019) [39]	R717 R290 R600a	T_{sat} = 1.06–31 °C p_{sat} = 2.15–11.06 bar x = 0–0.99	q = 5–130	G = 20–600	Fang et al. [144]	4.7 6.5 10.2	–	–
Fang, Xianshi (2023) [40]	R600a	T_{sat} = 38.5 °C – x = 0.05–0.79	–	G = 115–365	–	–	Nualboonrueng et al. [145]: Non-annular flow Annular flow	32.52 10.18
Fries (2019) [42]	R290	– p_{sat} = 12–16 bar –	–	G = 300–400	Thome [146] (for low x) Cavallini and Zecchin [112] (for high x)	– –	Friedel [142]	–
Fries (2020) [43]	R290 R1270	– p_r = 0.25 –	–	G = 300, 450, 600	–	–	Friedel [142]	* ±20% (all data)
Fronk (2016) [44]	R717	T_{sat} = 30–60 °C p_r = 0.10–0.23 –	–	G = 75–225	Annular flow model: $\mathrm{Nu}_a = \frac{hD}{k_l} = 0.023\mathrm{Re}_l^{0.8}\mathrm{Pr}_l^{0.4}\left(1 + 0.27\left(\frac{U_v}{U_l}\right)^{0.21} \mathrm{f}_i^{-0.46}\right)$ $\frac{U_v}{U_l} = \left(\frac{x}{1-x}\right)\left(\frac{\rho_l}{\rho_v}\right)\left(\frac{1-\varepsilon}{\varepsilon}\right)$ $\delta = \frac{1}{2}(D - D_i) = \frac{D}{2}\left(1 - \sqrt{\varepsilon}\right)$ $\varepsilon = \frac{\beta}{1 + \bar{V}_{vj}/j}$ $\bar{V}_{vj} = 0.336\mathrm{X}^{0.25}Ca_l^{0.154}\left(\sqrt{\frac{\rho_l}{\rho_v}} - 1\right)^{0.81} j$ $\mathrm{X} = \sqrt{\frac{(dp/dz)_l}{(dp/dz)_v}}$ $Ca_l = \frac{\mu_l(1-q)G}{\rho_l \sigma}$ $f = \begin{cases} \frac{16}{\mathrm{Re}} & for\ \mathrm{Re} < 2000 \\ 0.079\mathrm{Re}^{-0.25} & for\ \mathrm{Re} \geq 2000 \end{cases}$	12.8	–	–

					Non-annular flow model: $\mathrm{Nu}_{wavy} = \left[\left(1 + 0.741\left[\frac{1-x}{x}\right]^{0.3321}\right)^{-1}\mathrm{Nu}_{film} + \mathrm{Nu}_{pool}\right]$ $\mathrm{Nu}_{film} = \left(\frac{D}{k_l}\right)0.725\left(\frac{k_l^3\rho_l(\rho_l-\rho_v)gh_{lv}}{\mu_l D(T_{sat}-T_{w,i})}\right)^{0.25}$ $\mathrm{Nu}_{pool} = 0.023\mathrm{Re}_l^{0.8}\mathrm{Pr}_l^{0.4}(1-x^{0.087})$			
Gao (2018) [46]	R717	T_{sat} = −15.8–5 °C – –	q = 9–21	G = 50–100	Gungor and Winterton [147]	19.6	Müller-Steinhagen and Heck [129]	16.1
Gao (2019) [47]	R717	T_{sat} = −15.8–4.6 °C – x = 0–0.9	–	G = 20–200	–	–	Based on Müller-Steinhagen and Heck [129], $\nabla p_f = \mathrm{F}(1-x)^{1/3} + \mathrm{B}x^3$ $\mathrm{F} = \mathrm{A} + (1 + 0.007695\mathrm{Bd}^{-0.03573}{\mathrm{Re}_{lo}}^{0.3940})(\mathrm{B} - \mathrm{A})x$ $\mathrm{A} = \left(\frac{dp}{dz}\right)_{lo} = \mathrm{f}_{lo}\frac{2G^2}{\rho_l D}$; $\mathrm{B} = \left(\frac{dp}{dz}\right)_{vo} = \mathrm{f}_{vo}\frac{2G^2}{\rho_v D}$ $If\ \mathrm{Re}_{lo} \le 1187\ \mathrm{f}_{lo} = \frac{16}{\mathrm{Re}_{lo}}$; $If\ \mathrm{Re}_{lo} > 1187\ \mathrm{f}_{lo} = \frac{0.079}{{\mathrm{Re}_{lo}}^{0.25}}$	13.5
Ghazali (2022) [48]	R290	T_{sat} = 5–25 °C – x = 0.4–1	q = 2.5–60	G = 50–500	Based on Mohd-Yunos et al. [75], $h_{tp} = Sh_{nb} + \mathrm{F}h_{lo}$ $h_{nb} = 55\mathrm{p}_\mathrm{r}^{2.12}(-0.4343ln\mathrm{p}_r)^{-0.55}M^{-0.5}q^{0.67}$ $h_{lo} = 0.023\mathrm{Re}_l^{0.8}\mathrm{Pr}_l^{0.4}\frac{k_l}{D}$ $\mathrm{S} = b_1(\phi_f^2)^{b_2}\mathrm{Bo}^{b_3}$ $\mathrm{F} = MAX\left[\left(b_4(\phi_f^2)^{b_5} - b_6\right), 1\right]$ $for\ x \le 1\ \ b_1\ to\ b_6 = 0.176, 0.096, -0.117, 0.1, 0.748, -0.076$	17.02	–	–
Ghorbani (2017) [49]	R600a	T_{sat} = 36.2–45.6 – x = 0.06–0.78	–	G = 110–372	Shah [89]	13 AD	–	–
Guo (2018) [50]	R1234ze(E) R290 R161 R41	T_{sat} = 35–45 °C – x = 0–1	q = 8–30	G = 200–400	Based on Koyama et al. [148], $\phi_v^2 = 1 + 15.6\left(\frac{v_l}{v_v}\right)^{0.17} \times$ $\times\left(1 - e^{-0.6\sqrt{\mathrm{We}_\mathrm{l}^{0.8}\mathrm{Bd}^{0.625}}}\right)\mathrm{X}_{tt} + \mathrm{X}_{tt}^2$	21.6 (R290)	–	–
Huang (2012) [51]	R134a R507a	T_{sat} = 1.9–13 –	q = 1.9–10.8	G = 5.6–52.3	$\mathrm{Nu}_{tp} = 1.87 \times 10^{-3}\left(\frac{qd_0}{k_l T_{sat}}\right)^{0.56}\left(\frac{i_{lg}d_0}{\alpha_l^2}\right)^{0.31}\mathrm{Pr}_l^{0.33}$	7.3 (all data)	–	–

	R12, R717	x_{out} = 0.2–0.95			$d_0 = 0.0146\,\theta\left[\frac{2\sigma}{g(\rho_l-\rho_g)}\right]^{0.5}$ $\theta = 35° \; for \; hydrocarbon \; refrigerants$			
Ilie (2022) [53]	R717	T_{sat} = −9–(−2) °C – x = 0.5	q = 4–7.3	G = 1.8–2.6	Shah [113]	14.23	–	–
Inoue (2018) [54]	R32, R410a, R1234ze(E) R152a	T_{sat} = 35 °C – –	–	G = 100–400	$\mathrm{Nu} = 0.17\sqrt{\mathrm{f}_v}(\phi_v/\mathrm{X}_{tt})(\mu_l/\mu_v)^{0.1}\{x/(1-x)\}^{0.1}\mathrm{Re}_l^{0.87}$ $\mathrm{f}_v = 0.26\mathrm{Re}_v^{-0.38}$	* ±30% (all data) * ±30% R290 External data [65]	–	–
Kanizawa (2016) [55]	R134a R245fa R600a	T_{sat} = 21.5–58.3 °C – x = 0.01–0.93	q = 5–185	G = 49–2200	$h_{tp} = \mathrm{F}h_c + Sh_{nb}$ $h_{nb} = 0.0546\frac{k_l}{d_b}\left[\left(\frac{\rho_v}{\rho_l}\right)^{0.5}\left(\frac{q d_b}{k_l T_{sat}}\right)\right]^{0.670}\left(\frac{\rho_l-\rho_v}{\rho_l}\right)^{-4.33}$ $\times\left(i_{lv}d_b^2\left(\frac{\rho_l c_{pl}}{k_l}\right)^2\right)^{0.248}$ $d_b = 0.51\sqrt{2\sigma/[g(\rho_l-\rho_v)]}$ $h_c = 0.023\frac{k_l}{d}\mathrm{Re}_l^{0.8}\mathrm{Pr}_l^{1/3}$ $\mathrm{F} = 1 + \frac{2.50\mathrm{X}^{-1.32}}{1+\mathrm{We}_{u_v}^{0.24}}$ $\mathrm{S} = \frac{1.06\mathrm{Bd}^{-8.10^{-3}}}{1+0.12(\mathrm{Re}_{2p,mod}/10000)^{0.86}}$	11 (all data) No good agreement (R600a)	–	–
Khan, T.S. (2012) [56]	R717	T_{sat} = −25–(−2)°C – x_{out} = 0.5–0.9	q = 21–44	G = 8.5–27	$\mathrm{Nu}_{tp} = 82.5(\mathrm{Re}_{eq}\mathrm{Bo}_{eq})^{-0.085}(\mathrm{p}_r)^{0.21}$	* 75% ± 4%	$\mathrm{f}_{tp} = 212(\mathrm{Re}_{eq})^{-0.51}(\mathrm{p}_r)^{0.53}$	* 90% ± 5%
Khan, M.S. (2012) [57]	R717	T_{sat} = −25–(−2) °C – x_{out} = 0.5–0.9	q = 21–44	G = 5.5	$\mathrm{Nu}_{tp} = 169(\mathrm{Re}_{eq}\mathrm{Bo}_{eq})^{-0.04}(\mathrm{p}_r)^{0.52}$	* 70% ± 4%	$\mathrm{f}_{tp} = 673{,}336(\mathrm{Re}_{eq})^{-1.3}(\mathrm{p}_r)^{0.9}$	* 90% ± 7%
Koyama (2014) [58]	R717	– p_{sat} = 0.7, 0.9 MPa –	q = 10, 15, 20	G = 5–7.5	For δ = 1 mm, $\frac{h}{h_{liq}} = 52.2\left(\frac{1}{\mathrm{X}_{vv}}\right)^{0.90}$ $h_{liq} = 0.023\left(\frac{k_l}{D_h}\right)\left[\frac{G(1-x)D_h}{\mu_l}\right]^{0.8}\mathrm{Pr}_l^{0.4}$	* 85% ± 30%	–	–
					For δ = 2 and 5 mm, $\frac{h}{h_{liq}} = 48.6\left(\frac{1}{\mathrm{X}_{vv}}\right)^{0.79}$	* 88% ± 30%		
Lee (2010) [59]	R290	T_{sat} = 40 °C – x = 0–0.9	–	G = 35.5–178.8	Haraguchi et al. [149]	13.75	–	–
	R600a					6.57		

Lillo (2018) [60]	R290	T_{sat} = 25–35 °C – x = 0–1	q = 2.5–40.0	G = 150–500	Based on Wojtan et al. [150], $h_{wet} = (h_{cb}^3 + h_{nb}^3)^{1/3}$ $h_{cb} = 0.0133\mathrm{Re}_\delta^{0.69}\mathrm{Pr}_l^{0.4}\frac{\lambda_l}{\delta}$ $h_{nb} = 0.8h_{Cooper}$ $h_{cb,new} = 0.5h_{cb}$ $h_{nb,new} = 1.7h_{nb}$	8.2	Friedel [142]	20.8
Liu (2016) [61]	R290	T_{sat} = 40, 50 °C p_{sat} = 1.37–1.71 MPa x = 0.1–0.9	–	G = 200–500	Kim et al. [151]	13	Kim and Mudawar [152]	±30%
Liu (2018) [62]	R600a R227ea, R245fa	T_{sat} = 27.5–45.5 °C – x = 0–0.8	q = 3.60–10.50	G = 32.20–116.8	$h_{tp} = a\mathrm{Bo}^b\mathrm{Fr}_{lo}^c\mathrm{Bd}^d\left(\frac{\rho_l}{\rho_v}\right)^e\frac{k_l}{D_h}$ a = 17022, b = 0.939, c = 0.347, d = 0.581, e = 0.23	14.93 (all data) 17.09 (R600a)	–	–
Longo (2012) [63]	R600a R290 R1270	T_{sat} = 9.8–20.2 °C – x = 0.21–1	q = 4.3–19.6	G = 6.6–23.9	Cooper [153] Gorenflo [154] Gorenflo [154]	17.2 16.2 27.1	$\Delta p_f(kPa) = 1.525\,KE/V\,(Jm^{-3})$ $KE/V = G^2/(2\rho_m)$ $KE/V = Kinetic\ energy\ per\ unit\ volum$	8.8 (all data)
Longo (2017) [64]	R290 R1270	T_{sat} = 30, 35, 40 °C p_{sat} = 1.075–1.650 MPa x = 0.12–0.95	–	G = 75–400	Akers et al. [155]	9.0 13.0	Friedel [142]	14.5 12.4
Longo (2020) [65]	R600a	T_{sat} = 5–20 °C p_{sat} = 1.195–3.045 bar x = 0.08–0.75	q = 15–30	G = 100–300	Fang et al. [144]	6.2	Wang et al. [156]	15.49
Longo (2023) [66]	R290 R1270	T_{sat} = 9.9–10.4 °C p_{sat} = 0.63–0.79 MPa x = 0.24–1	q = 2.9–28.3	G = 5.0–17.8	Longo et al. [157]	7.7 6.9	–	–
López-Belchí (2016) [67]	R290	T_{sat} = 30, 40, 50 °C p_{sat} = 1.08–1.71 MPa –	q = 15.76–32.25	G = 175–350	Koyama et al. [158]	18.44	Sun and Mishima [159]	6.88
Macdonald (2016) [68]	R290	T_{sat} = 30–94 °C – –	–	G = 150–450	Cavallini et al. [160]	24	Garimella et al. [161]	26
Macdonald (2016) [69]	R290	T_{sat} = 30–94 °C – –	–	G = 150–450	$h_{adjusted} = h_{condensation}\mathrm{X}_{LM}$ $h_{condensation} = \frac{h_{film}\theta + h_{pool}(2\pi - \theta)}{2\pi}$	11	$\frac{dp}{dz} = \left(\frac{dp}{dz}\right)_l + \mathrm{C}\left[\left(\frac{dp}{dz}\right)_l\left(\frac{dp}{dz}\right)_v\right]^{0.5}$ $\left.\frac{dp}{dz}\right\vert_l = \frac{1}{2}\frac{\mathrm{f}_l\rho_l v_l^2}{d_h}\ where\!: v_l = \frac{G(1-x)}{\rho_l}$	18

					$X_{LM} = \left(\left(\frac{k_{l,wall-subcool}}{k_{l,sat}}\right)^2 - 0.3\right)\frac{1}{p_r^{0.1}}$		$\left.\frac{dp}{dz}\right\|_v = \frac{1}{2}\frac{f_v \rho_v v_v^2}{d_h}\ where: v_v = \frac{G(1-x)}{\rho_v}$ $C = 20Re^{-0.15}S_r^{1.15}Bd^{-0.2}$ $S_r = v_v/v_l$	
Macdonald (2017) [70]	R290	T_{sat} = 30–75 °C p_r = 0.25–0.67 –	–	G = 150–450	Based on Macdonald and Garimella [69], $h_{corrected} = h_{correlation}\chi_{\Delta T}$ $\chi_{\Delta T} = \left(\left(\frac{k_{l,wall-subcool}}{k_{l,sat}}\right)^2 - 0.3\right)\frac{1}{p_r^{0.1}}$	5.4	–	–
Maher (2020) [71]	R134a R245fa R125, R744 R236ea, R22, R152a R32, R410a R1234ze(E) R290, R600a R1234yf	T_{sat} = 25–55 °C – –	–	G = 35.5–2094	–	–	$\left(\frac{\Delta p}{\Delta L}\right)_{tp} = \frac{G_{tp}^2}{2D\rho_{tp}}\left(0.79Re_{tp}^{-0.25}\right)^{1.4} +$ $+\left[0.17\left(0.69 ln Re_{tp} - 2.2\right)^{-1.5}\right]^{1/0.7}$ $Re_{tp} = \frac{G_{tp}D}{[(1-x)\mu_l + x\mu_v]^{0.94}\left(\frac{1-x}{\mu_l} + \frac{x}{\mu_v}\right)^{1-0.9}}$	30 (all data)
Maqbool (2012) [72]	R717	T_{sat} = 23, 33, 43 °C – –	q = 15–355	G = 100–500	–	–	Based on Tran et al. [162], $\left(\frac{dp}{dz}\right)_f = \left(\frac{dp}{dz}\right)_{Lo}\Phi_{LO}^2$ $\Phi_{LO}^2 = 1 + (4.3Y^2 - 1)[0.2Co^{1.2}x^{0.875} \times$ $\times (1-x)^{0.875} + x^{1.75}]$ $Y^2 = \frac{\left(\frac{dp}{dz}\right)_{VO}}{\left(\frac{dp}{dz}\right)_{LO}}$	16
Maqbool (2012) [73]	R717	T_{sat} = 23, 33, 43 °C – –	q = 15–355	G = 100–500	Cooper [163]	20	–	–
Maqbool (2013) [74]	R290	T_{sat} = 23, 33, 43 °C – –	q = 5–280	G = 100–500	Cooper [164]	18	Müller-Steinhagen and Heck [129]	17
Mohd-Yunos (2020) [75]	R290	T_{sat} = −35–25 °C – –	q = 5–190	G = 63.9–480	Based on Choi et al. [25], $h_{tp} = Sh_{nb} + Fh_{lo}$ $Case\ I: for\ 0.0 < x < 1.0$ $S = 2\left(\phi_f^2\right)^{-0.073}Bo^{0.128}$ $F = MAX\left[\left(1.074\left(\phi_f^2\right)^{0.178} - 0.38\right), 1\right]$ $Case\ II: for\ 0 < x \le 0.6$ $S = 0.8\left(\phi_f^2\right)^{0.124}Bo^{0.093}$ $F = MAX\left[\left(1.226\left(\phi_f^2\right)^{0.107} - 0.28\right), 1\right]$ $for\ 0.6 < x < 1.0$ $S = 1.989\left(\phi_f^2\right)^{-0.867}Bo^{-0.322}$	33.16 25.26	–	–

					$F = MAX\left[\left(1.534\left(\phi_f^2\right)^{-0.293} + 0.754\right), 1\right]$			
Moreira (2021) [76]	R134a R600a R290 R1270	T_{sat} = 35 °C – x = 0–1	q = 5–60	G = 50–250	$h_{tp} = \mathrm{Nu}\,\frac{\lambda_l}{d}$ $\mathrm{Nu} = J_h \mathrm{Pr}_l^{1/3}$ $J_h = \begin{cases} 0.0053\,\mathrm{Re}_{eq} & \mathrm{Re}_{eq} \geq 25{,}000 \\ 0.79\,\mathrm{Re}_{eq}^{0.51} & \mathrm{Re}_{eq} < 25{,}000 \end{cases}$	–	–	–
Morrow (2021) [77]	R717 R290 R600a	T_{sat} = 24–60 °C – x = 0–1	–	G = 20–800	Shah [90] Kim [151] Shah [165]	41 14 15	–	–
Murphy (2019) [78]	R290	T_{sat} = 47, 74 °C p_{sat} = 1.6, 2.8 MPa x = 0.1–0.9	–	G = 75–150	$\mathrm{Nu} = 0.0841\,\frac{\mathrm{Pr}_l \mathrm{Re}_l^{1.329}}{T^+}\,F^{1.263}$ $F = \left(\frac{f_v}{8}\right)^{0.5}\left(\frac{x}{1-x}\right)^{0.5}\left(1 - 2.85X^{0.523}\right)$ $T^+ = \begin{cases} .707\mathrm{Pr}_l \mathrm{Re}_l^{0.5} & \mathrm{Re}_l < 50 \\ 5\mathrm{Pr}_l + 5ln\left[1 + \mathrm{Pr}_l\left(0.09636\mathrm{Re}_l^{0.585} - 1\right)\right] & 50 < \mathrm{Re}_l < 1125 \\ 5\mathrm{Pr}_l + 5ln\left(1 + 5\mathrm{Pr}_l\right) + 2.5ln\left(0.00313\mathrm{Re}_l^{0.812}\right) & \mathrm{Re}_l > 1125 \end{cases}$	13.4	$\left(\frac{dp}{dz}\right)_f = \frac{1}{2} f_{int}\,\frac{(Gx)^2}{\rho_v \alpha^{2.5}}\,\frac{1}{D}$ $\frac{f_{int}}{f_l} = 0.0019X^{0.6}\mathrm{Re}_{l,actual}^{0.930}\varphi^{-0.121}$	12
Nasr (2015) [79]	R600a	– p_{avg} = 5–6 bar x = 0–0.7	q = 10–27	G = 130–380	Gungor-Winterton [128]	12.23	–	–
Oh (2011) [80]	R22, R134a, R410A, R290, R744	T_{sat} = 0–15 °C – x = 0–1	q = 5–40	G = 50–600	$h_{tp} = Sh_{nbc} + Fh_l$ $S = 0.279\left(\phi_f^2\right)^{-0.029}\mathrm{Bo}^{-0.098}$ $F = MAX\left[\left(0.023\phi_f^{2.2} + 0.76\right), 1\right]$ $h_{nbc} = 55\mathrm{p}_r^{2.12}\left(-0.4343ln\mathrm{p}_r\right)^{-0.55}M^{-0.5}q^{0.67}$ $h_l = \begin{cases} = 4.36\,\frac{k_l}{D} & if\ \mathrm{Re}_l < 2300 \\ = \frac{(\mathrm{Re}_l - 1000)\mathrm{Pr}_l\left(\frac{f_l}{2}\right)\left(\frac{k_l}{D}\right)}{1 + 12.7\left(\mathrm{Pr}_l^{2/3} - 1\right)\left(\frac{F_f}{2}\right)^{0.5}} & if\ 3000 \leq \mathrm{Re}_l \leq 10^4 \\ = \frac{\mathrm{Re}_l \mathrm{Pr}_l\left(\frac{f_l}{2}\right)\left(\frac{k_l}{D}\right)}{1 + 12.7\left(\mathrm{Pr}_l^{2/3} - 1\right)\left(\frac{F_f}{2}\right)^{0.5}} & if\ 10^4 \leq \mathrm{Re}_l \leq\times 10^6 \\ = 0.023\,\frac{k_l}{D}\left[\frac{G(1-x)D}{\mu_l}\right]^{0.8}\left(\frac{C_{pl}\mu_l}{k_l}\right)^{0.4} & \mathrm{Re}_l \leq\times 10^6 \end{cases}$	15.28 (all data)	–	–
Pamitran (2009) [81]	R290	T_{sat} = 0, 5, 10 °C – x = 0–1	q = 5–20	G = 50–400	$h_{tp} = Sh_{nbc} + Fh_{lo}$ $S = 0.6226\left(\phi_f^2\right)^{0.1068}\mathrm{Bo}^{0.0777}$ $h_{nbc} = 55\mathrm{p}_r^{0.12}\left(-0.4343ln\mathrm{p}_r\right)^{-0.55}M^{-0.5}q^{0.67}$ $F = 0.023\phi_f^2 + 0.977$ $h_{lo} = 0.023\,\frac{\lambda_l}{D}\left[\frac{G(1-x)D}{\mu_l}\right]^{0.8}\left(\frac{C_{pl}\mu_l}{k_l}\right)^{0.4}$ $\phi_f^2 = 1 + \frac{C}{X} + \frac{1}{X^2}$ $C(tt) = 20, C(vt) = 12, C(tv) = 10, C(vv) = 5$	8.27	–	–
Pamitran (2011) [82]	R290 R717	T_{sat} = 0–10 °C –	q = 5–70	G = 50–600	$h_{tp} = Fh_{lo} + Sh_{pb}$	19.81 (all data)	–	–

	R744	x = 0–1			$h_{lo} = 0.023\frac{k_l}{D}\left[\frac{G(1-x)D}{\mu_l}\right]^{0.8}\left(\frac{c_{pl}\mu_l}{k_l}\right)^{0.4}$ $F = Max[(0.009(\varphi_l^2)^2 + 0.76), 1]$ $h_{pb} = 55p_r^{0.12}(-0.4343 ln p_r)^{-0.55}M^{-0.5}q^{0.67}$ $S = C_{ref}(\phi_f^2)^{-0.2093}Bo^{0.7402}$ $C_{ref,R717} = 0.45\ C_{ref,R290} = 0.38$	17.94 (R290) 22.52 (R717)		
Patel (2018) [83]	R290, R22 R1234yf, R1234ze, R410a, R32	T_{sat} = 30–50 °C – x = 0.1–0.9	–	G = 150–800	–	–	$\phi_{New}^2 = 1 + \frac{C}{X} + \frac{1}{X^2}$ $C_{New} = 0.3572Re_{lo}^{0.05021}Su_{vo}^{0.099}F^{0.025}H^{0.015}$ $Su_{vo}^c = \frac{\rho_v \sigma d_h}{\mu_v^2}$, $\left(\frac{dp}{dz}\right)_{tp} = \left(\frac{dp}{dz}\right)_l \phi_l^2$	10.08
Pham (2019) [84]	R22, R32, R410a, R290	T_{sat} = 48 °C – x = 0.1–0.9	q = 3–15	G = 50–500	$h = 2.76Bo^{0.053}Re_{eq}^{0.528}\left(\frac{1-x}{Pr_l}\right)^{-0.386}\left((1-x)^{0.8} + \frac{x}{p_r}\right)^{-0.76}\left(\frac{g}{Gh_{lv}}\frac{A_o}{A_i}\right)^{0.305}\left(\frac{\Phi_v}{X_{tt}}\right)^{-0.045}\frac{k_l}{d}$ $\phi_v^2 = 1 + CX_{tt} + X_{tt}^2$ $C = \lambda x^{0.35}(1-x)^{0.25}\left(\frac{p}{p_c}\right)^{0.31}Re_{tp}^{0.09}We_{tp}^{0.09}$ $\lambda = 24(1 - 1.355\beta + 1.947\beta^2 - 1.701\beta^3 + 0.956\beta^4 - 0.254\beta^5)$	18.14	–	–
Qiu (2015) [85]	R600a	T_{sat} = 20 °C – x = 0.05–0.85	q = 5–10	G = 200–400	Shah [121]	21.75	Groennerud [166]	19.07 (G=400) 28.55 (G=200)
Sempértegui-Tapia (2017) [86]	R134a R1234ze(E), R1234yf R600a	T_{sat} = 31, 41 °C – x = 0–0.93	q = 15–145	G = 200–800	Based on Kanizawa et al. [55], $h_{tp} = [(Fh_l)^2 + (Sh_{nb})^2]^{0.5}$ h_l *according to Dittus and Boelter*, h_{nb} *according to Stephan and Abdelsalam* $F = 1 + \frac{2.55X_{tx}^{-1.04}}{(1 + We_{uG}^{-0.194})}$ $S = \frac{1.427Bd^{0.032}}{1 + 0.1086(10^{-4}Re_l F^{1.25})^{0.981}}$	11.4 (all data) 14.0 (R600a)	–	–
Sempértegui-Tapia (2017) [87]	R134a, R1234ze(E) R1234yf R600a	T_{sat} = 31,41 °C – x = 0.05–0.95	–	G = 100–1600	–	–	Based on Müller-Steinhagen and Heck [129] $\left(\frac{dp}{dz}\right)_{tp} = F(1-x)^{1/\lambda} + \left(\frac{dp}{dz}\right)_{vo}x^{\lambda}$ $F = \left(\frac{dp}{dz}\right)_{lo} + \omega\left(\left(\frac{dp}{dz}\right)_{vo} - \left(\frac{dp}{dz}\right)_{lo}\right)x$ $\omega = 3.01e^{-0.00464Re_{vo}/1000}$; $\lambda = 2.31$ $D_{eq} = \sqrt{\frac{4A}{\pi}}$; $\left(\frac{dp}{dz}\right)_{ko} = 2f_{ko}\frac{G^2}{D_{eq}\rho_k}$	10.2 (all data) 9.3 (R600a) 7.2 (R290, external data [36])

							$f_{ko} = \frac{16}{\mathrm{Re}_{ko}}\ laminar\ flow, circular\ channel$	
Shafaee (2016) [88]	R600a	– p_{avg} = 4–6 bar x = 0.08–0.7	q = 18.6–26.1	G = 109.2–505	Shah [121]	15	–	–
Shah (2009) [89]	R718 halocarbon Rs HC Rs organics	– p_r = 0.0008–0.9 x = 0.01–0.99	–	G = 4–820	$h_I = h_{lo}\left(\frac{\mu_l}{14\mu_g}\right)^n\left[(1-x)^{0.8} + \frac{3.8x^{0.76}(1-x)^{0.04}}{\mathrm{p}_r^{0.38}}\right]$ $h_{lo} = 0.023\mathrm{Re}_{lo}^{0.8}\mathrm{Pr}_l^{0.4}$ $n = 0.0058 + 0.557\mathrm{p}_r$ $h_{Nu} = 1.32\mathrm{Re}_l^{-1/3}\left[\frac{\rho_l(\rho_l-\rho_g)gk_l^3}{\mu_l^2}\right]^{1/3}$ Boundary between Regime I and II: $\mathrm{J}_g \geq 0.98(\mathrm{Z}+0.263)^{-0.62}$ $h_{tp} = \begin{cases} h_{tp} = h_I & in\ Regime\ I \\ h_{tp} = h_I + h_{Nu} & in\ Regime\ II \\ h_{tp} = h_{Nu} & vertical\ tubes\ in\ Regime\ III \end{cases}$	14.4 (all data) 11.2,13.7 (R600a) 16.4,15.210.5,20.5 (R290) 17.2,32.6 (R1270)	–	–
Shah (2016) [90]	R718, R744, halocarbon Rs, HC Rs	– p_r = 0.0055–0.94 x = 0.02–0.99	–	G = 20–1400	$h_I = h_{lo}\left[1 + 1.128x^{0.817}\left(\frac{\rho_l}{\rho_v}\right)^{0.3685}\left(\frac{\mu_l}{\mu_v}\right)^{0.2363}\times\left(1-\frac{\mu_v}{\mu_l}\right)^{2.144}\mathrm{Pr}_l^{-0.1}\right]$ $h_{lo} = 0.023\mathrm{Re}_{lo}^{0.8}\mathrm{Pr}_l^{0.4}\ k_l/D$	15.5 (all data) 21.3 (R290)	–	–
Shah (2017) [91]	R718 R744 R717 halocarbon Rs cryogens HC Rs	– p_r = 0.0046– 0.787 –	–	G = 15–2437	$h_{tp} = \mathrm{F}h_{Shah}$ $\mathrm{F} = h_{tp}/h_{Shah} = (2.1 - 0.008\ \mathrm{We}_{GT} - 110\mathrm{Bo}) \geq 1$ *For horizontal channels with* $\mathrm{Fr}_l < 0.01, \mathrm{F} = 1$	18.6 (all data) 21.6 (R717) 9.2 (R290) 11.4,40.1 (R600a)	–	–
Shah (2017) [92]	R718, R744 cryogens, R12, R113 R22, R134a HC Rs (R50, R290)	– p_r = 0.0046–0.99 –	–	G = 3.7–5176	$h_{tp} = q/(T_w - T_{sat})$ $q = h_v\mathrm{F}_{dc}(T_w - T_v)$ $\begin{cases} For\ \mathrm{p}_r > 0.8, & \mathrm{F}_{dc} = 2.64\mathrm{p}_r - 1.11 \\ For\ \mathrm{p}_r \leq 0.8, & \mathrm{F}_{dc} = 1 \end{cases}$	19.4 (all data) 28.3 (R290)	–	–
Shah (2021) [93]	R718, HC Rs, R717, halocarbon Rs	– p_r = 0.0083–0.8 x = 0–1	q = 2.5–93.5	G = 2.3–165	Based on Longo et al. [167], $h_{grav} = 1.32\phi\mathrm{Re}_{lo}^{-1/3}\left[\frac{\rho_l(\rho_l-\rho_g)gk_l^3}{\mu_l^2}\right]^{1/3}$ $h_{fc} = 1.875\phi\mathrm{Re}_{eq}^{0.445}\mathrm{Pr}_l^{1/3}k_l$ $\begin{cases} for\ \mathrm{Re}_{eq} < 1600, h_{tp} = larger\ of\ h_{grav}\ and\ h_{fc} \\ for\ \mathrm{Re}_{eq} \geq 1600, h_{tp} = h_{fc} \end{cases}$	20.9 (all data) 16.6,23.6 (R717) 13.5,17.4 (R600a) 6.5,11.0,25.8 (R290) 13.8 (R1270)	–	–

Shah (2022) [94]	R718, R744 halocarbon Rs, HC Rs, R717 cryogens, chemicals	– p_r = 0.0046–0.787 –	–	*G* = 15–2437	$h_{tp} = F_{st}\psi h_l$ $\psi = h_{tp}/h_l$ $h_{lo} = 0.023\left(\frac{G(1-x)d}{\mu_l}\right)^{0.8} Pr_l^{0.4}\left(\frac{\lambda_l}{d}\right)$ $\psi_{cb} = 2/J^{0.8}$ $\psi_{bs} = \psi_0\left(1+\frac{0.16}{J^{0.87}}\right)$ $\psi_0 = 1 + 560Bo^{0.65}$ $F_{st} = (2.1 - 0.008We_v - 110Bo) \geq 1$	18.8 (all data) 18.2 (HC Rs)	–	–
Tao (2019) [95]	HFCs HC Rs HFOs R744	T_{sat} = −34.4–72.1 °C p_{sat} = 1.0–24.2 *x* = 0–1	*q* = 2.5–66.5	*G* = 2–150	Longo et al. [167]	25.5 (all data)	$f_{TP} = (4.207 - 2.673\beta^{-0.46}) \times$ $\times\,(4200 - 5.41Bd^{1.2})Re_{eq}^{-0.95}\left(\frac{p_{sat}}{p_{cr}}\right)^{0.3}$	31.2 (all data)
Tao (2020) [96]	R717	– p_{sat} = 630–930 kPa *x* = 0.05–0.65	–	*G* = 21–78	$h_{gc} = 0.36Co^{-0.28}\left[\frac{g\rho_l(\rho_l-\rho_g)\Delta h_{lg}\lambda_l^3}{\mu_l \Delta T d_h}\right]^{0.25} Pr_l^{0.333}$	7.4	$\Delta P_{TP} = \Delta P_L + 2\sqrt{\Delta P_L \Delta P_G} + x\Delta P_G$ $\Delta P_L = f_L\frac{G_L^2}{2\rho_l}\frac{L_p}{d_h} = f_L\frac{G^2(1-x)^2}{2\rho_l}\frac{L_p}{d_h}$ $\Delta P_L = f_G\frac{G_G^2}{2\rho_g}\frac{L_p}{d_h} = f_G\frac{G^2x^2}{2\rho_g}\frac{L_p}{d_h}$	14.6
Turgut (2016) [98]	R717	T_{sat} = −14–14 °C *x* = 0.1–0.6 –	*q* = 12–25	*G* = 50–160	–	–	Gronnerud [168]	13.9
Turgut (2021) [99]	R290	T_{sat} = −35–43 °C – *x* = 0.01–0.99	*q* = 2.5–227.0	*G* = 50–600	Based on Wattelet et al. [169], $X_{tt} = \left(\frac{1-x}{x}\right)^{C_1}\left(\frac{\rho_v}{\rho_l}\right)^{C_2}\left(\frac{\mu_l}{\mu_v}\right)^{C_3}$ $F = 1 + C_4X_{tt}^{C_5}$ $h_{nb} = C_6p_r^{C_7}(-log(p_r))^{C_8}M^{C_9}Q^{C_{10}}$ $h_{cb} = C_{11}Re_l^{C_{12}}Pr_l^{C_{13}}(k_l/D_h)$ $h_{tp} = \left(h_{nb}^{C_{14}} + (Fh_{cb})^{C_{14}}\right)^{1/C_{14}}$ *C_1 to C_{14} reported in the article* [99]	19.1	–	–
Turgut (2022) [100]	R600a	T_{sat} = −34.4– 43 °C *x* = 0.01– 0.96	*q* = 5–240	*G* = 16.3–500	$h_{tp} = (h_{nb}^{4.1684} + (Fh_{cb})^{6.8901})^{1/4.3074}$ $h_{nb} = 7.4756p_r^{0.9797}(-ln(p_r))^{1.9161}M^{0.2722}q^{0.6351}$ $F = 1 + 4.9531X_{tt}^{-0.991}$ $X_{tt} = \left(\frac{1-x}{x}\right)^{0.6171}\left(\frac{\rho_v}{\rho_l}\right)^{0.3111}\left(\frac{\mu_v}{\mu_l}\right)^{0.2527}$ $h_{cb} = 0.0058Re_l^{0.5758}Pr_l^{0.2523}(k_l/D_h)$	17.3	–	–
	R717	T_{sat} = 6–40 °C – *x* = 0.01– 0.94	*q* = 5–140	*G* = =49–2200	$h_{tp} = 0.6177M^{0.3111}Bo^{0.2527}Fr_l^{4.9531}Bd^{-0.991}\left(\frac{\mu_l}{\mu_v}\right)^{7.4756}$ $\times\times\left(\frac{\rho_v}{\rho_l}\right)^{0.9797} Y\left(\frac{k_l}{D_h}\right)$ $Y = \begin{cases} 0.2722 & if\ p_r < 1.9161 \\ 0.6351 - p_r^{0.0058} & otherwise \end{cases}$	12.4		
Umar (2022) [101]	R290	T_{sat} = 8.7–10.8 °C	*q* = 5–20	*G* = 50–180	–	–	Li and Hibiki [170]	19.47

		– x = 0.1–0.9						
Wang, S. (2014) [102]	R290	T_{sat} = −35–(−1.9) °C – –	q = 11.7–87.1	G = 62–104	Liu and Winterton [117]	7.5	Müller-Steinhagen and Heck [129]	17.0
Wang, H. (2016) [103]	R717	– p_{sat} = 0.19–1.6 x = 0.002–0.997	q = 2.0–240	G = 10–600	Kandlikar [171] Stephan [172]	40.9 40.9	–	–
Wen (2018) [104]	R290	T_{sat} = 40 °C p_{sat} = 1.37 MPa –	–	G = 400–800	Thome et al. (2003) [146]	7.27	Friedel [142]	7.59
Yang (2017) [105]	R600a	– p_{sat} = 0.215–0.415 MPa –	q = 10.6–75.0	G = 67–194	Liu and Winterton [117]	11.5	Based on Müller-Steinhagen and Heck [129], $\Delta p_{frict} = \left\{[a+2(b-a)x](1-x)^{1/3}+bx^{3}\right\} \times \left[0.2875 + 0.0534(1-x)^{-0.1208}\mathrm{We}_{tp}^{0.423}\left(log_{10}\mathrm{Fr}_{tp}\right)^{-0.5222}\right]$ $a = \mathrm{f}_l \frac{G^2}{2d\rho_l}, b = \mathrm{f}_v \frac{G^2}{2d\rho_v}$ $If\ \mathrm{Re}_l and\ \mathrm{Re}_v \le 1187, \mathrm{f}_l = \frac{64}{\mathrm{Re}_l}, \mathrm{f}_v =$ $If\ \mathrm{Re}_l and\ \mathrm{Re}_v > 1187, \mathrm{f}_l = \frac{0.3164}{\mathrm{Re}_l^{1/4}}, \mathrm{f}_v =$	16.6
Yuan (2017) [106]	R134a, R22, R717, R744 R236fa, R245fa R1234ze	– p_r = 0.01–0.77 x = 0.10–0.98	q = 3–240	G = 50–1290	$h_{tp} = [h_{cv}^2 + h_{nb}^2]^{1/2}$ $h_{cv} = 7.0 \times 10^{-3} t^{+1.00}\mathrm{Re}_v^{0.14}\mathrm{Pr}_l^{0.80}\frac{k_l}{t}$ $h_{nb} = 0.69\ h_{nb,Shekriladze}$ $h_{nb,Shekriladze} = 0.0122 \times \frac{k_l}{r_0}\left(\frac{[p(\rho_v{}^{-1}-\rho_l{}^{-1})]^{0.5}\sigma c_l \rho_l^2 T_{sat}}{\mu_l h_{lv}^2 \rho_v^2}\right)^{0.25}\left(\frac{r_0^2\rho_v h_{lg} q}{\sigma k_l T_{sat}}\right)^{0.7}$ $t^+ = \frac{1}{\sqrt{2}}\mathrm{Re}_{lf} \quad for \quad \mathrm{Re}_{lf} \le 162$ $t^+ = 0.6246\,\mathrm{Re}_{lf}^{0.5244} \quad for \quad 162 \le \mathrm{Re}_{lf} \le 2785$ $t^+ = 0.03221\,\mathrm{Re}_{lf}^{0.8982} \quad for \quad \mathrm{Re}_{lf} \ge 2785$	13.7 (all data) 12.9 (R717)	–	–
Zhang, Y. (2019) [107]	R290 R600a	T_{sat} = −35–40 °C – x = 0–0.99	q = 5–135	G = 50–500	$h_{tp} = [(\mathrm{f}_{cb}h_{cb})^2 + (\mathrm{f}_{nb}h_{nb})^2]^{0.5}$ $h_{cb} = 0.023\mathrm{Re}_{lo}^{0.8}\mathrm{Pr}_l^{0.4}\,\lambda_l/D$ $h_{nb} = 55\mathrm{p}_r^{0.12-0.2logRa}(-log\mathrm{p}_r)^{-0.55}M^{-0.5}q^{2/3}$ $\mathrm{f}_{nb} = \frac{a_1\mathrm{Cn}^{a_5}}{1+a_2 2\mathrm{Re}_l^{a_3}\mathrm{f}_{cb}^{a_4}}(1+a_6\mathrm{Rtd}^{a_7}\mathrm{Pr}_l^{a_8}\mathrm{We}_{l,b}^{a_9}$	−3.6 (AD all data)	–	–

					$\mathrm{Rtd} = \frac{\lvert 1-\mathrm{Pr}_l^{-0.4}\rvert}{\mathrm{CnRe}_l^{0.5}}$ $\mathrm{f}_{cb} = b_1\{1+b_2\mathrm{X}_{tt}^{b_3}[1+b_4(1-\mathrm{Pr}_l^{-0.4})^{b_5}\mathrm{Pr}_l^{b_6}\mathrm{We}_v^{b_7}\mathrm{Bo}^{b_8}]\}^{b_9}$ $a_1\,to\,a_9 = 1.758, 0.596, 0.133, 0.1, -0.137, 2.455\times10^{-3}, -0.15, 2.0, 0.677$ $b_1\,to\,b_9 = 0.5, 1.0, -1.0, 1.044\times10^{-2}, 6.0, 5.5, 1.2, -0.2, 0.3$			
Zhang, J. (2021) [108]	R134a R236fa, R245fa, R1233zd (E) R1234ze(E) R290 R600a	T_{sat} = 30–90 °C – x_{out} = 0.01–0.05	–	G = 12–93	$h = 0.4703\mathrm{Re}_{eq}^{0.5221}\mathrm{Pr}_l^{1/3}\mathrm{Bd}^{0.1674}\rho^{*0.2126}\left(\frac{k_l}{D_h}\right)$ $D_h = 2b/\varphi \quad \gamma = \pi b/\lambda$ $\varphi = \left(1+\sqrt{1+\gamma^2}+4\sqrt{1+\gamma^2/2}\right)/6$	8.9 (all data) 11.0 (R1270, external data [173])	$\mathrm{f} = 11557.62\mathrm{Re}_{eq}^{-1.0041}\mathrm{Bd}^{0.3002}\rho^{*-0.426}$	10.3 (all data) 19.8 (R1270, external data [173])
Zhang, J. (2021) [109]	R134a R236fa, R245fa, R1233zd (E) R1234ze(E) R290 R600a	T_{sat} = 55–141 °C – x = 0.06–1	q = 12.3–37.5	G = 52–137	$h = h_{nb}+h_{cb} = Sh_{pool}+\mathrm{F}_{hl}$ F, S by Chen [174] $h_{cooper} = 35\mathrm{Pr}^{0.12}(-log_{10}\mathrm{Pr})^{-0.55}M^{-0.5}q^{0.67}$ $h_l = 0.023\mathrm{Re}_l^{0.8}\mathrm{Pr}_l^{0.4}\frac{k_l}{D_h}$ $\mathrm{F} = 2.35(\mathrm{X}_{tt}^{-1}+0.213)^{0.736}$ $\mathrm{S} = [1+2.53\times10^{-6}(\mathrm{Re}_l\mathrm{F}^{1.25})^{1.17}]^{-1}$	12.8 (all data) 10.9 (R290) 8.4 (R600a)	Zhang et al. [175]	11.1 (all data) 13.3 (R290) 9.9 (R600a)
Zhang, R. (2021) [110]	R717	T_{sat} = −10–10 °C – x = 0.1–1	q = 10–30	G = 40–200	Based on Kew and Conwell [176], Pre-dry out: $h_{tp} = 6.56\mathrm{Re}_{lo}^{0.536}\mathrm{Bo}^{0.274}\left(\frac{1}{1-x}\right)^{0.350}\frac{\lambda_l}{D}$ Post-dry out: $h_{tp} = 34.12\mathrm{Re}_{lo}^{0.371}\mathrm{Bo}^{0.10}\left(\frac{1}{1-x}\right)^{-0.557}\frac{\lambda_l}{D}$	10.4 11.4	Based on Müller-Steinhagen and Heck [177] $\left(\frac{dp}{dz}\right)_f = G\,(1-x)^{1.28}+\left(\frac{dp}{dz}\right)_{vo}x^{3.11}$ $G = \left(\frac{dp}{dz}\right)_{lo}+1.68x\left(\left(\frac{dp}{dz}\right)_{vo}-\left(\frac{dp}{dz}\right)_{lo}\right)$	19.6
Zhang, R. (2022) [111]	R717	T_{sat} = −10–10 °C – x = 0.1–1	q = 10–30	G = 40–200	Kew and Conwell [143]	20.84	Müller-Steinhagen and Heck [129]	23.71

R = refrigerant, ST, T_{sat} = saturation temperature, SP, p_{sat} = saturation pressure, p_r = reduced pressure, p_{avg} = average pressure, VQ = vapour quality, HC Rs = hydrocarbon refrigerants, cHT = condensation heat transfer, bHT = boiling heat transfer, aPD = adiabatic pressure drop, *AAD* = average absolute deviation, *AD* = average deviation; "*" refers to different ways to express the error with respect to *AAD*; "**" refers to the error in outlet pressure (p_o).

Table 3. Summary of the types of data, geometries and research highlights of the articles included in this review in cases of unusual configurations.

First Author/Year	R	Data	Geometry/Material/Orientation	Research Highlights
Abbas (2017) [178]	R717	Experimental study	Flooded triangular pitch plain tube bundle, d_o = 19.1 mm	Outside boiling HT
Abbas (2017) [179]	R717	Experimental study	Triangular pitch plain tube bundle, d_o = 19.1 mm	Effects of inlet vapor quality and exit degree of super heat on HT, outside boiling
Ahmadpour (2020) [180]	R600a	Experimental study	Horizontal copper MF tube, d_i = 14.18 mm	Condensation HT, effect of lubricating oil and nanoparticles on condensation HT
Aprin (2011) [181]	R290 R600a R601a	Experimental study	Staggered smooth tube bundle, d_o = 19.05 mm	Flow patterns, TP flow void fraction and convective boiling outside tube bundle
Ayub (2017) [182]	R717	Experimental study	Triangular pitch plain tube bundle, d_o = 19.1 mm	Effect of exit degree of super heat on HT, outside boiling
Ding (2017) [183]	R290	Experimental study	Shell side of LNG SWHE, d_i = 6 mm, θ = 4°	Flow patterns, TP downward flow boiling HT and PD
Ding (2018) [184]	R290	Experimental study	Shell side of LNG SWHE, d_o = 12 mm, θ = 4°	TP flow boiling HT and PD
Fernández-Seara (2016) [185]	R717	Experimental study	A plain and an integral-fin (1260 f.p.m.) titanium tube, d_o = 19.05 mm	Pool boiling HT
Gil (2019) [186]	RE170, R600a R601	Experimental study	Horizontal flat plate of a vessel, d = 72 mm	Nucleate boiling HT
Gong (2013) [187]	R600a	Experimental study	Vertical stainless-steel cylinder boiling vessel, d_i = 75 mm	Visualization study, nucleate pool boiling HT
Huang (2020) [188]	R717	Experimental study	Microchannel heat sink, d_h = 280 μm	Saturated flow boiling HT
Jin (2019) [189]	R134a, R290, R600a, R32, R1234ze(E)	Experimental study and data from [190,191]	Horizontal smooth copper tube, d_o = 19.05 mm	Falling film evaporation HT
Koyama (2014) [192]	R717	Experimental study	Titanium MF plate evaporator, channel height = 1, 2, 5 mm	Flow boiling HT
Li (2018) [193]	R290	Numerical simulation (ANSYS CFX 12.1)	SWHE, d_h = 14 mm, tilt angle 10°	Numerical study on forced convective condensation HT and frictional PD
Lin (2023) [194]	R134a, R32 R245fa, R1234ze(E) R410a, R123, R290 R600a	External experimental database (see [194])	Horizontal smooth tube, d_o = 16–25.35 mm	Falling film evaporation HT
Ma (2017) [195]	R600a	Experimental study	Smooth copper TPCT, d_i = 40 mm	Evaporation and condensation HT
Moon (2022) [196]	R600a	Experimental study	Horizontal MF tube, d_i = 6.36 mm	Evaporation HT and frictional PD
Pham (2022) [197]	R290	Experimental study	Horizontal MF copper tube, d_i = 6.3 mm	Flow patterns and flow condensation HT
Qiu (2015) [198]	R290	Numerical simulation CFD software ANSYS Fluent	Upright spiral tube, tilt angle = 10°, d_i = 14 mm	Forced convective condensation HT and frictional PD
Salman (2023) [199]	R290	Experimental study	Brazed PHE with OSF	Saturation flow boiling HT and frictional PD
	R717		Horizontal platinum wire,	Nucleate pool boiling HT

Sathyabhama (2010) [200]		External experimental database [201–203]	d = 0.3 mm Horizontal flat circular sur face of silver, d = 10 mm Horizontal, plain stainless-steel tube, d = 19.05 mm	
Shah (2017) [204]	R718, R717 halocarbon Rs HC Rs	External experimental database (see [204])	Copper/brass/steel, stainless steel single tubes and plain/enhanced tube bundles, d_i = 3 mm	Flow patterns, TP void fraction and flow boiling HT
Shah (2021) [205]	R718, R717, halocarbon Rs, HC Rs (R290, R600a)	External experimental database (see [205])	Horizontal copper/brass/aluminium-brass/stainless steel/copper-nickel single tube, top tube of a column of tubes, d_o = 12.7–50.8 mm	Falling film evaporation HT in full wetting and partial dryout regimes
Shete (2023) [206]	R134a, R32, R600a	Experimental study	A plain and five different re-entrant cavity (REC) copper tubes, d_i = 16.5 mm	Nucleated pool boiling HT
Tian (2022) [207]	R290	Experimental study	A smooth, a fin-enhanced horizontal U-shaped titanium tube, $d_{i1,2}$ = 16.65 mm	Enhanced pool boiling
Touhami (2014) [208]	R718, R717 halocarbon Rs HC Rs HFC	External experimental database (see [208])	Horizontal copper/carbon steel/stainless steel tubes, d_o = 4–51 mm	Pool boiling HT
Wen (2014) [209]	R600a	Experimental study	Circular copper tube with porous inserts, d_i = 7.5 mm	Flow boiling HT and PD, effect of the sizes of inserts on HT and PD
Wu (2021) [210]	R290	Experimental study	Horizontal copper MF tube, d_i = 6.3 mm	Condensation HT
Yan (2021) [211]	R1270	Experimental study	LHP, 2.5 mm × 2.5 mm channel	Flow patterns and condensation HT
Yang (2018) [212]	R290	Experimental study	Shell side of horizontal stainless steel HBHX, d_o = 14 mm, baffle angle 40°	Flow patterns and TP condensation HT
Yang (2019) [213]	R290	Experimental study	Shell side of vertical stainless steel HBHX, d_o = 14 mm, baffle angle 40°	Flow patterns and TP condensation HT
Yoo (2022) [214]	R290	Experimental study	Semicircular channel PCHE, d_h = 1.22 mm	Condensation HT and PD
Yu (2018) [215]	R290	Experimental study	Helical tube, helix angle = 10°, d_h = 10 mm	Forced convective condensation HT and frictional PD
Zhao (2023) [216]	R290	Experimental study	Horizontal copper MF tube, d_o = 7 mm	Flow patterns, boiling HT and frictional PD

R = refrigerant, TP = two phase, HT = heat transfer, PD = pressure drop, PHE = plate heat exchanger, MF = microfin, d_i, d_h, d_o = inner, hydraulic, outer diameter, HC Rs = hydrocarbon refrigerants, LNG = liquefied natural gas, SWHE = spiral wound heat exchanger, HBHX = helically baffled shell-and-tube heat exchanger, TPCT = two-phase closed thermosyphon, PCHE = printed circuit heat exchanger, LHP = loop heat pipe, OSF = offset strip fin, θ = winding angle, f.p.m. = fins per meter.

Table 4. Summary of the operating conditions, HTC and PD correlations of the papers included in this review, in cases of unusual configurations.

First Author/Year	R	ST/SP/VQ	Heat Flux (kW/m²)	Mass Flux (kg/m²s)	Best Reported HTC Correlation/New HTC Correlation	*AAD* (%)	Best Reported PD Correlation/New PD Correlation	*AAD* (%)
Abbas (2017) [178]	R717	T_{sat} = −20–(−1.7) °C – –	q = 5–45	–	$h_{tp} = 70q^{0.9-0.4p_r^{0.1}} p_r^{0.55}(-log p_r)^{-0.6}$	* ±15%	–	–
Abbas (2017) [179]	R717	T_{sat} = −20–(−1.7) °C – x_{in} = 0–0.30	q = 5–45	–	$h_{tp} = 70q^{0.9-0.4p_r^{0.1}} p_r^{0.55}(-log p_r)^{-0.6} e^{-0.075T_{sup}} e^{-0.5x_{in}}$	* 93% ± 20%		
Ahmadpour (2020) [180]	R600a	T_{sat} = 41.4–52.3 °C p_{sat} = 550–700 x = 0.03–0.76	–	G = 54–90	Yu and Koyama [217] Cavallini et al. [218] Kedzierski and Goncalves [219]	* ±20	–	–
Aprin (2011) [181]	R290 R600a R601a	– p = 0.2–12 bar –	q = 3–53	G = 8–15	$J_G < 0.15\ ms^{-1};\ h_1 = 55p_r^{0.12-0.2log(Ra/0.4)}[-log(p_r)]^{-0.55} M^{-0.5} q$ $J_G > 0.35\ ms^{-1};\ Nu = \frac{h_2 d_o}{\lambda_G} = 387p_r^{0.17} Re_v^{0.34} Pr_v^{0.33}$ $0.15\ ms^{-1} < J_G < 0.35\ ms^{-1};\ h = max(h_1, h_2)$	* 92% ± 20% (all data)	–	–
Ayub (2017) [182]	R717	T_{sat} = −20–(−1.7) °C – –	q = 5–45	–	$h_{tp} = 70q^{0.9-0.4p_r^{0.1}} p_r^{0.55}(-log p_r)^{-0.6} e^{-0.075T_{sup}}$	* ±15%		
Ding (2017) [183]	R290	– p_{sat} = 0.25 MPa x = 0.2–1	q = 4–10	G = 40–80	$h_{tp} = Eh_{cv} + Sh_{nb}$ $h_{cv} = 0.039\lambda_l \left(\frac{v^2}{g}\right)^{-1/3} Re^{0.09} Pr^{0.99}$ $h_{nb} = 55p_r^{0.12-0.4343lnRa}(-0.4343ln p_r)^{-0.55} M^{-0.5} q^{0.67}$ $E = 1 + (9.42 \times 10^{-6})(\phi^2)^{0.92} Re^{0.81}$ $S = (4.76 \times 10^{-5}) We^{-0.0047} Bo^{0.061} p_r^{0.094}$	* 98% ± 20%	–	–
Ding (2018) [184]	R290	T_{sat} = −19.4 °C p_{sat} = 0.25 Mpa x = 0.2–0.9	q = 4–10	G = 40–80	$h_{tp} = Eh_{cv} + Sh_{nb}$ $h_{cv} = 0.039\lambda_l \left(\frac{v^2}{g}\right)^{-1/3} Re_{film}^{0.04} Pr^{0.65}$ $h_{nb} = 55p_r^{0.12-0.4343lnRa}(-0.4343ln p_r)^{-0.55} M^{-0.5} q^{0.67}$ $E = 1 + 3.25 \times 10^{-4} (\phi_l{}^2)^{-0.47Pt_{radi}+1.03} Re_{film}^{0.040Pt_{long}+0.79}$ $S = -0.3 + 1.19We^{0.25} Bo^{0.068Pt_{long}+0.70Pt_{radi}-0.69}$ $Pt_{long} = \frac{p_{long} + D}{D};\ Pt_{radi} = \frac{p_{radi} + D}{D}$	* 95% ± 20%	$\Delta P_{frict,tp} = \phi_l^2 \Delta P_{frict,l}$ $\phi_l^2 = 1 + \frac{C}{X_{tt}} + \frac{1}{X_{tt}^2}$ $\Delta P_{frict,l} = \frac{2f_l N[G(1-x)]^2}{\rho_l}$ $C = 1416.31Re_l^{-0.53} U_v^{0.0041} Pt_{long}^{-2.41} Pt_{radi}^{-5.40} - 2$	* 95% ± 25%
Fernández Seara (2016) [185]	R717	T_{sat} = 4–10 °C – –	–	NA	$h_o = C(q/A_o)^{0.77} p_r^{1.31}$ $q = heat\ flow\ [W];\ A_o = \pi d_o L$ $\begin{cases} C = 87.35 & for\ plain\ tube \\ C = 110.46 & for\ integral-fin\ tube \end{cases}$	* ±5.5	–	–
Gil (2019) [186]	RE170, R600a R601	T_{sat} = 10 °C – –	q = 5–70	NA	$h_{nb} = 42 \frac{\lambda_l}{d_0} \left[\frac{q d_0}{\lambda_l T_{sat}}\right]^{C_1} (-log_{10} p_r)^{-1}$ $C_1 = 0.4p_r^{0.78} \left(\frac{\rho_v}{\rho_l}\right)^{-0.59}$ $d_0 = 0.0208\beta \left[\frac{\sigma}{g(\rho_l - \rho_v)}\right]$	3.5 (all data)	–	–

					$\beta = contact\ angle = 35°$			
Gong (2013) [187]	R600a	– p_{sat} = 0.1–0.5 MPa –	q = 20–150	NA	Jung et al. [220]	6.9	–	–
Huang (2020) [188]	R717	T_{sat} = 25, 35 °C – –	q = 60.2–134.3 W/cm²	G = 165–883	$h = 0.00061(\mathrm{S}+\mathrm{F})\mathrm{Re}_l\mathrm{Pr}_l^{0.4}\mathrm{Fa}^{0.11}\frac{\lambda_l}{d_h}\Big/ln\left(\frac{b\mu_{lf}}{\mu_{lw}}\right)$ $\mathrm{F} = 1250\mathrm{Bo}^{0.95}\mathrm{Re}_{lo}^{0.22}\left(\frac{x}{1-x}\right)^{1.06}$ $\mathrm{S} = 2000\mathrm{Bo}^{1.02}\mathrm{Re}_{lo}^{0.22};\quad b = 1.02$	5.2	–	–
Jin (2019) [189]	R134a, R290, R600a, R32 R1234ze(E)	T_{sat} = 6–10 °C – –	q = 10–60	–	Full wetting regime: $\mathrm{Nu} = 23.3\mathrm{Re}_r^{0.8174}\mathrm{Bo}^{0.6331}\mathrm{Pr}^{-0.0864}$ $\mathrm{Re}_r = 3.92\times10^2 - 3.5\times10^3$ $\mathrm{Bo} = 5.16\times10^{-3} - 3.30\times10^{-1}$ $\mathrm{Pr} = 1.77 - 4.46$	* 96.7% ± 30%	–	–
					Partial dryout regime: $\mathrm{Nu} = 11.7\mathrm{Re}_r^{0.8931}\mathrm{Bo}^{0.5278}\mathrm{Pr}^{-0.0287}$ $\mathrm{Re}_r = 1.95\times10^2 - 8.33\times10^2$ $\mathrm{Bo} = 2.2\times10^{-2} - 3.56\times10^{-1}$ $\mathrm{Pr} = 1.77 - 4.46$	* 97.5% ± 30%		
Koyama(2014) [192]	R717	– p_{sat} = 0.7, 0.9 MPa –	q = 10, 15, 20	G = 5–7.5	$For\ \delta = 1\ mm,$ $\frac{h}{h_l} = 48.0\left(\frac{1}{\mathrm{X}_{vv}}\right)^{0.95}$ $h_l = 0.023\left(\frac{\lambda_l}{d_h}\right)\left[\frac{G(1-x)d_h}{\mu_l}\right]^{0.8}\mathrm{Pr}_l^{0.4}$	* 92% ± 30%	–	–
					$For\ \delta = 2\ and\ 5\ mm,$ $\frac{h}{h_l} = 41.8\left(\frac{1}{\mathrm{X}_{vv}}\right)^{0.96}\quad (1/\mathrm{X}_{vv} \geq 1)$ $\frac{h}{h_l} = 47.1\left(\frac{1}{\mathrm{X}_{vv}}\right)^{0.51}\quad (1/\mathrm{X}_{vv} \leq 1)$	* 87% ± 30%		
Li (2018) [193]	R290	– p_{sat} = 1.2–2.0 MPa x = 0.15–0.95	q = 5–20	G = 150–350	$h_{tp} = 0.021\frac{\lambda_l}{d_h}\mathrm{Re}_{lo}^{0.8}\mathrm{Pr}_l^{0.43}\left(1+3.5\frac{d_h}{D}\right)\psi_{lo}$ $\psi_{lo} = \left[1+\left(\sum_{i=1}^{2}a_i x^{b_i}\right)\left(\frac{\rho_v}{\rho_l}\right)^c \mathrm{Fr}_{lo}^d\right]\times\times[\mathrm{Bo}(1-x)+1]^e$ $a_1 = 0.0830, a_2 = -0.076, b_1 = 0.8161, b_2 = 16.29$ $c = -1.364, d = 0.047, e = -543.1$	4.00	$\left(\frac{dp}{dl}\right)_{tp} = \left(\frac{dp}{dl}\right)_{lo} + \varphi_{lv}\left[\left(\frac{dp}{dl}\right)_{vo} - \left(\frac{dp}{dl}\right)_{lo}\right]$ $\left(\frac{dp}{dl}\right)_{lo} = \left[\frac{0.3164}{Re_{lo}^{0.25}} + 0.03\left(\frac{d_h}{D}\right)^{0.5}\right]\frac{G^2}{2\rho_l d_h}$ $\left(\frac{dp}{dl}\right)_{vo} = \left[\frac{0.3164}{\mathrm{Re}_{lo}^{0.25}} + 0.03\left(\frac{d_h}{D}\right)^{0.5}\right]\frac{G^2}{2\rho_v d_h}$ $\varphi_{lv} = \left(\sum_{i=1}^{3}a_i x^i\right)\left(\frac{\rho_l}{\rho_v}\right)^b\left(\sum_{i=1}^{3}c_i\mathrm{Fr}_{lo}^i\right)$ $a_1 = 0.5311, a_2 = 1.794, a_3 = -1.270, b = -0.1703$ $c_1 = 8.613, c_2 = -4.975, c_3 = 0.7734$	3.37

Lin (2023) [194]	R134a, R32 R245fa R1234ze(E) R410a, R123, R290, R600a	T_{sat} = 4.85–26.7 °C – –	q = 2.5–168	–	$\mathrm{Nu}_{wetting} = max(\mathrm{Nu}_{cv}, \mathrm{Nu}_{comb})$ $\mathrm{Nu}_{cv} = (\mathrm{Nu}_{lam}^5 + \mathrm{Nu}_{tur}^5)^{1/5}$ $\mathrm{Nu}_{lam} = 2.65\mathrm{Re}_{ff}^{-0.158}\mathrm{Ka}_{ff}^{0.0563}$ $\mathrm{Nu}_{tur} = 0.03\mathrm{Re}_{ff}^{0.2}\mathrm{Pr}^{0.7}$ $\mathrm{Nu}_{comb} = \mathrm{Nu}_{nb}\mathrm{S} + \mathrm{Nu}_{cv}\mathrm{E}$ $\mathrm{Nu}_{nb} = \frac{h_{nb}\lambda_l}{d}$ $h_{nb} = 10\frac{k_l}{d_{bubble}}\left[\frac{q d_{bubble}}{\lambda_l T_{sat}}\right]^a \mathrm{p}_r^{0.1}(1 - T_r)^{-1.4}(\mathrm{Pr}_l)^{-0.25}$ $a = 0.855\left(\frac{\rho_v}{\rho_l}\right)^{0.309} \mathrm{p}_r^{-0.437}$ $d_{bubble} = 0.511\left[\frac{2\sigma}{g(\rho_l - \rho_v)}\right]^{0.5}$ $\mathrm{S} = \mathrm{Pr}_l^{0.474}\mathrm{Re}_{ff}^{0.968}\mathrm{Bo}_{ff}^{1}\mathrm{Ka}_{ff}^{0.565}\mathrm{Ga}_{bubble}^{1}\mathrm{p}_r^{-0.037} \times$ $\times \pi_0^{-0.883}\left(\frac{\rho_l}{\rho_v}\right)^{-1}\left(\frac{q}{q_{cri}}\right)^{0.99}$ $\mathrm{E} = \mathrm{Pr}_l^{-0.465}\mathrm{Re}_{ff}^{0.642}\mathrm{Bo}_{ff}^{0.46}\mathrm{Ka}_{ff}^{-0.242}\mathrm{Ga}_{bubble}^{-1} \times$ $\times \mathrm{p}_r^{-0.253}\pi_0^{0.418}\left(\frac{\rho_l}{\rho_v}\right)^{1}\left(\frac{q}{q_{cri}}\right)^{-1}$ $\mathrm{Re}_{ff} = 4\Gamma/\mu$ $\mathrm{Bo}_{ff} = q(\pi d)/\Gamma i_{lv}$ $\mathrm{Ga}_{bubble} = g d_{bubble}^3 \nu_l^{-2}$ $\pi_0 = q^2 d(\rho_l - \rho_v)/i_{lv}^{5/2}\mu_l$ $q_{cri=}\left(\frac{\pi^2}{60}\right)(3^{0.25})\left[2g\left(\frac{\rho_l - \rho_v}{\rho_l + \rho_v}\right) + \frac{\sigma}{(\rho_l + \rho_v)R^2}\right]^{0.5} \times$ $\times\left[\frac{g(\rho_l - \rho_v)}{\sigma} + \frac{1}{2R^2}\right]^{-0.75}$	10 (all data)	–	–
					Simplified correlation $\mathrm{S} = \mathrm{Re}_{ff}^{0.043}\mathrm{Bo}_{ff}^{-0.182}$ $\mathrm{E} = \mathrm{Re}_{ff}^{-0.496}\mathrm{Bo}_{ff}^{-0.377}$	14 (all data)		
Ma (2017) [195]	R600a	T_{sat} = 54.6 °C p_{sat} = 0.77 MPa –	–	NA	Rohsenow [221]	10.3	–	–
Moon (2022) [196]	R600a	T_{sat} = −25–(−10) °C – x = 0.2–0.9	q = 9–15	G = 20–40	$h = h_{nb} + h_{cv}$ $h_{nb} = 0.9664 h_{Cooper}\mathrm{S}$ $h_{Cooper} = 55\mathrm{p}_r^{0.12}[-log(\mathrm{p}_r)]^{0.55}M^{0.5}q^{0.67}$ $\mathrm{S} = 1.36\mathrm{X}_{tt}^{0.36}$ $h_{cv} = 1.0274 h_{lo}\left[1 + 1.128x^{0.8170}\left(\frac{\rho_l}{\rho_v}\right)^{0.3685}\left(\frac{\mu_l}{\mu_v}\right)^{0.2363} \times \left(1 - \frac{\mu_l}{\mu_v}\right)^{2.144}\mathrm{Pr}_l^{0.1}\right]\mathrm{Rx}^{2.14}(\mathrm{BdFr})^{-0.2531}\left(\frac{G_0}{G}\right)^{0.0677}$ $h_{lo} = 0.023\frac{\lambda_l}{d}\mathrm{Re}_{lo}^{0.8}\mathrm{Pr}_l^{0.333}$	8.26	$\left(\frac{dp}{dz}\right)_f = \phi_{lo}^2\left(\frac{dp}{dz}\right)_{f,lo} = \phi_{lo}^2 2\mathrm{f}_{lo}\frac{G^2}{d\rho_l}A$ $A = 2.358\left(\frac{G}{G_{40}}\right)^{1.2464}$; $\mathrm{f}_{lo} = \frac{64}{Re_{lo}}$; $G_{40} = 40$ $\phi_{lo}^2 = \mathrm{Z} + 1.3529\mathrm{FH}(1 - \mathrm{E})^W$ $\mathrm{Z} = (1 + x)^2 + x^2\frac{\rho_l}{\rho_v}\left(\frac{\mu_v}{\mu_l}\right)^{0.2}$ $\mathrm{F} = x^{0.9525}(1 + x)^{0.414}$	4.82

							$\mathrm{H} = \left(\frac{\rho_l}{\rho_v}\right)^{1.132}\left(\frac{\mu_v}{\mu_l}\right)^{0.44}\left(1-\frac{\mu_v}{\mu_l}\right)^{3.542}$ $1-\mathrm{E} = -0.331 ln\left[\frac{\mu_l G x}{\rho_v \sigma}\right] - 0.0919$ $\begin{cases} \mathrm{E} = 0.95 \;\; if\; \mathrm{E} > 0.96 \\ \mathrm{E} = 0 \;\; if\; \mathrm{E} < 0 \end{cases}$ $\mathrm{W} = 1.398\mathrm{p}_r$	
Pham (2022) [197]	R290	T_{sat} = 48 °C – –	q = 3–9	G = 100–300	$h = \frac{\lambda_l}{d_i} 0.007079\mathrm{Re}^{0.1112}\mathrm{Ja}^{-0.232x}\mathrm{Pr}^{-0.68} \times$ $\times\, \mathrm{p}_r^{-0.578x^2}\left(-log(\mathrm{Pr})\right)^{-0.474x^2}\mathrm{Sv}^{2.531x}$	8.54	–	–
Qiu (2015) [198]	R290	– – x = 0.1–0.9	–	G = 150–250	Boyko [222]	8.8	Fuchs [223]	4.05
Salman (2023) [199]	R290	T_{sat} = 5–20 °C – x = 0.14–0.89	q = 7.5–15	G = 20–60	$\mathrm{Nu} = \mathrm{Z}_1\left(\mathrm{Re}_{eq}\right)^{Z_2}(\mathrm{Re}_l)^{Z_3}(\mathrm{Pr})^{Z_4}$ $Z_1 to Z_4 = 2.251, 0.549, 0.043, 0.333$	10	$\mathrm{f}_{tp} = \mathrm{Z}_1\left(\mathrm{Re}_{eq}\right)^{Z_2}(\mathrm{Re}_l)^{Z_3}\left(\frac{\rho_l}{\rho_v}\right)^{Z_4}$ $\mathrm{Re}_{eq} < 2500;\; \mathrm{Z}_1 to \mathrm{Z}_4 = 0.061, 1.251, -0.501, -0.951$ $\mathrm{Re}_{eq} > 2500;\; \mathrm{Z}_1 to \mathrm{Z}_4 = 0.091, 1.101, -0.551, -1.021$	14
Sathyabhama (2010) [200]	R717	– p [201] = 0.7 MPa p [202] = 0.7 MPa p [203] = 0.4 MPa –	q [201] = 72–1000 q [202] = 72–2800 q [203] = 8–60	NA	Kruzhilin [224] Mostinski [225] Mostinski [225]	7.54 (AD) −3.16 (AD) 29.8 (AD)	–	–
Shah (2017) [204]	R718, R717 halocarbon Rs HC Rs	– p_r = 0.005–0.2866 x = 0–0.98	q = 1–1000	G = 0.17–1391	Regime I—Intense Boiling Regime (Y_{IB} > 0.0008): $\mathrm{Y}_{IB} = \mathrm{F}_{pb}\mathrm{Bo}\mathrm{Fr}^{0.3}$ $\mathrm{F}_{pb} = h_{pb,actual}/h_{Cooper}$ $\mathrm{F}_{pb} = 1$ unless test data or an alternative correlation is used $h_{tp} = \mathrm{F}_{pb}h_{Cooper}$ $h_{Cooper=55.1q^{0.67}\mathrm{p}_r^{0.12}(-log\mathrm{p}_r)^{-0.55}M^{-0.55}}$ Regime II—Convective Boiling Regime (0.00021<Y_{IB} ≤0.0008): $\varphi = \varphi_0$ Regime III—Convection Regime (Y_{IB} ≤ 0.00021): $\varphi = \frac{2.3}{\mathrm{Z}^{0.08}\mathrm{Fr}^{0.22}}$ $\mathrm{Z} = \left(\frac{1-x}{x}\right)^{0.8}\mathrm{p}_r^{0.4}$	5.2 (all data) 24.25 (R717) 14.3 (R600a)	–	–
Shah (2021) [205]	R718, R717, halocarbon Rs, HC Rs (R290, R600a)	– p_r = 0.00059–0.19144 –	q = 1–208	–	$h_{tp} is\ the\ larger\ of\ h_{c,lam} and \left(h_{pb} + h_{c,turb}\right)$ $h_{c,lam} = 0.821\left(\frac{\mathrm{v}^2}{g\lambda^3}\right)^{-1/3}\mathrm{Re}_l^{-0.22}$ $h_{c,turb} = 0.0038\left(\frac{\mathrm{v}^2}{g\lambda^3}\right)^{-1/3}\mathrm{Re}_l^{0.4}\left(\frac{\mathrm{v}}{\alpha}\right)^{0.65}$ h_{pb} from Mostinski for HC Rs: $h_{pb} = 0.00417q^{0.7}p_c^{0.69}(1.8\mathrm{p}_r^{0.17} + 4\mathrm{p}_r^{1.2} + 10\mathrm{p}_r^{10})$ h_{pb} from Cooper for all other fluids: $h_{pb} = 55\mathrm{p}_r^{0.12}(-0.4343 ln\mathrm{p}_r)^{-0.55}M^{-0.5}q^{0.67}$	17.4 (all data) 16.9 (HC Rs) 13.0 (R717)	–	–

Shete (2023) [206]	R134a, R32 R600a	T_{sat} = 7–10 °C – –	q = 6.92–51.71	NA	Plain: Stephan and Abdesalam [226] For REC tubes: $\text{Nu} = \text{Re}^{0.773}\text{Pr}_l^{0.036}\left(\frac{p_{sat}}{p_c}\right)^{2.721}\left(\frac{\rho_l}{\rho_v}\right)^{2.765}\beta^{-0.1617}$ β = mouth size to fin height ratio	* ±30% * ±20%	–	–
Tian (2022) [207]	R290	T_{sat} = 20–40 °C – –	q = 2.5–10.5	NA	Smooth tube: R-J [227] Enhanced tube: Copper [153]	10.93 11.48	–	–
Touhami (2014) [208]	R718, R717 halocarbon Rs HC Rs, HFC	– p = 0.2–106.87 bar –	q = 0–670	–	$h = 0.5p_c^{0.10}l_c^{-0.20}c_p^{0.40}H_{lv}^{-0.67}\mu^{-0.27}\lambda^{0.60}p^{-010}Ra_q^{0.07}d^{-0.20}q^{0.67}$	32% (all data)	–	–
Wen (2014) [209]	R600a	T_{sat} = 10 °C – x = 0.076–0.87	q = 12–65	G = 120–1100	$\text{Nu} = 8.332\text{Bo}^{0.35}\text{Re}^{0.48}\text{Pr}^{0.74}\varepsilon^{0.47}$	* 95% ± 20%	$\text{f} = 21.093\text{Re}^{-0.731}\varepsilon^{-6.558}$	* 95% ± 20%
Wu (2021) [210]	R290	T_{sat} = 40–55 °C p_{sat} = 1.37–1.91 MPa x = 0–1	q = 3–8	G = 100–250	Yu et al. [217]	15.52	–	–
Yan (2021) [211]	R1270	T_{sat} = 283 K – –	q = 5–70	G = 2.2–26.5	Cavallini et al. [228]	* ±20	–	–
Yang (2018) [212]	R290	– – x = 0.1–0.9	q = 3–7	G = 20–40	$\frac{h_s}{\lambda_l}\left[\frac{\mu_l^2}{\rho_l(\rho_l-\rho_v)g}\right]^{1/3} =$ $= \left[\left(1.11\text{Re}_{film}^{-0.3}\right)^4 + \left(0.068\text{Re}_{film}^{0.2}\right)^4\right]^{1/4}$ $\text{Re}_{film} = \frac{4\Gamma}{x\mu_l} = \frac{4\pi dq}{x\mu_l i_{fv}}$	* 86% ± 10%	–	–
Yang (2019) [213]	R290	– – x = 0.2–0.9	q = 3–7	G = 20–40	$h = \lambda_l\left[\frac{\rho_l(\rho_l-\rho_v)g}{\mu_l^2}\right]^{1/3}\left[\frac{a\text{Re}_{film}^b(1+\text{Re}_v^c)}{1.08\text{Re}_{film}^{1.22}-5.2}\right]$ $(48.5 < \text{Re}_{film} < 684.6, 6150 < \text{Re}_v < 61153)$ $a = 0.00063, b = 1.4, c = 0.5$	* 93% ± 20%	–	–
Yoo (2022) [214]	R290	T_{sat} = −5.47–7.92 p_{sat} = 400–600 kPa x = 0–1	–	G = 40–90	$\text{Nu} = 1.18\text{Re}_{eq,tes,h}^{1/3}\text{Pr}_{l,test,h}^{1/3}$	* ±15	Lockhart and Martinelli [229]	–
Yu (2018) [215]	R290	T_{sat} = −40–27 °C – x = 0.1–0.9	q = 1.4–9.6	G = 200–400	Shah [113]	* ±20	Müller-Steinhagen and Heck [129]	* ±20
Zhao (2023) [216]	R290	T_{sat} = −23.55–(−4.35) °C p_{sat} = 0.215–0.415 MPa x = 0–0.96	q = 10.6–73.0	G = 70–190	Cavallini [230]	29.39	Rollmann and Spindler [118]	16.24

R = refrigerant, ST, T_{sat} = saturation temperature, SP, p_{sat} = saturation pressure, p_r = reduced pressure, p_{avg} = average pressure, VQ = vapour quality, HC Rs = hydrocarbon refrigerants, *AAD* = average absolute deviation, *AD* = average deviation; "*" refers to different ways to express the error with respect to *AAD*.

As described, Tables 3 and 4 refer to unusual configurations. In fact, among N = 135 articles included, N = 34 articles discuss different geometries, or different motion or heat transfer regimes. More specifically, N = 12 articles refer to various geometrical configurations (e.g., helicoidal tubes or heat pipes, etc.); N = 6 articles are related to the heat transfer in cases of microfin tubes; N = 6 analyse the pool boiling heat transfer; N = 6 deal with external HTC; and N = 3 study falling film evaporation. One article refers to a thermosyphon configuration.

The most investigated refrigerants are propane and isobutane. The majority of the articles were published after 2017.

The following paragraphs provide some details of the articles summarised in Tables 1 and 2.

3.1. Distribution of Articles over Time

As mentioned above, this research focused on the last fifteen years. Figure 2 shows a sharp increase in the number of studies between 2015 and 2016. This may be due to a growing interest in natural refrigerants, perhaps as a result of technological developments, regulatory changes or increased environmental awareness. Of particular note is Regulation (EU) No 517/2014 [231], which came into force on 1 January 2015 and aims to reduce F-gas emissions in the EU by limiting gases with a high global warming potential (GWP).

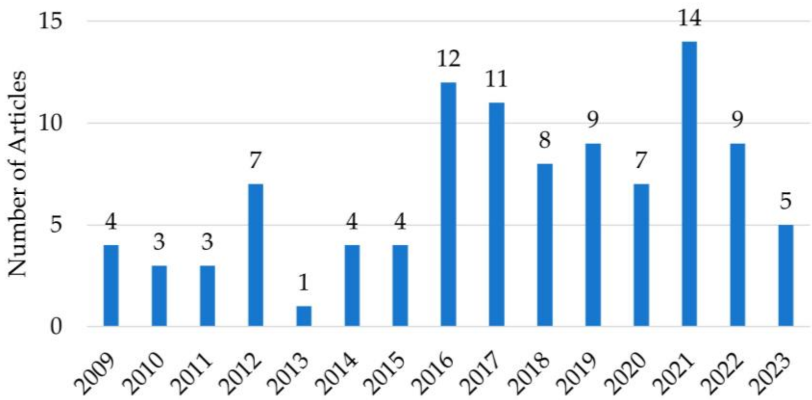

Figure 2. Number of studies published in the last 15 years.

3.2. Research Approach

3.2.1. Data

When analysing the authors' approach to the experimental data on heat transfer coefficient and pressure drop, it can be seen that N = 71 were carried out by the authors using their own experimental data, while N = 28 used external experimental databases from other studies. As shown in Figure 3, only N = 2 articles used numerical simulations.

Focusing on each refrigerant (Figure 4), the use of own experimental data is predominant for R290, R600a and R1270. For R717, both approaches are used equally.

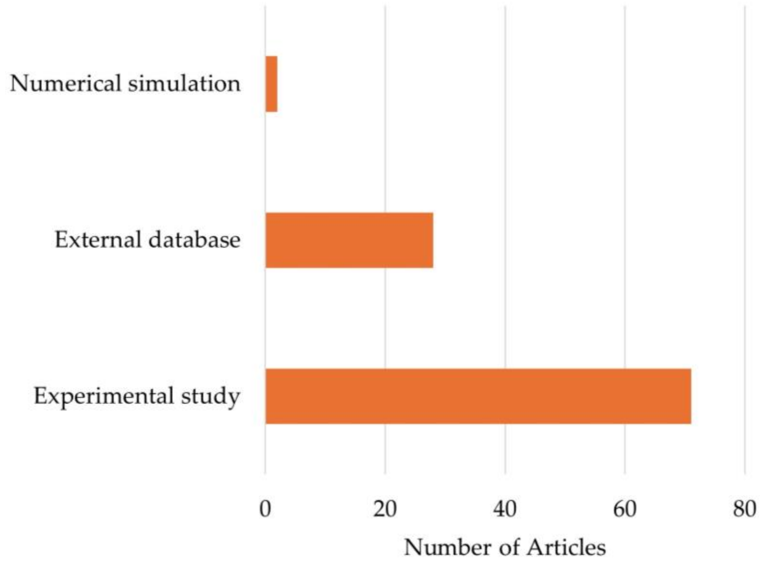

Figure 3. Number of articles by type of data used.

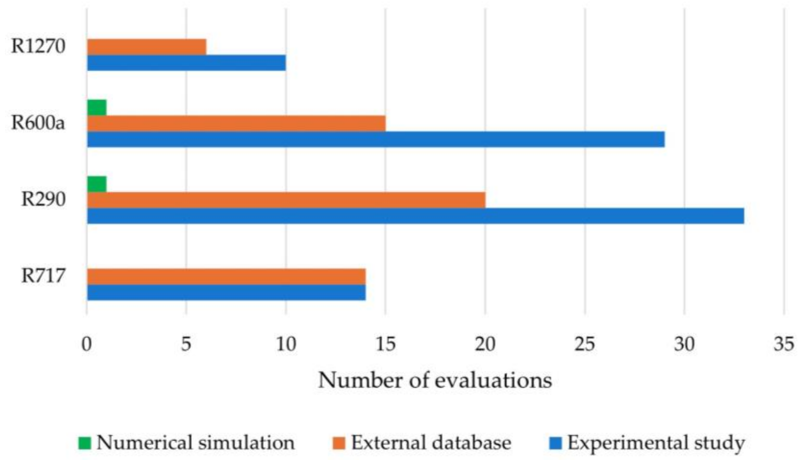

Figure 4. Number of evaluations by type of data used for each refrigerant.

3.2.2. HTC and PD Correlations

Figure 5 shows the authors' different approaches to the correlations. In particular, a new correlation was developed in N = 47 of the HTC evaluations, while in N = 38, the authors reported the correlation from the literature that best predicted the data.

For pressure drop, the number of best correlations already published (N = 30) outweighed the development of a new model (N = 21).

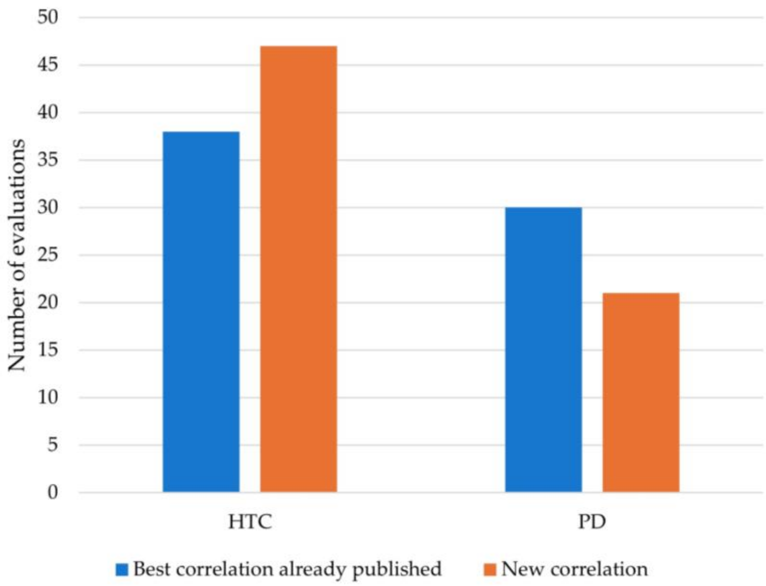

Figure 5. Number of evaluations related to new correlations and best correlations already published for HTC and PD.

3.2.3. Test Conditions

Of the 101 selected papers, N = 50 deal only with HTC, N = 16 deal only with pressure drop and the rest (N = 35) analyse both HTC and pressure drop.

A closer analysis of the 85 HTC papers shows in Figure 6 that most of them (N = 53) deal with the evaporating condition, N = 30 with condensation and only N = 2 with the heat transfer correlations under both conditions (Figure 6).

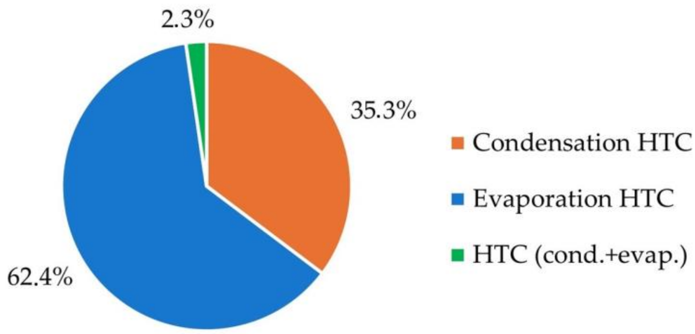

Figure 6. Percentage distribution of HTC articles.

3.3. Operating Conditions

3.3.1. Hydraulic Diameters

An analysis of the geometries used, reported in Figure 7, shows that the most commonly studied diameters range from 0.5 to 9 mm, with the largest number of evaluations in the (1, 2] mm range. The (0, 0.5] and (9, 50] mm ranges are of less interest to the authors.

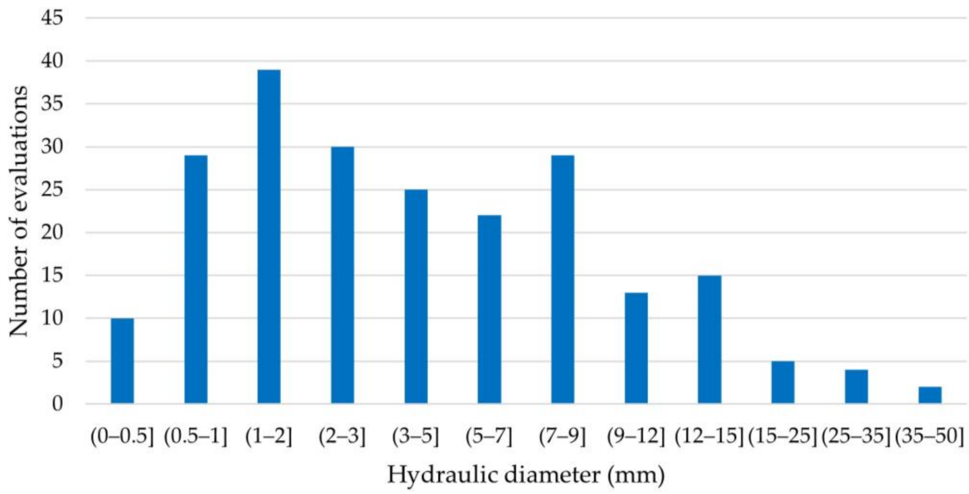

Figure 7. Number of evaluations related to each hydraulic diameter range.

3.3.2. Saturation Temperatures

From the analysis of saturation temperatures in the evaporating condition shown in Figure 8, most of the authors' evaluations cover the range from −40 to 40 °C. Less studied are the conditions from 50 to 150 °C. On the other hand, for the condensing condition, the low temperatures (from −40 to 20 °C) are the least studied, followed by the range (50, 100] °C. The most evaluated range is 30–40 °C, followed by 40–50 °C and 20–30 °C.

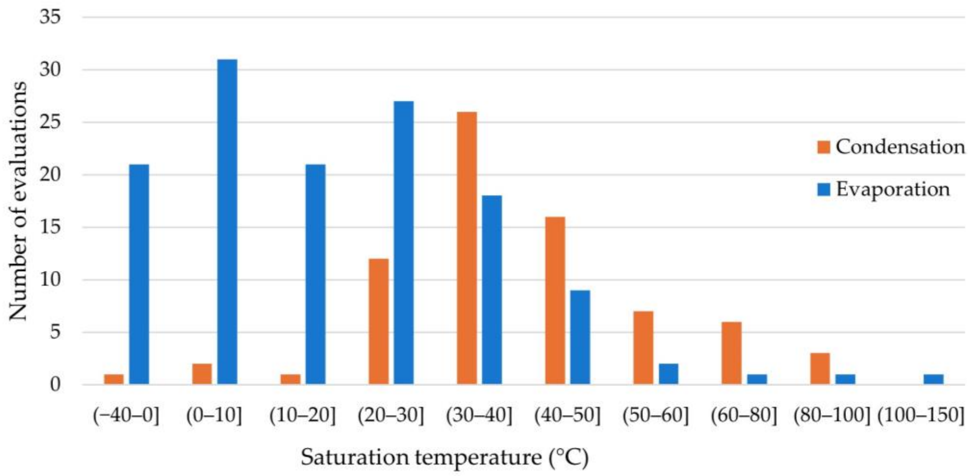

Figure 8. Number of evaluations related to each saturation temperature range for evaporating and condensing conditions.

3.3.3. Vapour Quality

From the vapour quality data summarised in Table 2 and shown in Figure 9, it can be seen that all ranges were investigated.

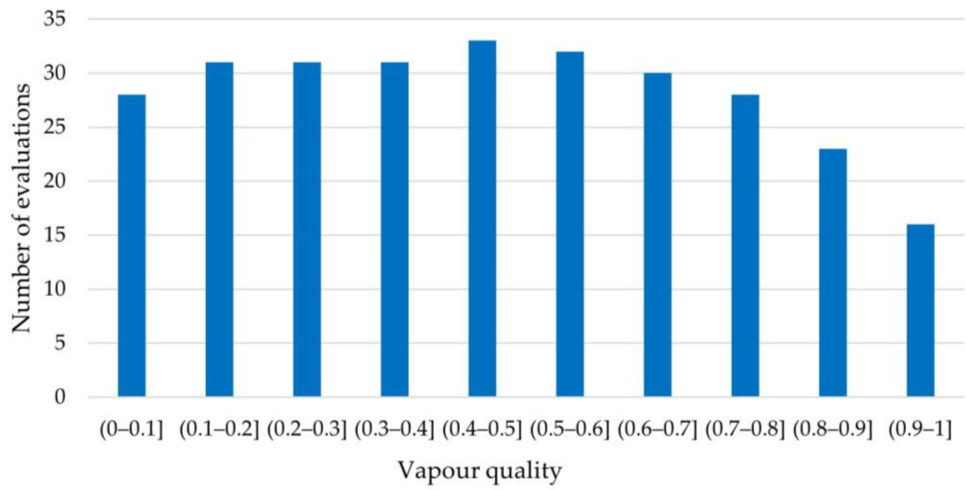

Figure 9. Number of evaluations related to each vapour quality range.

3.3.4. Specific Heat Flux

The analysis of the specific heat flux data shows a higher interest in the heat flux values from 0 to 30 kW/m^2, with a peak in the range from 10 to 20 kW/m^2, as shown in Figure 10. For the range from 30 to 740 kW/m^2, a decreasing trend in the number of evaluations is observed as the heat flux increases.

Focusing on the specific heat fluxes studied for each refrigerant, a similar trend is found for all of them.

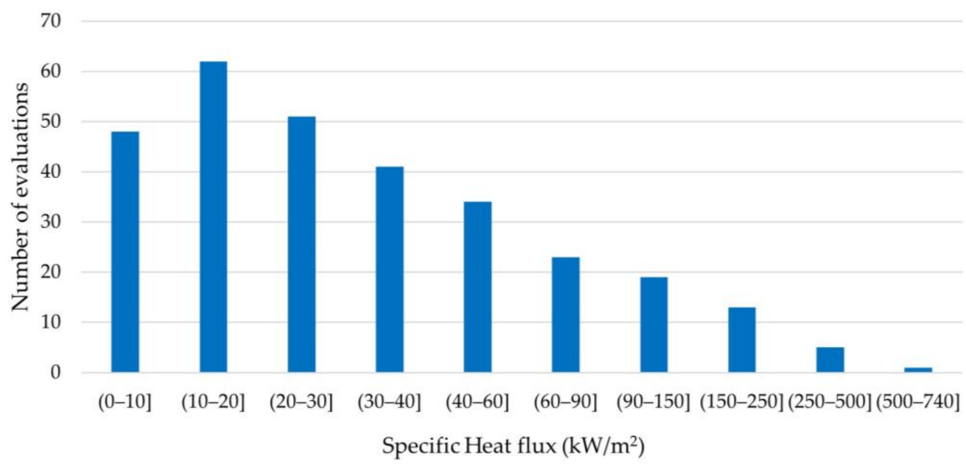

Figure 10. Number of evaluations related to each specific heat flux range.

3.3.5. Specific Mass Flux

As shown in Figure 11, the most studied specific mass fluxes range from 0 to 600 kg/m^{2}s; the intervals from 600 to 5600 kg/m^{2}s are less adopted.

Focusing on the specific mass fluxes adopted for each refrigerant, a similar trend is found for all of them.

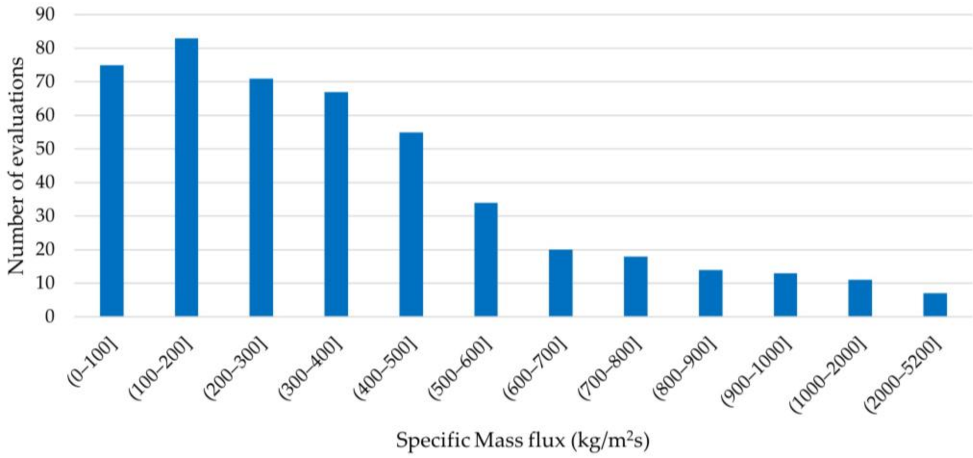

Figure 11. Number of evaluations related to each specific mass flux range.

3.4. Refrigerants

Among the selected articles, most concern propane and isobutane, as shown in Figure 12.

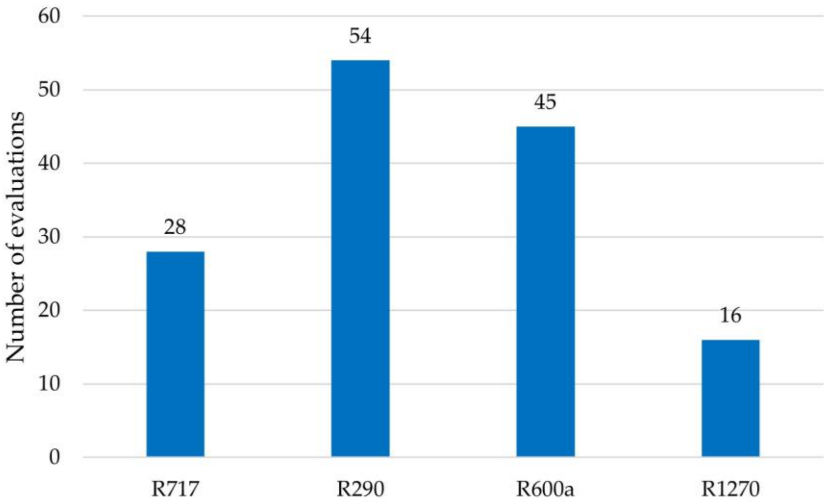

Figure 12. Number of evaluations related to each refrigerant.

Hydraulic Diameters and Saturation Temperatures

An analysis of the diameters used in ammonia studies shows that diameters from 0.5 to 15 mm are all widely studied, with a greater focus on those from 1 to 3 mm. Less used are the (0, 0.5] mm range and diameters from 15 to 50 mm.

Based on the R600a geometry data, the most studied diameter range is that from 0.5 to 12 mm, with the highest number of evaluations relating to the (7, 9] and (1, 2] mm ranges. Of less interest to authors are the (0, 0.5] mm range and diameters from 12 to 50 mm.

For propane, most of the authors' evaluations cover the range from 0.5 to 15 mm, with a focus on the (0.5, 3] mm range. As with ammonia, the (0, 0.5] mm range and diameters from 15 to 50 mm are less commonly used. The few evaluations on R1270 take into account all the diameter ranges.

Looking more closely at the saturation temperature ranges for each refrigerant, the evaluations for ammonia cover the range from 20 °C to 60 °C in the condensing conditions.

For R1270, R600a and R290, the range of condensing saturation temperatures considered is wider, from −40 °C to 80 °C, and the most evaluated range is from 30 to 40 °C.

When analysing the evaporation temperatures, it can be seen that for ammonia, most of the authors' evaluations cover the range −40 °C to 50 °C, whereas for R1270, the studies focus on saturated temperatures from 0 °C to 30 °C.

For R600a and R290, the most commonly used temperatures are from 0 °C to 40 °C and from −40 °C to 40 °C, respectively.

For evaporating temperatures above 50 °C, there are no evaluations for R717 and R1270, while there are a few for R600a and R290.

4. Correlations

Correlations for HTC and pressure drop for each refrigerant are considered below, focusing on error ranges and best correlations. Only articles where the error was evaluated in terms of absolute average deviation are considered, and an *AAD* threshold of 12% is used to identify the best models.

4.1. R717

Out of a total of 28 studies on ammonia, only 20 that expressed the error in terms of *AAD* were included in this analysis. In particular, for the condensation HTC, the Tao [96] correlation predicts the experimental data well, with an *AAD* of 7.4%. The maximum error in terms of *AAD* is 41% for the Shah correlation, as reported in [77]. For the evaporation HTC the proposed correlations show errors ranging from 4.7% to 40.9%, the best being those of Fang [144], Choi [25] and Zhang [110] with *AAD*s of 4.7%, 11.09% and 11.4%, respectively. For PD, the *AAD* ranges from 9.5% to 23.7%; the correlation by Moreno, Quiben and Thome [131] shows a good prediction of the data with an *AAD* of 9.5%.

4.2. R1270

Of the 16 studies on R1270, the 9 that reported the error in terms of *AAD* were considered. For the condensation HTC, the errors range from 11.0% to 32.6% and the most reliable correlations are those of Dorao and Fernandino [122] and Zhang [108] with an *AAD* of 11.0%. For the evaporating condition, the best predictions of the data are the Longo [157], Liu and Winterton [117] and Sun and Mishima [141] models, with *AAD*s of 6.9%, 8.5% and 8.6%, respectively. The maximum error is 27.1% for the Gorenflo correlation, as reported in [154].

For PD, the average absolute deviation ranges from 4.4% to 19.8%; the correlations by Xu and Fang [119], Macdonald and Garimella [69] and Friedel [142] show the best predictions of the data with *AAD*s of 4.4%, 6.4% and 7.3%, respectively.

4.3. R600a

Of the 45 studies on R600a, only 23 report the *AAD* error. In particular, for the condensation HTC, the correlations by Dorao and Fernandino [122], Haraguchi et al. [149], Cao [23] and Shah [89] predict the experimental data well, with *AAD*s of 5.8%, 6.57%, 9.8% and 11.2%, respectively. The maximum error in terms of *AAD* is 17.4%, as reported in [93].

Regarding the evaporation HTC, the proposed correlations show errors ranging from 6.2% to 40.1%, and the best ones are those of Fang et al. [144], Shah [121], Shah [91] and Liu and Winterton [117], with *AAD*s of 6.2% and 10.2% (for [65] and [39], respectively), 6.4%, 11.4% and 11.5%, respectively.

For PD, the AAD ranges from 6.6% to 32.52%; the correlations by Xu and Fang [119], Xu and Fang [124], Cao [23], Sempértegui-Tapia [87], Zhang [175] and Nualboonrueng [145] show good predictions of the data with *AAD*s of 6.6%, 11.0%, 7.3%, 9.3%, 9.9% and 10.18%.

4.4. R290

Out of a total of 54 studies on propane, only 38 that reported the error in terms of *AAD* were included in this analysis. For the condensation HTC, the errors range from 4.9% to 25.8% and the most reliable correlations are those by Dorao and Fernandino [122], Macdonald [70], Shah [93], Moser [138], Thome [146], Akers [155], Shah [89] and Macdonald [69] with *AAD*s of 4.9%, 5.4%, 6.5% and 11%, 7.22%, 7.27%, 9.0%, 10.5% and 11%, respectively. For the evaporating condition, the best predictions of the data are by the models by Liu and Winterton [117], Fang et al. [144], Longo et al. [157], Lillo [60], Pamitran [81], Shah [91], Choi [25], Zhang [109] and Aizuddin et al. [115] with *AAD*s of 6.2% and 7.5% (for [10] and [102], respectively), 6.5%, 7.7%, 8.2%, 8.27%, 9.2%, 10.02%, 10.9% and 11.6%, respectively. The maximum error is 33.16%, as reported in [75].

For PD, the average absolute deviation ranges from 6.88% to 20.8%; the correlation by Sun and Mishima [159], Sempértegui-Tapia [87], Friedel [142], Macdonald and Garimella [69], Del Col et al. [140], Patel [83], Choi [24] and Xu and Fang [119] show the best predictions of the data with *AAD*s of 6.88%, 7.2%, 7.59%, 7.9%, 9.1%, 10.08%, 10.84% and 11.7%, respectively.

5. Discussion

Of the four refrigerants considered in this review, R600a has the most reliable correlation for condensing HTC, with a maximum *AAD* error of 17.4%. For evaporating HTC, the smallest maximum error is found for R1270 and is equal to 27.1%.

For pressure drop, for both R1270 and R290, the correlations proposed by the authors show good reliability in predicting the data, with maximum *AAD*s of 19.8% and 20.8%, respectively.

Considering the intervals studied by the authors, the widest diameter range of validity of the correlations is 2–49 mm in [89]; the widest saturation temperature range of validity is from −34.4 °C to 72.1 °C for condensation in [95] and from 55 °C to 141 °C for evaporation in [109]. For specific mass flux and specific heat flux, the widest ranges of validity are 3.7–5176 kg/m^{2}s in [92] and 3–736 kW/m^2 in [26], respectively.

Among the articles reported in Tables 1 and 2, propane and isobutane are the most studied refrigerants.

The use of the authors' own experimental data predominates over the use of external experimental databases. For HTC, most of the studies deal with the development of a new correlation, whereas for pressure drop, the number of best correlations that are already published prevails.

Of the 101 papers selected, 50 deal only with HTC, 16 deal only with pressure drop and the remaining 35 analyse both HTC and pressure drop; most of the HTC papers deal with the evaporating condition.

With regard to the geometries, the most commonly studied diameters range from 0.5 to 9 mm, with the largest number of evaluations concerning the (1, 2] mm range.

Among the unusual configurations, 12 papers refer to various geometrical configurations (e.g., helicoidal tubes or heat pipes, etc.), 6 papers refer to heat transfer in the case of microfin tubes, 6 papers analyse the pool boiling heat transfer, 6 papers deal with external HTC, and 3 papers study falling film evaporation. One paper deals with a thermosyphon configuration. It could be noted that limited attention has been directed in the available literature to providing experimental correlations for configurations widely used in practice (such as shell-and-tube heat exchangers, different types of fins, falling film heat transfer, etc.).

Regarding the analysis of saturation temperatures in the evaporating conditions, most of the authors' evaluations cover the range from −40 to 40 °C; for the condensing condition, most of the authors studied the temperature range from 20 to 50 °C.

It should be noted that a small number of evaluations (and, therefore, correlations) focus on high-temperature condensation (50–80 °C). These temperature ranges could be studied in view of the high-temperature applications of heat pumps. In fact, in the near future, high-temperature heat pumps could be installed in buildings that have not yet been subject to energy-saving measures. Many studies are dedicated to propane, as efforts are also focused on it for domestic applications (small machines). For centralised applications in residential or public buildings, the use of high-capacity and high-temperature machines could be considered; in this case, propane or ammonia could be interesting and should be reconsidered and further investigated.

6. Conclusions

In this work, available data on the existing correlations of heat transfer coefficient and pressure drop for natural refrigerants have been collected through a systematic search.

For the articles considered in this review, the operating conditions are reported in terms of diameter, saturation temperatures, vapour quality, specific heat flux and specific mass flux. The results show that more attention is paid to the evaporation behaviour with respect to condensation and that two refrigerants (propane and isobutane) are diffusely studied.

The available literature has limited focus on providing experimental correlations for natural refrigerants in configurations that are widely used in practice.

In the studies reported in this review, the correlation in the case of high condensation temperature is reported in a few cases. This lack of information requires further investigation in view of the applications of heat pumps in heating systems, without modification to the distribution systems in buildings that have not yet been subject to energy-saving measures.

Author Contributions: Conceptualization, A.C. and A.D.; methodology, A.C. and A.D.; software, A.C. and A.D.; validation A.C. and A.D.; formal analysis, A.C. and A.D.; investigation, A.C. and A.D.; resources, A.D.; data curation, A.C. and A.D.; writing—original draft preparation, A.C. and A.D.; writing—review and editing, A.C. and A.D.; visualization, A.C. and A.D.; supervision, A.D.; project administration, A.D.; funding acquisition, A.D. All authors have read and agreed to the published version of the manuscript.

Funding: This research was funded by Ministero dell'Università e della Ricerca MUR, grant D.M. 1061/2021 finanziati tramite il Programma Operativo Nazionale (PON) "Ricerca e Innovazione" 2014–2020—Azione IV.4 "Dottorati e contratti di ricerca su tematiche dell'innovazione" e Azione IV.5 "Dottorati su tematiche green".

Conflicts of Interest: The authors declare no conflicts of interest. The funders had no role in the design of the study; in the collection, analyses, or interpretation of data; in the writing of the manuscript; or in the decision to publish the results.

Nomenclature

Roman	
c_p	Specific heat capacity [J/kgK]
d	Diameter [m]
g	Acceleration of gravity [m/s^2]
G	Specific Mass flux [kg/m^{2}s]
h	Heat transfer coefficient [W/m^{2}K]
h_{lv}	Latent heat of vaporization [J/kg]
i	Specific enthalpy [J/kg]
J_v	Vapour superficial velocity [m/s]
L_h	Heated length [m]
M	Molecular mass [kg/kmol]
N	Number of tube rows per meter
p	Pressure [Pa]
p_r	Reduced pressure, $p_r = p_{sat}/p_c$
q	Specific Heat flux [W/m^2]
Ra	Mean roughness height [μm]
Rx	Area enhancement [–]
SV	Specific volume, $\mathrm{SV} = \frac{(V_v - V_l)}{V} = \frac{V_v - V_l}{xV_v + (1-x)V_l}$
T	Temperature [°C]
x	Vapour quality [–]
Greek letters	
β	Chevron angle [°]
β^*	Reduced chevron angle [–]

δ	Channel height [m]
Δp	Pressure drop [Pa]
θ	Winding angle [°]
λ	Thermal conductivity [W/mK]
μ	Dynamic viscosity [Pa·s]
ν	Kinematic viscosity [m^2/s]
ρ	Density [kg/m^3]
ρ^*	Density ratio, $\rho^* = \rho_l/\rho_v$
ρ_{tp}	Two phase density, $\rho_{tp} = \left(\frac{x}{\rho_v} + \frac{1-x}{\rho_l}\right)^{-1}$
σ	Surface tension [N/m]
Subscripts	
avg	Average
c	Critical
cb	Convective boiling
eq	Equivalent
exp	Experimental
flat	Flattened tubes
frict	Frictional
h	Hydraulic
i	Inner
l	Liquid
lf	Liquid film
lo	Liquid only
loc	Local
nb	Nucleate Boiling
o	Outer
pb	Pool boiling
pred	Predicted
sat	Saturation
v	Vapour
vo	Vapour only
w	Wall
Abbreviations	
AD	Average deviation
aPD	Adiabatic flow pressure drop
AAD	Absolute average deviation
CFCs	Chlorofluorocarbons
f.p.m.	Fins per meter
GWP	Global warming potential
HBHX	Helically baffled shell-and-tube heat exchanger
HCFCs	Hydrochlorofluorocarbons
HC Rs	Hydrocarbon refrigerants
HFCs	Hydrofluorocarbons
HFO	Hydrofluoroolefin
HT	Heat transfer
bHT	Boiling heat transfer
cHT	Condensation heat transfer
HTC	Heat transfer coefficient
LHP	Loop heat pipe
LNG	Liquefied natural gas
MF	Microfin
ODF	Offset strip fin
ODP	Ozone depletion potential
PCHE	Printed circuit heat exchanger
PD	Pressure drop
PHE	Plate heat exchanger

R	Refrigerant
ST	Smooth tube
SWHE	Spiral wound heat exchanger
TP	Two phase
TPCT	Two-phase closed thermosyphon
VQ	Vapour quality
Dimensionless numbers	
Bo	Boiling number, $\text{Bo} = \frac{q}{Gh_{lv}}$
Bd	Bond number, $\text{Bd} = \frac{g(\rho_l - \rho_v)d^2}{\sigma}$
Cn	Confinement number, $\text{Cn} = \frac{(\sigma/g(\rho_l - \rho_v))^{0.5}}{d}$
Co	Convection number, $\text{Co} = \left(\frac{1-x}{x}\right)^{0.8}\left(\frac{\rho_v}{\rho_l}\right)^{0.5}$
Fa	Fang number, $\text{Fa} = \frac{(\rho_l - \rho_v)\sigma}{G^2 d}$
ϕ_f^2	Two-phase frictional multiplier (Chisholm), $\phi_f^2 = 1 + \frac{C}{X_{tt}} + \frac{1}{X_{tt}^2}$
Fr_l	Liquid Froude number, $\text{Fr}_l = \frac{[G(1-x)]^2}{gd\rho_l^2}$
f	Friction factor ≡ Darcy factor, $\text{f} = \frac{2\Delta p}{\rho v^2}\frac{d}{L}$
f_{Fann}	Fanning friction factor, $\text{f}_{Fann} = \frac{\Delta p}{2\rho v^2}\frac{d}{L}$
Ja	Jacob's number, $\text{Ja} = \frac{h_{lv}}{c_{pl}\Delta T_s}$
Ka	Kapitza number, $\text{Ka} = \mu^4\, g/\rho\sigma^3$
Nu	Nusselt number, $\text{Nu} = \frac{hL}{\lambda}$
Pr	Prandtl number, $\text{Pr} = \frac{c_p\mu}{\lambda}$
Re_{eq}	Equivalent Raynolds number, $\text{Re}_{eq} = \frac{Gd_h}{\mu_l}\left[(1+x) + x\left(\frac{\rho_l}{\rho_v}\right)^{0.5}\right]$
Re_l	Liquid Reynolds number, $\text{Re}_l = \frac{(1-x)Gd}{\mu_l}$
Re_v	Vapour Reynolds number, $\text{Re}_v = \frac{xGd}{\mu_v}$
Re_{ko}	Liquid only (*k* = *l*) or vapor only (*k* = *v*) Re, $\text{Re}_{ko} = \frac{Gd}{\mu_k}$
We	Weber number, $\text{We} = \frac{G^2 d}{\rho\sigma}$
X_{tt}	Lockhart–Martinelli parameter, $X_{tt} = \left(\frac{\rho_v}{\rho_l}\right)^{0.5}\left(\frac{\mu_l}{\mu_v}\right)^{0.1}\left(\frac{1-x}{x}\right)^{0.9}$ (Turbulent–Turbulent flow)
X_{vv}	Lockhart–Martinelli parameter, $X_{vv} = \left(\frac{\rho_v}{\rho_l}\right)^{0.5}\left(\frac{\mu_l}{\mu_v}\right)^{0.5}\left(\frac{1-x}{x}\right)^{0.5}$ (Laminar–Laminar flow)

References

1. Council of the European Union. *Proposal for a Regulation of the European Parliament and of the Council on Fluorinated Greenhouse Gases, Amending Directive (EU) 2019/1937 and Repealing Regulation (EU) No 517/2014*; European Commission: Brussels, Belgium. 2023. Available online: https://eur-lex.europa.eu/legal-content/EN/TXT/?uri=consil%3AST_14409_2023_INIT (accessed on 12 January 2024).
2. Sunden, B.; Meyer, J.; Dirker, J.; John, B.; Mukkamala, Y. Local Measurements in Heat Exchangers: A Systematic Review and Regression Analysis. *Heat Transf. Eng.* **2021**, *43*, 1529–1565.
3. Cavallini, A.; Del Col, D.; Rossetto, L. Heat transfer and pressure drop of natural refrigerants in minichannels (low charge equipment). *Int. J. Refrig.* **2013**, *36*, 287–300.
4. Thome, J.; Cheng, L.; Ribatski, G.; Vales, L. Flow boiling of ammonia and hydrocarbons: A state-of-the-art review. *Int. J. Refrig.* **2008**, *31*, 603–620.
5. Liberati, A.; Altman, D.G.; Tetzlaff, J.; Mulrow, C.; Gøtzsche, P.C.; Ioannidis, J.P.A.; Clarke, M.; Devereaux, P.J.; Kleijnen, J.; Moher, D. The PRISMA statement for reporting systematic reviews and meta-analyses of studies that evaluate healthcare interventions: Explanation and elaboration. *BMJ Clin. Res. Ed.* **2009**, *339*, b2700.
6. Ağra, O.; Teke, I. Determination of the heat transfer coefficient during annular flow condensation in smooth horizontal tubes. *J. Therm. Sci. Technol.* **2012**, *32*, 151–159.
7. Ahmadpour, M.M.; Akhavan-Behabadi, M.A.; Sajadi, B.; Salehi-Kohestani, A. Effect of lubricating oil on condensation characteristics of R600a inside a horizontal U-shaped tube: Experimental study. *Int. J. Therm. Sci.* **2019**, *145*, 106007.

8. Akbar, R.; Oh, J.; Pamitran, A. Evaluation of Heat Transfer Coefficient of Two-Phase Flow Boiling with R290 in Horizontal Mini Channel. *J. Adv. Res. Fluid Mech. Therm. Sci.* **2021**, *88*, 88–95.
9. Ali, M.S.; Anwar, Z.; Mujtaba, M.A.; Khidmatgar, A.; Goodarzi, M. Two-phase frictional pressure drop with pure refrigerants in vertical mini/micro-channels. *Case Stud. Therm. Eng.* **2021**, *23*, 100824.
10. Allymehr, E.; Pardiñas, Á.; Eikevik, T.; Hafner, A. Characteristics of evaporation of propane (R290) in compact smooth and microfinned tubes. *Appl. Therm. Eng.* **2020**, *181*, 115880.
11. Allymehr, E.; Pardiñas, Á.; Eikevik, T.; Hafner, A. Comparative analysis of evaporation of Isobutane (R600a) and Propylene (R1270) in compact smooth and microfinned tubes. *Appl. Therm. Eng.* **2021**, *188*, 116606.
12. Allymehr, E.; Pardiñas, Á.; Eikevik, T.; Hafner, A. Condensation of Hydrocarbons in Compact Smooth and Microfinned Tubes. *Energies* **2021**, *14*, 2647.
13. Amalfi, R.L.; Vakili-Farahani, F.; Thome, J.R. Flow boiling and frictional pressure gradients in plate heat exchangers. Part 2: Comparison of literature methods to database and new prediction methods. *Int. J. Refrig.* **2016**, *61*, 185–203.
14. Amalfi, R.L.; Vakili-Farahani, F.; Thome, J.R. Flow boiling and frictional pressure gradients in plate heat exchangers. Part 1: Review and experimental database. *Int. J. Refrig.* **2016**, *61*, 166–184.
15. Anwar, Z.; Palm, B.; Khodabandeh, R. Flow Boiling Heat Transfer and Dryout Characteristics of R600a in a Vertical Minichannel. *Exp. Therm. Fluid Sci.* **2015**, *36*, 1230–1240.
16. Arima, H.; Kim, J.H.; Okamoto, A.; Ikegami, Y. Local boiling heat transfer characteristics of ammonia in a vertical plate evaporator. *Int. J. Refrig.* **2010**, *33*, 359–370.
17. Asim, M.; Anwar, Z.; Farooq, M.; Shaukat, R.; Imran, S.; Abbas, M.M.; Ali, Q. Flow boiling heat transfer characteristics of low GWP refrigerants in a vertical mini-channel. *Therm. Sci.* **2022**, *26*, 63–76.
18. Ayub, Z.H.; Khan, T.S.; Salam, S.; Nawaz, K.; Ayub, A.H.; Khan, M.S. Literature Survey and a Universal Evaporation Correlation for Plate type Heat Exchangers. *Int. J. Refrig.* **2019**, *99*, 408–418.
19. Başaran, A.; Benim, A.C.; Yurddas, A. Numerical Simulation of the Condensation Flow of the Isobutane (R600a) inside Microchannel. *Heat Transf. Eng.* **2021**, *43*, 337–361.
20. Başaran, A.; Yurddaş, A. Thermal modeling and designing of microchannel condenser for refrigeration applications operating with isobutane (R600a). *Appl. Therm. Eng.* **2021**, *198*, 117446.
21. Butrymowicz, D.; Śmierciew, K.; Karwacki, J.; Borsukiewicz, A.; Gagan, J. Experimental Investigations of Flow Boiling Heat Transfer under Near-Critical Pressure for Selected Working Fluids. *Sustainability* **2022**, *14*, 14029.
22. Butrymowicz, D.; Śmierciew, K.; Gagan, J.; Dudar, A.; Lukaszuk, M.; Zou, H.; Łapiński, A. Investigations of Performance of Mini-Channel Condensers and Evaporators for Propane. *Sustainability* **2022**, *14*, 14249.
23. Cao, X.; Wang, X.; Song, Q.; Wang, D.; Li, Y. Experimental investigation on the heat transfer and pressure drop characteristics of R600a in a minichannel condenser with different inclined angles. *Appl. Therm. Eng.* **2021**, *196*, 117227.
24. Choi, K.-I.; Pamitran, A.S.; Oh, J.-T.; Saito, K. Pressure drop and heat transfer during two-phase flow vaporization of propane in horizontal smooth minichannels. *Int. J. Refrig.* **2009**, *32*, 837–845.
25. Choi, K.-I.; Oh, J.-T.; Saito, K.; Jeong, J. Comparison of heat transfer coefficient during evaporation of natural refrigerants and R-1234yf in horizontal small tube. *Int. J. Refrig.* **2014**, *41*, 210–218.
26. Cioncolini, A.; Thome, J.R. Algebraic turbulence modeling in adiabatic and evaporating annular two-phase flow. *Int. J. Heat Fluid Flow* **2011**, *32*, 805–817.
27. Da Silva, P.F.; de Oliveira, J.D.; Copetti, J.B.; Macagnan, M.; Cardoso, E. Flow boiling pressure drop and flow patterns of R-600a in a multiport minichannels. *Int. J. Refrig.* **2023**, *148*, 13–24.
28. Da Silva Lima, R.J.; Quibén, J.M.; Kuhn, C.; Boyman, T.; Thome, J.R. Ammonia two-phase flow in a horizontal smooth tube: Flow pattern observations, diabatic and adiabatic frictional pressure drops and assessment of prediction methods. *Int. J. Heat Mass Transf.* **2009**, *52*, 2273–2288.
29. Dalkilic, A.S.; Ağra, Ö.; Teke, I.; Wongwises, S. Comparison of frictional pressure drop models during annular flow condensation of R600a in a horizontal tube at low mass flux and of R134a in a vertical tube at high mass flux. *Int. J. Heat Mass Transf.* **2010**, *53*, 2052–2064.
30. Darzi, M.; Akhavan-Behabadi, M.A.; Sadoughi, M.K.; Razi, P. Experimental study of horizontal flattened tubes performance on condensation of R600a vapor. *Int. Commun. Heat Mass Transf.* **2015**, *62*, 18–25.
31. De Oliveira, J.D.; Biancon Copetti, J.; Passos, J.C. An experimental investigation on flow boiling heat transfer of R-600a in a horizontal small tube. *Int. J. Refrig.* **2016**, *72*, 97–110.
32. De Oliveira, J.D.; Biancon Copetti, J.; Passos, J.C. Experimental investigation on flow boiling pressure drop of R-290 and R-600a in a horizontal small tube. *Int. J. Refrig.* **2017**, *84*, 165–180.
33. De Oliveira, J.D.; Passos, J.C.; Biancon Copetti, J.; Van der Geld, C.W.M. Flow boiling heat transfer of propane in 1.0 mm tube. *Exp. Therm. Fluid Sci.* **2018**, *96*, 243–256.
34. De Oliveira, J.D.; Passos, J.C.; Biancon Copetti, J.; Van der Geld, C.W.M. On flow boiling of R-1270 in a small horizontal tube: Flow patterns and heat transfer. *Appl. Therm. Eng.* **2020**, *178*, 115403.
35. De Oliveira, J.D.; Passos, J.C.; Biancon Copetti, J.; Cardoso, E.M.; de Souza, R.R. Flow boiling pressure drop of R-1270 in 1.0 mm tube. *Appl. Therm. Eng.* **2023**, *231*, 120885.
36. Del Col, D.; Bortolato, M.; Bortolin, S. Comprehensive experimental investigation of two-phase heat transfer and pressure drop with propane in a minichannel. *Int. J. Refrig.* **2014**, *47*, 66–84.

37. Del Col, D.; Azzolin, M.; Bortolin, S.; Berto, A. Experimental results and design procedures for minichannel condensers and evaporators using propylene. *Int. J. Refrig.* **2017**, *83*, 23–38.
38. Elfaham, M.; Tang, C. A Comparative Analysis of Two-Phase Flow Boiling Heat Transfer Coefficient and Correlations for Hydrocarbons and Ethanol. *Energies* **2023**, *16*, 5931.
39. Fang, X.; Zhuang, F.; Chen, C.; Wu, Q.; Chen, Y.; Chen, Y.; He, Y. Saturated flow boiling heat transfer: Review and assessment of prediction methods. *Heat Mass Transf.* **2019**, *55*, 197–222.
40. Fang, X.; Qiu, G.; Che, X.; Chen, J.; Cai, W. Evaluation of prediction models on frictional pressure drop for condensation flow in horizontal circular tubes. *Energy Sources A Recovery Util. Environ. Eff.* **2023**, *45*, 6305–6316.
41. Moghaddam, H.A.; Sarmadian, A.; Shafaee, M.; Enayatollahi, H. Flow pattern maps, pressure drop and performance assessment of horizontal tubes with coiled wire inserts during condensation of R-600a. *Int. J. Heat Mass Transf.* **2020**, *148*, 119062.
42. Fries, S.; Skusa, S.; Luke, A. Heat transfer and pressure drop of condensation of hydrocarbons in tubes. *Heat Mass Transf.* **2019**, *55*, 33–40.
43. Fries, S.; Deeb, M.; Luke, A. Influence of Surface Roughness on Pressure Drop in Two-Phase Flow of Saturated Hydrocarbons. *Chem. Ing. Tech.* **2020**, *92*, 608–612.
44. Fronk, B.; Garimella, S. Condensation of ammonia and high-temperature-glide zeotropic ammonia/water mixtures in minichannels—Part II: Heat transfer models. *Int. J. Heat Mass Transf.* **2016**, *101*, 1357–1373.
45. Fronk, B.; Garimella, S. Condensation of ammonia and high-temperature-glide ammonia/water zeotropic mixtures in minichannels—Part I: Measurements. *Int. J. Heat Mass Transf.* **2016**, *101*, 1343–1356.
46. Gao, Y.; Shao, S.; Zhan, B.; Chen, Y.; Tian, C. Heat transfer and pressure drop characteristics of ammonia during flow boiling inside a horizontal small diameter tube. *Int. J. Heat Mass Transf.* **2018**, *127*, 981–996.
47. Gao, Y.; Feng, Y.; Shao, S.; Tian, C. Two-phase pressure drop of ammonia in horizontal small diameter tubes: Experiments and correlation. *Int. J. Refrig.* **2019**, *98*, 283–293.
48. Ghazali, M.A.H.; Mohd-Yunos, Y.; Pamitran, A.S.; Jong-Taek, O.; Mohd-Ghazali, N. Development of a new correlation for pre-dry out evaporative heat transfer coefficient of R290 in a microchannel. *Int. J. Air-Cond. Refrig.* **2022**, *30*, 15.
49. Ghorbani, B.; Akhavan-Behabadi, M.A.; Ebrahimi, S.; Vijayaraghavan, K. Experimental investigation of condensation heat transfer of R600a/POE/CuO nano-refrigerant in flattened tubes. *Int. Commun. Heat Mass Transf.* **2017**, *88*, 236–244.
50. Guo, Q.; Li, M.; Gu, H. Condensation heat transfer characteristics of low-GWP refrigerants in a smooth horizontal mini tube. *Int. J. Heat Mass Transf.* **2018**, *126*, 26–38.
51. Huang, J.; Sheer, T.; Bailey-McEwan, M. Heat transfer and pressure drop in plate heat exchanger refrigerant evaporators. *Int. J. Refrig.* **2012**, *35*, 325–335.
52. Huang, J.; Bailey-McEwan, M.; Sheer, T. Performance Analysis of Plate Heat Exchangers used as Refrigerant Evaporators. In Proceedings of the 22nd International Congress of Refrigeration, Beijing, China, 21–26 August 2007.
53. Ilie, A.; Girip, A.; Calotă, R.; Călin, A. Investigation on the Ammonia Boiling Heat Transfer Coefficient in Plate Heat Exchangers. *Energies* **2022**, *15*, 1503.
54. Inoue, N.; Hirose, M.; Jige, D.; Ichinose, J. Correlation for Condensation Heat Transfer in a 4.0 mm Smooth Tube and Relationship with R1234ze(E), R404A, and R290. *Appl. Sci.* **2018**, *8*, 2267.
55. Kanizawa, F.T.; Tibiriçá, C.B.; Ribatski, G. Heat transfer during convective boiling inside microchannels. *Int. J. Heat Mass Transf.* **2016**, *93*, 566–583.
56. Khan, T.S.; Khan, M.S.; Chyu, M.-C.; Ayub, Z.H. Experimental investigation of evaporation heat transfer and pressure drop of ammonia in a 60° chevron plate heat exchanger. *Int. J. Refrig.* **2012**, *35*, 336–348.
57. Khan, M.S.; Khan, T.S.; Chyu, M.-C.; Ayub, Z.H. Experimental investigation of evaporation heat transfer and pressure drop of ammonia in a 30° chevron plate heat exchanger. *Int. J. Refrig.* **2012**, *35*, 1757–1765.
58. Koyama, K.; Chiyoda, H.; Arima, H.; Ikegami, Y. Experimental study on thermal characteristics of ammonia flow boiling in a plate evaporator at low mass flux. *Int. J. Refrig.* **2014**, *38*, 227–235.
59. Lee, H.-S.; Son, C.-H. Condensation heat transfer and pressure drop characteristics of R-290, R-600a, R-134a and R-22 in horizontal tubes. *Heat Mass Transf.* **2010**, *46*, 571–584.
60. Lillo, G.; Mastrullo, R.; Mauro, A.W.; Viscito, L. Flow boiling heat transfer, dry-out vapor quality and pressure drop of propane (R290): Experiments and assessment of predictive methods. *Int. J. Heat Mass Transf.* **2018**, *126*, 1236–1252.
61. Liu, N.; Xiao, H.; Li, J. Experimental investigation of condensation heat transfer and pressure drop of propane, R1234ze(E) and R22 in minichannels. *Appl. Therm. Eng.* **2016**, *102*, 63–72.
62. Liu, J.; Liu, J.; Li, R.; Xu, X. Experimental study on flow boiling characteristics in a high aspect ratio vertical rectangular mini-channel under low heat and mass flux. *Exp. Therm. Fluid Sci.* **2018**, *98*, 146–157.
63. Longo, G.A. Hydrocarbon Refrigerant Vaporization Inside a Brazed Plate Heat Exchanger. *J. Heat Transf.* **2012**, *134*, 101801.
64. Longo, G.A.; Mancin, S.; Righetti, G.; Zilio, C. Saturated vapour condensation of HFC404A inside a 4 mm ID horizontal smooth tube: Comparison with the long-term low GWP substitutes HC290 (Propane) and HC1270 (Propylene). *Int. J. Heat Mass Transf.* **2017**, *108*, 2088–2099.
65. Longo, G.A.; Mancin, S.; Righetti, G.; Zilio, C. Flow boiling heat transfer capabilities of R134a low GWP substitutes inside a 4 mm id horizontal smooth tube: R600a and R152a. *Heat Mass Transf.* **2020**, 1–19. https://doi.org/10.1007/s00231-020-02991-x.
66. Longo, G.A.; Mancin, S.; Righetti, G.; Zilio, C. Hydrocarbon refrigerants boiling local heat transfer coefficients inside a Brazed Plate Heat Exchanger (BPHE). *Int. J. Refrig.* **2023**, *156*, 113–122.

67. Lopez-Belchi, A.; Illán-Gómez, F.; García-Cascales, J.R.; Vera-García, F. Condensing two-phase pressure drop and heat transfer coefficient of propane in a horizontal multiport mini-channel tube: Experimental measurements. *Int. J. Refrig.* **2016**, *68*, 59–75.
68. Macdonald, M.; Garimella, S. Hydrocarbon condensation in horizontal smooth tubes: Part I—Measurements. *Int. J. Heat Mass Transf.* **2016**, *93*, 75–85.
69. Macdonald, M.; Garimella, S. Hydrocarbon condensation in horizontal smooth tubes: Part II—Heat transfer coefficient and pressure drop modeling. *Int. J. Heat Mass Transf.* **2016**, *93*, 1248–1261.
70. Macdonald, M.; Garimella, S. Effect of Temperature Difference on In-Tube Condensation Heat Transfer Coefficients. *J. Heat Transf.* **2017**, *139*, 2546597.
71. Maher, D.; Hana, A.; Habib, S. New Correlations for Two Phase Flow Pressure Drop in Homogeneous Flows Model. *Therm. Eng.* **2020**, *67*, 92–105.
72. Maqbool, M.H.; Palm, B.; Khodabandeh, R. Flow boiling of ammonia in vertical small diameter tubes: Two phase frictional pressure drop results and assessment of prediction methods. *Int. J. Therm. Sci.* **2012**, *54*, 1–12.
73. Maqbool, M.H.; Palm, B.; Khodabandeh, R. Boiling heat transfer of ammonia in vertical smooth mini channels: Experimental results and predictions. *Int. J. Therm. Sci*. **2012**, *54*, 13–21.
74. Maqbool, M.H.; Palm, B.; Khodabandeh, R. Investigation of two phase heat transfer and pressure drop of propane in a vertical circular minichannel. *Exp. Therm. Fluid Sci.* **2013**, *46*, 120–130.
75. Mohd-Yunos, Y.; Mohd-Ghazali, N.; Mohamad, M.; Pamitran, A.S.; Oh, J.-T. Improvement of two-phase heat transfer correlation superposition type for propane by genetic algorithm. *Heat Mass Transf.* **2020**, *56*, 1087–1098.
76. Moreira, T.A.; Ayub, Z.H.; Ribatski, G. Convective condensation of R600a, R290, R1270 and their zeotropic binary mixtures in horizontal tubes. *Int. J. Refrig.* **2021**, *130*, 27–43.
77. Morrow, J.A.; Huber, R.A.; Nawaz, K.; Derby, M.M. Flow condensation heat transfer performance of natural and emerging synthetic refrigerants. *Int. J. Refrig.* **2021**, *132*, 293–321.
78. Murphy, D.L.; Macdonald, M.P.; Mahvi, A.J.; Garimella, S. Condensation of propane in vertical minichannels. *Int. J. Heat Mass Transf.* **2019**, *137*, 1154–1166.
79. Nasr, M.; Akhavan-Behabadi, M.A.; Momenifar, M.R.; Hanafizadeh, P. Heat transfer characteristic of R-600a during flow boiling inside horizontal plain tube. *Int. Commun. Heat Mass Transf.* **2015**, *66*, 93–99.
80. Oh, J.-T.; Pamitran, A.S.; Choi, K.-I.; Hrnjak, P. Experimental investigation on two-phase flow boiling heat transfer of five refrigerants in horizontal small tubes of 0.5, 1.5 and 3.0 mm inner diameters. *Int. J. Heat Mass Transf.* **2011**, *54*, 2080–2088.
81. Pamitran, A.S.; Choi, K.-I.; Oh, J.-T.; Park, K.-W. Two-phase flow heat transfer of propane vaporization in horizontal minichannels. *J. Mech. Sci. Tech.* **2009**, *23*, 599–606.
82. Pamitran, A.S.; Choi, K.-I.; Oh, J.-T.; Nasruddin, N. Evaporation heat transfer coefficient in single circular small tubes for flow natural refrigerants of C_3H_8, NH_3, and CO_2. *Int. J. Multiph. Flow* **2011**, *37*, 794–801.
83. Patel, T.; Parekh, A.; Tailor, P. Theoretical analysis of two-phase frictional pressure drop during condensing in horizontal mini channel. *Int. J. Mech. Eng. Tech.* **2018**, *9*, 61–71.
84. Pham, Q.V.; Choi, K.-I.; Oh, J.-T. Condensation Heat Transfer Characteristics and Pressure Drops of R410A, R22, R32, and R290 in Multiport Rectangular Channel. *Sci. Technol. Built. Environ.* **2019**, *25*, 1325–1336.
85. Qiu, J.; Zhang, H.; Yu, X.; Qi, Y.; Lou, J.; Wang, X. Experimental investigation of flow boiling heat transfer and pressure drops characteristic of R1234ze(E), R600a, and a mixture of R1234ze(E)/R32 in a horizontal smooth tube. *Adv. Mech. Eng.* **2015**, *7*, 1687814015606311. https://doi.org/10.1177/16878140156063.
86. Sempértegui Tapia, D.F.; Ribatski, G. Flow boiling heat transfer of R134a and low GWP refrigerants in a horizontal micro-scale channel. *Int. J. Heat Mass Transf.* **2017**, *108*, 2417–2432.
87. Sempértegui Tapia, D.F.; Ribatski, G. Two-phase frictional pressure drop in horizontal micro-scale channels: Experimental data analysis and prediction method development. *Int. J. Refrig.* **2017**, *79*, 143–163.
88. Shafaee, M.; Alimardani, F.; Mohseni, S.G. An empirical study on evaporation heat transfer characteristics and flow pattern visualization in tubes with coiled wire inserts. *Int. Commun. Heat Mass Transf.* **2016**, *76*, 301–307.
89. Shah, M.M. An Improved and Extended General Correlation for Heat Transfer During Condensation in Plain Tubes. *HVAC&R Res.* **2009**, *15*, 889–913.
90. Shah, M.M. A correlation for heat transfer during condensation in horizontal mini/micro channels. *Int. J. Refrig.* **2016**, *64*, 187–202.
91. Shah, M.M. Unified correlation for heat transfer during boiling in plain mini/micro and conventional channels. *Int. J. Refrig.* **2016**, *74*, 606–626.
92. Shah, M.M. Comprehensive correlation for dispersed flow film boiling heat transfer in mini/macro tubes. *Int. J. Refrig.* **2017**, *78*, 32–46.
93. Shah, M.M. Heat transfer during condensation in corrugated plate heat exchangers. *Int. J. Refrig.* **2021**, *127*, 180–193.
94. Shah, M.M. New general correlation for heat transfer during saturated boiling in mini and macro channels. *Int. J. Refrig.* **2022**, *137*, 103–116.
95. Tao, X.; Infante Ferreira, C.A. Heat transfer and frictional pressure drop during condensation in plate heat exchangers: Assessment of correlations and a new method. *Int. J. Heat Mass Transf.* **2019**, *135*, 996–1012.
96. Tao, X.; Infante Ferreira, C.A. NH_3 condensation in a plate heat exchanger: Flow pattern based models of heat transfer and frictional pressure drop. *Int. J. Heat Mass Transf.* **2020**, *154*, 119774.

97. Tao, X.; Dahlgren, E.; Leichsenring, M.; Infante Ferreira, C.A. NH_3 condensation in a plate heat exchanger: Experimental investigation on flow patterns, heat transfer and frictional pressure drop. *Int. J. Heat Mass Transf.* **2020**, *151*, 119374.
98. Turgut, O.E.; Coban, M.T.; Asker, M. Comparison of flow boiling pressure drop correlations for smooth macrotubes. *Heat Transf. Eng.* **2016**, *37*, 487–506.
99. Turgut, O.E.; Coban, M.T. A New Saturated Two-Phase Flow Boiling Correlation Based on Propane (R290) Data. *Arab. J. Sci. Eng.* **2021**, *46*, 7851–7874.
100. Turgut, O.E.; Genceli, H.; Asker, M.; Coban, M.T. Novel Saturated Flow Boiling Correlations for R600a and R717 Refrigerants. *Heat Transf. Eng.* **2022**, *43*, 1579–1609.
101. Umar, F.; Oh, J.T.; Pamitran, A.S. Evaluation of Pressure Drop of Two-Phase Flow Boiling with R290 in Horizontal Mini Channel. *J. Adv. Res. Fluid Mech. Therm. Sci.* **2022**, *89*, 160–166.
102. Wang, S.; Gong, M.Q.; Chen, G.F.; Sun, Z.H.; Wu, J.F. Two-phase heat transfer and pressure drop of propane during saturated flow boiling inside a horizontal tube. *Int. J. Refrig.* **2014**, *41*, 200–209.
103. Wang, H.; Fang, X. Evaluation Analysis of Correlations of Flow Boiling Heat Transfer Coefficients Applied to Ammonia. *Heat Transf. Eng.* **2016**, *37*, 32–44.
104. Wen, J.; Gu, X.; Wang, S.; Li, Y.; Tu, J. The comparison of condensation heat transfer and frictional pressure drop of R1234ze(E), Propane and R134a in a horizontal mini-channel. *Int. J. Refrig.* **2018**, *92*, 208–224.
105. Yang, Z.; Gong, M.; Chen, G.; Zou, X.; Shen, J. Two-phase flow patterns, heat transfer and pressure drop characteristics of R600a during flow boiling inside a horizontal tube. *Appl. Therm. Eng.* **2017**, *120*, 654–671.
106. Yuan, S.; Cheng, W.-L.; Nian, Y.-L.; Zhong, Q.; Fan, Y.-F.; He, J. Evaluation of prediction methods for heat transfer coefficient of annular flow and a novel correlation. *Appl. Therm. Eng.* **2017**, *114*, 10–23.
107. Zhang, Y.; Tan, H.; Li, Y.; Shan, S.; Liu, Y. A modified heat transfer correlation for flow boiling in small channels based on the boundary layer theory. *Int. J. Heat Mass Transf.* **2019**, *132*, 107–117.
108. Zhang, J.; Elmegaard, B.; Haglind, F. Condensation heat transfer and pressure drop correlations in plate heat exchangers for heat pump and organic Rankine cycle systems. *Appl. Therm. Eng.* **2021**, *183*, 116231.
109. Zhang, J.; Haglind, F. Experimental analysis of high temperature flow boiling heat transfer and pressure drop in a plate heat exchanger. *Appl. Therm. Eng.* **2021**, *196*, 117269.
110. Zhang, R.; Liu, J.; Zhang, L. Boiling Heat Transfer and Visualization for R717 in a Horizontal Smooth Mini-tube. *Int. J. Refrig.* **2021**, *131*, 275–285.
111. Zhang, R.; Liu, J.; Zhang, L. Flow boiling heat transfer and dryout characteristics of ammonia in a horizontal smooth mini-tube. *Int. J. Therm. Sci.* **2022**, *171*, 107224.
112. Cavallini, A.; Zecchin, R. A dimensionless correlation for heat transfer in forced convection condensation. In Proceedings of the 5th International Heat Transfer Conference Digital Library, Tokyo, Japan, 3–7 September 1974.
113. Shah, M.M. A general correlation for heat transfer during film condensation inside pipes. *Int. J. Heat Mass Transf.* **1979**, *22*, 547–556.
114. Traviss, D.P.; Rohsenow, W.M.; Baron, A.B. Forced convection condensation inside tubes: A heat transfer equation for condenser design, *ASHRAE Transact*. **1973**, *79*, 157–165.
115. Aizuddin, N.; Mohd-Ghazali, N.; Yushazaziah, M.-Y. Analysis of Convective Boiling Heat Transfer Coefficient Correlation of R290. *J. Mech.* **2018**, *41*, 39–44.
116. Cavallini, A.; Del Col, D.; Matkovic, M.; Rossetto, L. Frictional pressure drop during vapour–liquid flow in minichannels: Modelling and experimental evaluation. *Int. J. Heat Fluid Flow* **2009**, *30*, 131–139.
117. Liu, Z.; Winterton, R.H. A general correlation for saturated and subcooled flow boiling in tubes and annuli, based on a nucleate pool boiling equation. *Int. J. Heat Mass Transf.* **1991**, *34*, 2759–2766.
118. Rollmann, P.; Spindler, K. New models for heat transfer and pressure drop during flow boiling of R407C and R410A in a horizontal microfin tube. *Int. J. Therm. Sci.* **2016**, *103*, 57–66.
119. Xu, Y.; Fang, X. A new correlation of two-phase frictional pressure drop for evaporating flow in pipes. *Int. J. Refrig.* **2012**, *5*, 2039–2050.
120. Diani, A.; Mancin, S.; Rossetto, L. R1234ze(E) flow boiling inside a 3.4 mm ID microfin tube. *Int. J. Refrig.* **2014**, *47*, 105–119.
121. Shah, M.M. Chart correlation for saturation boiling heat transfer: Equation and further study. *ASHREA Trans*. **1982**, *88*, 186–196.
122. Dorao, C.A.; Fernandino, M. Simple and general correlation for heat transfer during flow condensation inside plain pipes. *Int. J. Heat Mass Transf.* **2018**, *122*, 290–305.
123. Cavallini, A.; Del Col, D.; Mancin, S.; Rossetto, L. Condensation of pure and near-azeotropic refrigerants in microfin tubes: A new computational procedure. *Int. J. Refrig.* **2009**, *32*, 162–174.
124. Xu, Y.; Fang, X. A new correlation of two-phase frictional pressure drop for condensing flow in pipes. *Nucl. Eng. Des.* **2013**, *263*, 87–96.
125. Li, W.; Wu, Z. A General Correlation for Evaporative Heat Transfer in Micro/Mini-Channels. *Int. J. Heat Mass Transf.* **2010**, *53*, 1778–1787.
126. Mahmoud, M.; Karayiannis, T. A Statistical Correlation for Flow Boiling Heat Transfer in Micro Tubes, In Proceedings of the 3rd European Conference on Microfluidics-Microfluidics, Heidelberg, Germany, 3–5 December 2012.
127. Sakamatapan, K.; Wongwises, S. Pressure drop during condensation of R134a flowing inside a multiport minichannel. *Int. J. Heat Mass Transf.* **2014**, *75*, 31–39.

128. Gungor, K.E.; Wintertone, R.H.S. A general correlation for flow boiling in tubes and annuli. *Int. J. Heat Mass Transf.* **1986**, *29*, 351–358.
129. Müller-Steinhagen, H.; Heck, K. A simple friction pressure drop correlation for two-phase flow in pipes. *Chem. Eng. Process. Process Intensif.* **1986**, *20*, 297–308.
130. Hwang, Y.W.; Kim, M.S. The pressure drop in microtubes and the correlation development. *Int. J. Heat Mass Transf.* **2006**, *49*, 1804–1812.
131. Moreno Quibén, J.; Thome, J.R. Flow pattern based two-phase frictional pressure drop model for horizontal tubes. Part II: New phenomenological model. *Int. J. Heat Fluid Flow* **2007**, *28*, 1060–1072.
132. Chen, I.Y.; Yang, K.S.; Chang, Y.J.; Wang, C.C. Two-phase pressure drop of air– water and R-410a in small horizontal tubes. *Int. J. Multiph. Flow* **2001**, *27*, 1293–1299.
133. Mishima, K.; Hibiki, T. Some characteristics of air–water two-phase flow in small diameter vertical tubes. *Int. J. Multiph. Flow* **1996**, *22*, 703–712.
134. Jung, D.; Radermacher, R. Prediction of pressure drop during horizontal annular flow boiling of pure and mixed refrigerants, *Int. J. Heat Mass Transf.* **1989**, *32*, 2435–2446.
135. Kim, S.-M.; Mudawar, I. Universal approach to predicting saturated flow boiling heat transfer in mini/micro-channels—Part II. Two-phase heat transfer coefficient. *Int. J. Heat Mass Transf.* **2013**, *64*, 1239–1256.
136. Zhang, W.; Hibiki, T.; Mishima, K. Correlations of two-phase frictional pressure drop and void fraction in mini-channel. *Int. J. Heat Mass Transf.* **2010**, *53*, 453–465.
137. Bertsch, S.S.; Groll, E.A.; Garimella, S.V. A composite heat transfer correlation for saturated flow boiling in small channels. *Int. J. Heat Mass Transf.* **2009**, *52*, 2110–2118.
138. Moser, K.; Webb, R.; Na, B. A new equivalent Reynolds number model for condensation in smooth tubes. *J. Heat Transf.* **1998**, *120*, 410–417.
139. Thome, J.R.; Dupont, V.; Jacobi, A.M. Heat transfer model for evaporation in microchannels. Part I: Presentation of the model. *Int. J. Heat Mass Transf.* **2004**, *47*, 3375–3385.
140. Del Col, D.; Bisetto, A.; Bortolato, M.; Torresin, D.; Rossetto, L. Experiments and updated model for two phase frictional pressure drop inside minichannels. *Int. J. Heat Mass Transf.* **2013**, *67*, 326–337.
141. Sun, L.; Mishima, K. An evaluation of prediction methods for saturated flow boiling heat transfer in mini-channels. *Int. J. Heat Mass Transf.* **2009**, *52*, 5323–5329.
142. Friedel, L. Improved friction pressure drop correlations for horizontal and vertical two phase flow. In Proceedings of the European Two Phase Flow Group Meeting, Paper E2, Ispra, Italy, 5–8 June 1979.
143. Kew, P.A.; Cornwell, K. Correlations for the prediction of boiling heat transfer in small-diameter channels. *Appl. Therm. Eng.* **1997**, *17*, 705–715.
144. Fang, X.; Wu, Q.; Yuan, Y. A general correlation for saturated flow boiling heat transfer in channels of various sizes and flow directions. *Int. J. Heat Mass Transf.* **2017**, *107*, 972–981.
145. Nualboonrueng, T.; Wongwises, S. Two-phase flow pressure drop of HFC-134a during condensation in smooth and micro-fin tubes at high mass flux. *Int. Commun. Heat Mass Transf.* **2004**, *31*, 991–1004.
146. Thome, J.R.; Cavallini, A.; El-Hajal, J. Condensation in horizontal tubes, part 2: New heat transfer model based on flow regimes. *Int. J. Heat Mass Transf* **2003**, *46*, 3365–3387.
147. Gungor, K.E.; Winterton, R.H.S. Simplified general correlation for saturated flow boiling and comparison with data. *Chem. Eng. Res. Des.* **1987**, *65*, 148–156.
148. Koyama, S.; Kuwara, K.; Nakashita, K. Condensation of refrigerant in a multiport channel. In Proceedings of the 1st International Conference on Microchannels and Minichannels, Rochester, NY, USA, 24–25 April 2003.
149. Haraguchi, E.; Koyama, H.; Fujii, H. Condensation of refrigerant HCFC-22, HFC-134a and HCFC-123 in a horizontal smooth tube. *Trans. JSME* **1994**, *60*, 2117–2126.
150. Wojtan, L.; Ursenbacher, T.; Thome, J.R. Investigation of flow boiling in horizontal tubes: Part II—Developement of a new heat transfer model for stratified-wavy, dryout and mist flow regimes. *Int. J. Heat Mass Transf.* **2005**, *48*, 2970–2985.
151. Kim, S.M.; Mudawar, I. Universal approach to predicting heat transfer coefficient for condensing mini/micro-channel flow. *Int. J. Heat Mass Transfer* **2013**, *56*, 238–250.
152. Kim, S.M.; Mudawar, I. Universal approach to predicting two-phase frictional pressure drop for adiabatic and condensing mini/micro-channel flows. *Int. J. Heat Mass Transfer* **2012**, *55*, 3246–3261.
153. Cooper, M.G. Heat Flows Rates in Saturated Pool Boiling—A Wide Ranging Examination Using Reduced Properties. In *Advances in Heat Transfer*; Elsevier: Amsterdam, The Netherlands, 1984; Volume 16, pp. 157–239.
154. Gorenflo, D. Pool Boiling. In *VDI Heat Atlas*; Springer: Dusseldorf, Germany, 1993; pp. Ha1–Ha25.
155. Akers, W.W.; Deans, H.A.; Crosser, O.K. Condensing heat transfer within horizontal tubes. *Chem. Eng. Prog. Symp. Ser.* **1959**, *55*, 171–176.
156. Wang, C.C.; Chiang, C.S.; Lu, D.C. Visual observation of two-phase flow pattern of R-22, R-134a, and R-407C in a 6.5-mm smooth tube. *Exp. Therm. Fluid Sci.* **1997**, *15*, 395–405.
157. Longo, G.A.; Mancin, S.; Righetti, G.; Zilio, C. A new computational procedure for refrigerant boiling inside Brazed Plate Heat Exchangers (BPHEs). *Int. J. Heat Mass Transf.* **2015**, *91*, 144–149.

158. Koyama, S.; Kuwahara, K.; Nakashita, K.; Yamamoto, K. An experimental study on condensation of refrigerant R134a in a multi-port extruded tube. *Int. J. Refrig.* **2003**, *26*, 425–432.
159. Sun, L.; Mishima, K. Evaluation analysis of prediction methods for two-phase flow pressure drop in mini-channels. *Int. J. Multiph. Flow* **2009**, *35*, 47–54.
160. Cavallini, A.; Del Col, D.; Doretti, L.; Matkovic, M.; Rossetto, L.; Zilio, C.; Censi, G. Condensation in horizontal smooth tubes: A new heat transfer model for heat exchanger design. *Heat Transf. Eng*. **2006**, *27*, 31–38.
161. Garimella, S.; Agarwal, A.; Killion, J. Condensation pressure drop in circular microchannels. *Heat Transf. Eng*. **2005**, *26*, 28–35.
162. Tran, T.N.; Chyu, M.C.; Wambsganss, M.W.; France, D.M. Two phase pressure drop of refrigerants during flow boiling in small channels: An experimental investigation and correlation development. *Int. J. Multiph. Flow* **2000**, *26*, 1739–1754.
163. Cooper, M.G. Flow boiling–the 'apparentaly nucleate' regime. *Int. J. Heat Mass Transf.* **1989**, *32*, 459–464.
164. Cooper, M.G. Saturated nucleate pool boiling, a simple correlation. *Int. Chem. Eng. Symp. Series* **1984**, *86*, 785–793.
165. Shah, M.M. General correlation for heat transfer during condensation in plain tubes: Further development and verification. *ASHRAE Trans.* **2013**, *119*, 3–11.
166. Ould Didi, M.B.; Kattan, N.; Thome, J.R. Prediction of two-phase pressure gradients of refrigerants in horizontal tubes. *Int. J. Refrig.* **2002**, *25*, 935–947.
167. Longo, G.A.; Righetti, G.; Zilio, C. A new computational procedure for refrigerant condensation inside herringbone-type Brazed Plate Heat Exchangers. *Int. J. Heat Mass Transf.* **2015**, *82*, 530–536.
168. Gronnerud, R. *Investigation of Liquid Hold-Up, Flow Resistance and Heat Transfer in Circulation Type Evaporators, Part IV: Two-Phase Flow Resistance in Boiling Refrigerants, Annexe 1972-1, Bull. de l'Institut du Froid*; International Institute of Refrigeration: Paris, France, 1979.
169. Wattelet, J.P.; Chato, J.C.; Souza, A.L.; Christofersen, B.R. Evaporative characteristics of R-12, R134a, and a mixture at low mass fuxes. *ASHRAE Trans.* **1994**, *100*, 603–615.
170. Li, X.; Hibiki, T. Frictional pressure drop correlation for two-phase flows in mini and micro single channels. *Int. J. Multiph. Flow* **2017**, *90*, 29–45.
171. Kandlikar, S.G. A Model for Predicting the Two-Phase Flow Boiling Heat Transfer Coefficient in Augmented Tube and Compact Heat Exchanger Geometries. *J. Heat Transf.* **1991**, *113*, 966–972.
172. Stephan, K. *Heat Transfer in Condensation and Boiling*; Springer: New York, NY, USA, 1992.
173. Longo, G.A. Heat transfer and pressure drop during hydrocarbon refrigerant condensation inside a brazed plate heat exchanger. *Int. J. Refrig*. **2010**, *33*, 944–953.
174. Chen, J.C. Correlation for boiling heat transfer to saturated fluids in convective flow. *Ind. Eng. Chem. Process Des. Dev.* **1966**, *5*, 322–329.
175. Zhang, J.; Desideri, A.; Kærn, M.R.; Ommen, T.S.; Wronski, J.; Haglind, F. Flow boiling heat transfer and pressure drop characteristics of R134a, R1234yf and R1234ze in a plate heat exchanger for organic Rankine cycle units. *Int. J. Heat Mass Transf.* **2017**, *108*, 1787–1801.
176. Cheng, L.; Ribatski, G.; Thome, J.R. New prediction methods for CO_2 evaporation inside tubes: Part II—An updated general flow boiling heat transfer model based on flow patterns. *Int. J. Heat Mass Transf.* **2008**, *51*, 125–135.
177. Mori, H.; Yoshida, S.; Ohishi, K.; Kokimoto, Y. Dryout quality and post dryout heat transfer coefficient in horizontal evaporator tubes. In Proceedings of the 3rd European Thermal Sciences Conference, Heidelberg, Germany, 10–13 September 2000.
178. Abbas, A.; Ayub, Z.H. Experimental study of ammonia flooded boiling on a triangular pitch plain tube bundle. *Appl. Therm. Eng.* **2017**, *121*, 484–491.
179. Abbas, A.; Ayub, Z.H.; Ayub, A.H.; Chattha, J.A. Shell side direct expansion evaporation of ammonia on a plain tube bundle with inlet quality effect in the presence of exit superheat. *Int. J. Refrig.* **2017**, *82*, 11–21.
180. Ahmadpour, M.M.; Akhavan-Behabadi, M.A.; Sajadi, B.; Salehi-Kohestani, A. Experimental study of R600a/oil/MWCNT nano-refrigerant condensing flow inside micro-fin tubes. *Heat Mass Transf.* **2020**, *56*, 749–757.
181. Aprin, L.; Mercier, P.; Tadrist, L. Local heat transfer analysis for boiling of hydrocarbons in complex geometries: A new approach for heat transfer prediction in staggered tube bundle. *Int. J. Heat Mass Transf.* **2011**, *54*, 4203–4219.
182. Ayub, Z.H.; Abbas, A.; Ayub, A.H.; Khan, T.S.; Chattha, J.A. Shell side direct expansion evaporation of ammonia on a plain tube bundle with exit superheat effect. *Int. J. Refrig.* **2017**, *76*, 126–135.
183. Ding, C.; Hu, H.; Ding, G.; Chen, J.; Mi, X.; Yu, S.; Li, J. Experimental investigation on downward flow boiling heat transfer characteristics of propane in shell side of LNG spiral wound heat exchanger. *Int. J. Refrig.* **2017**, *84*, 13–25.
184. Ding, C.; Hu, H.; Ding, G.; Chen, J.; Mi, X.; Yu, S. Influences of tube pitches on heat transfer and pressure drop characteristics of two-phase propane flow boiling in shell side of LNG spiral wound heat exchanger. *Appl. Therm. Eng.* **2018**, *131*, 270–283.
185. Fernández-Seara, J.; Pardiñas, Á.A.; Diz, R. Heat transfer enhancement of ammonia pool boiling with an integral-fin tube. *Int. J. Refrig.* **2016**, *69*, 175–185.
186. Gil, B.; Fijałkowska, B. Experimental Study of Nucleate Boiling of Flammable, Environmentally Friendly Refrigerants. *Energies* **2019**, *13*, 160.
187. Gong, M.; Wu, Y.; Ding, L.; Cheng, K.; Wu, J. Visualization study on nucleate pool boiling of ethane, isobutane and their binary mixtures. *Exp. Therm. Fluid Sci.* **2013**, *51*, 164–173.
188. Huang, Y.; Yang, Q.; Zhao, J.; Miao, J.; Shen, X.; Fu, W.; Wu, Q.; Guo, Y. Experimental Study on Flow Boiling Heat Transfer Characteristics of Ammonia in Microchannels. *Microgravity Sci. Technol.* **2020**, *32*, 477–492.

189. Jin, P.-H.; Zhang, Z.; Mostafa, I.; Zhao, C.-Y.; Ji, W.-T.; Tao, W.-Q. Heat transfer correlations of refrigerant falling film evaporation on a single horizontal smooth tube. *Int. J. Heat Mass Transf.* **2019**, *133*, 96–106.
190. Jin, P.-H.; Zhao, C.-Y.; Ji, W.-T.; Tao, W.-Q. Experimental investigation of R410A and R32 falling film evaporation on horizontal enhanced tubes. *Appl. Therm. Eng.* **2018**, *137*, 739–748.
191. Jin, P.-H.; Zhang, Z.; Mostafa, I. Low GWP refrigerant R1234ze(E) falling film evaporation on a single horizontal plain tube and enhanced tubes with reentrant cavities. In Proceedings of the 9th Asian Conference on Refrigeration and Air Conditioning, Sapporo, Japan, 10–13 June 2018.
192. Koyama, K.; Chiyoda, H.; Arima, H.; Okamoto, A.; Ikegami, Y. Measurement and prediction of heat transfer coefficient on ammonia flow boiling in a microfin plate evaporator. *Int. J. Refrig.* **2014**, *44*, 36–48.
193. Li, S.; Cai, W.; Chen, J.; Zhang, H.; Jiang, Y. Numerical study on the flow and heat transfer characteristics of forced convective condensation with propane in a spiral pipe. *Int. J. Heat Mass Transf.* **2018**, *117*, 1169–1187.
194. Lin, H.-Y.; Murugan, M.; Yang, C.-M.; Nawaz, K.; Wang, C.-C. Universal Correlation for Falling Film Evaporation on a Horizontal Plain Tube. *Int. J. Refrig.* **2023**, *146*, 261–273.
195. Ma, L.; Shang, L.; Zhong, D.; Ji, Z. Experimental investigation of a two-phase closed thermosyphon charged with hydrocarbon and Freon refrigerants. *Appl. Energy* **2017**, *207*, 665–673.
196. Moon, S.H.; Lee, D.; Kim, M.; Kim, Y. Evaporation heat transfer coefficient and frictional pressure drop of R600a in a micro-fin tube at low mass fluxes and temperatures. *Int. J. Heat Mass Transf.* **2022**, *190*, 122769.
197. Pham, Q.V.; Oh, J.-T. Flow condensation heat transfer of propane refrigerant inside a horizontal micro-fin tube. *Int. J. Air-Cond. Refrig.* **2022**, *30*, 14.
198. Qiu, G.D.; Cai, W.H.; Wu, Z.Y.; Yao, Y.; Jiang, Y.Q. Numerical Simulation of Forced Convective Condensation of Propane in a Spiral Tube. *J. Heat Transf.* **2015**, *137*, 041502.
199. Salman, M.; Prabakaran, R.; Kumar, P.G.; Lee, D.; Kim, S.C. Saturation flow boiling characteristics of R290 (propane) inside a brazed plate heat exchanger with offset strip fins. *Int. J. Heat Mass Transf.* **2022**, *202*, 123778.
200. Sathyabhama, A.; Hegde, R. Prediction of nucleate pool boiling heat transfer coefficient. *Therm. Sci.* **2010**, *14*, 353–364.
201. Inoue, T.; Monde, M.; Teruya, Y. Pool Boiling Heat Transfer in Binary Mixtures of Ammonia and Water. *Int. J. Heat Mass Transf.* **2002**, *45*, 4409–4415.
202. Arima, H.; Monde, M.; Mitsutake, Y. Heat Transfer in Pool Boiling of Ammonia Water Mixture. *Int. J. Heat Mass Transf.* **2003**, *39*, 535–543.
203. Zeng, X.; Chyu, M.-C.; Ayub, Z.H. Evaporation Heat Transfer Performance of Nozzle-Sprayed Ammonia on a Horizontal Tube. In *Thermal Sciences 2000. Proceedings of the International Thermal Science Seminar*; Begel House Inc.: Danbury, CT, USA, 2000; Volume 1, pp. 136–149.
204. Shah, M.M. A correlation for heat transfer during boiling on bundles of horizontal plain and enhanced tubes. *Int. J. Refrig.* **2017**, *78*, 47–59.
205. Shah, M.M. A general correlation for heat transfer during evaporation of falling films on single horizontal plain tubes. *Int. J. Refrig.* **2021**, *130*, 424–433.
206. Shete, U.N.; Kumar, R.; Chandra, R. Pool boiling heat transfer enhancement of R134a, R32, and R600a using reentrant cavity surfaces. *Exp. Heat Transf.* **2023**, *36*, 528–547.
207. Tian, Z.; Wang, F.; Gu, B.; Zhang, Y.; Gao, W. Enhanced pool boiling of propane on horizontal U-shaped tubes in a large-scale confined space. *Int. J. Refrig.* **2022**, *133*, 19–29.
208. Touhami, B.; Abdelkader, A.; Mohamed, T. Proposal for a correlation raising the impact of the external diameter of a horizontal tube during pool boiling. *Int. J. Therm. Sci.* **2014**, *84*, 293–299.
209. Wen, M.-Y.; Jang, K.-J.; Ho, C.-Y. The characteristics of boiling heat transfer and pressure drop of R-600a in a circular tube with porous inserts. *Appl. Therm. Eng.* **2014**, *64*, 348–357.
210. Wu, J.; Zou, S.; Wang, L.; Dai, Y. Condensation heat transfer of R290 in micro-fin tube with inside diameter of 6.3 mm. *Exp. Heat Transf.* **2021**, *34*, 1–17.
211. Yan, K.; Xie, R.; Li, N.; Xu, G.; Wu, Y. Experimental Investigation and Visualization Study of the Condensation Characteristics in a Propylene Loop Heat Pipe. *J. Therm. Sci.* **2021**, *30*, 1803–1813.
212. Yang, G.; Hu, H.; Ding, G.; Chen, J.; Yang, W.; Hu, S.; Pang, X. Experimental investigation on heat transfer characteristics of two-phase propane flow condensation in shell side of helically baffled shell-and-tube condenser. *Int. J. Refrig.* **2018**, *88*, 58–66.
213. Yang, G.; Ding, G.; Chen, J.; Yang, W.; Hu, S. Experimental study on shell side heat transfer characteristics of two-phase propane flow condensation for vertical helically baffled shell-and-tube exchanger. *Int. J. Refrig.* **2019**, *107*, 134–144.
214. Yoo, J.W.; Nam, C.W.; Yoon, S.H. Experimental study of propane condensation heat transfer and pressure drop in semicircular channel printed circuit heat exchanger. *Int. J. Heat Mass Transf.* **2022**, *182*, 121939.
215. Yu, J.; Chen, J.; Li, F.; Cai, W.; Lu, L.; Jiang, Y. Experimental investigation of forced convective condensation heat transfer of hydrocarbon refrigerant in a helical tube. *Appl. Therm. Eng.* **2018**, *129*, 1634–1644.
216. Zhao, C.; Guo, H.; Hanwen, X.; Nie, F.; Gong, M.; Yang, Z. Boiling heat transfer and pressure drop of R290 in a micro-fin tube. *Int. J. Refrig.* **2023**, *155*, 195–206.
217. Yu, J.; Koyama, S. Condensation heat transfer of pure refrigerants in microfin tubes. In Proceedings of the 1998 International Refrigeration Conference at Purdue, West Lafayette, IN, USA, 14–17 July 1998.

218. Cavallini, A.; Doretti, L.; Klammsteiner, A.; Longo, L.G.; Rossetto, L. Condensation of new refrigerants inside smooth and enhanced tubes. In Proceedings of the 9th International Congress of Refrigeration, Hague, The Netherlands, 20–25 August 1995.
219. Kedzierski, M.A.; Goncalves, J.M. Horizontal convective condensation of alternative refrigerants within a micro-fin tube. *J. Enhanc. Heat Transf.* **1999**, *6*, 161–178.
220. Jung, D.; Lee, H.; Bae, D.; Oho, S. Nucleate boiling heat transfer coefficients of flammable refrigerants. *Int. J. Refrig*. **2004**, *27*, 409–414.
221. Rohsenow, W.M. A method of correlating heat transfer data for surface boiling of liquids. *Trans ASME* **1952**, *74*, 969–976.
222. Boyko, L.D.; Kruzhilin, G.N. Heat Transfer and Hydraulic Resistance During Condensation of Steam in a Horizontal Tube and in a Bundle of Tubes. *Int. J. Heat Mass Transf.* **1967**, *10*, 361–373.
223. Fuchs, P.H. Pressure Drop and Heat Transfer during Flow of Evaporating Liquid in Horizontal Tubes and Bends. Ph.D. Thesis, NTH, Trondheim, Norway, 1975.
224. Kruzhilin, G.N. Free Convection Transfer of Heat from a Horizontal Plate and Boiling Liquid. *Dokl. AN SSSR Rep. USSR Acad. Sci.* **1947**, *58*, 1657–1660.
225. Mostinski, I.L. Application of the Rule of Corresponding States for Calculation of Heat Transfer and Critical Heat Flux. *Teploenergetika* **1963**, *4*, 66–71.
226. Stephan, K.; Abdelsalam, M. Heat-transfer correlations for natural convection boiling. *Int. J. Heat Mass Transf.* **1980**, *23*, 73–87.
227. Ribatski, G.; Jabardo, J.M.S. Experimental study of nucleate boiling of halocarbon refrigerants on cylindrical surfaces. *Int. J. Heat Mass Transf.* **2003**, *46*, 4439–4451.
228. Cavallini, A.; Censi, G.; Del Col, D. Condensation of halogenated refrigerants inside smooth tubes. *HVAC&R Res.* **2002**, *8*, 429–451.
229. Lockhart, R.W.; Martinelli, R.C. Proposed correlation of data for isothermal two phase, two component flow in pipes. *Chem. Eng. Prog.* **1949**, *45*, 39–48.
230. Cavallini, A.; Del Col, D.; Doretti, L.; Longo, G.A.; Rossetto, L. Refrigerant vaporization inside enhanced tubes: A heat transfer model. *Heat Technol.* **1999**, *17*, 29–36.
231. The European Parliament and the Council of the European Union. REGULATION (EU) No 517/2014 of the European Parliament and of the Council of 16 April 2014 on Fluorinated Greenhouse Gases and Repealing Regulation (EC) No 842/2006, Official Journal of the European Union, 20 May 2014. Available online: https://eur-lex.europa.eu/legal-content/EN/TXT/?uri=CELEX%3A32014R0517 (accessed on 12 January 2024).